8-2012

Magnetic, Optical and Dielectric Effects on Photovoltaic Processes in Organic Solar Cells

HUIDONG ZANG
hzang2@utk.edu

To the Graduate Council:

I am submitting herewith a dissertation written by HUIDONG ZANG entitled "Magnetic, Optical and Dielectric Effects on Photovoltaic Processes in Organic Solar Cells." I have examined the final electronic copy of this dissertation for form and content and recommend that it be accepted in partial fulfillment of the requirements for the degree of Doctor of Philosophy, with a major in Materials Science and Engineering.

Bin Hu, Major Professor

We have read this dissertation and recommend its acceptance:

Roberto S. Benson, Jimmy Mays, Ilia N. Ivanov

Accepted for the Council:
Dixie L. Thompson

Vice Provost and Dean of the Graduate School

(Original signatures are on file with official student records.)

To the Graduate Council:

I am submitting herewith a dissertation written by Huidong Zang entitled "Magnetic, Optical and Dielectric Effects on Photovoltaic Processes in Organic Solar Cells." I have examined the final paper copy of this dissertation for form and content and recommend that it be accepted in partial fulfillment of the requirements for the degree of Doctor of Philosophy, with a major in Materials Science and Engineering.

_____

Bin Hu, Major Professor

We have read this dissertation
and recommend its acceptance:

_____

Bin Hu

_____

Roberto S. Benson

_____

Jimmy Mays

_____

Ilia N. Ivanov

Accepted for the Council:

_____

Carolyn R. Hodges

Vice Provost and Dean of the Graduate School

Magnetic, Optical and Dielectric Effects on Photovoltaic Processes in Organic Solar Cells

A Dissertation

Presented for the

Doctor of Philosophy

Degree

The University of Tennessee, Knoxville

Huidong Zang

August 2012

Dedication

I dedicate this dissertation to my parents!

Acknowledgements

I am sincerely and heartily grateful to my advisor Dr. Bin Hu for his five years of guidance and support for my research and dissertation. I learned a lot from him, most importantly the capability to solve problems. I am sure it would have not been possible for me to finish my dissertation without his help. Also, I would like to thank my committee members, Dr. Roberto S. Benson, Dr. Jimmy Mays, and Dr. Ilia N. Ivanov for their instructive advice and great support.

I would like to show my gratitude to my collaborators at the Oak Ridge National Laboratory (ORNL) for their great help in providing facilities and many valuable discussions. They are Dr. David B.Geohegan, Dr. Ilia Ivanov, and Dr. Kai Xiao. I also would like to thank Dr. Luping Yu and Dr. Yongye Liang from The University of Chicago for providing materials and fruitful discussions.

I owe sincere and earnest thankfulness to my former group members, Dr. Yue Wu, Dr. Zhihua Xu, Dr. Liang Yan, Dr. Ming Shao, Dr. Tho Nguyen, Jaime Sullivan, Dr. Xinjun Xu, Dr. Youzhi Wu, Dr. Lianbin Niu and my present group members Dr. Dehua Hu, Dr. Lei He, Yu-Che Hisao, Mingxing Li, Qing Liu, undergraduate students Michael Stanford and Jackie Cann. I would like to thank them for their numerous discussions and great support.

Finally, I must express my great appreciation to my parents and other family members in China, as well as my wife, Wei Jiang, who provided me the strongest support during the years in the graduate school. Thank you all.

Abstract

Organic bulk heterojunction photovoltaics have attracted extensive attention during the past decade due to the global energy crisis, and it had been nominated as one of the most promising substitution for the next generation of green energy. Organic Photovoltaics, also named as "plastic solar cells", have many advantages including super-low cost, flexibility, and compatibility with the ink printing fabrication technique, etc. Although the photovoltaic efficiency of the organic bulk heterojunction is still not as high as that of the inorganic ones, its great potential makes it the most promising solar cells in the future. In this dissertation, Chapter 1 presents a basic introduction to the concepts of conjugated polymers, the widely utilized materials in photovoltaic devices, and the fundamental device physics. Meanwhile, some basic spintronics was also discussed in this chapter. Finally, the peer publications review is briefly discussed in order to cover the academic progress in this field. Chapter 2 and Chapter 3 systematically study the origin of open circuit voltage in organic photovoltaics. Chapter 4 and Chapter 5 study the magnetic field effect on photocurrent change of bulk heterojunction and double layer photovoltaics, respectively. Chapter 6 focuses on the "intra-molecular" interaction effect on internal photovoltaic processes in new low band gap materials based on magnetic field effect and photoassisted dielectric response techniques. Finally, Chapter 7 gives a short conclusion for the entire dissertation.

Contents

List of Tables xi

List of Figures xii

1 Introduction 1

1.1 History of solar energy conversion: photovoltaics 1

1.1.1 Inorganic photovoltaics 1

1.1.2 Organic photovoltaics 2

1.2 Organic Photovoltaic materials 2

1.2.1 Π-conjugated organic semiconductors 2

1.2.2 Materials for bulk heterojunction photovoltaics 4

1.3 Bulk heterojunction photovoltaics 4

1.3.1 Device architecture 4

1.3.2 Working principle 4

1.3.3 Electrical characterization 6

1.3.4 Magneto-optical characterization and experimental setup . . . 8

1.4 Photophysics in organic materials and photovoltaics 9

1.4.1 Singlet and triplet excited states 9

1.4.2 Exciton, polaron pair, and charge-transfer complex 11

1.4.3 Zeeman effect 13

1.4.4 Spin-Orbit coupling 14

1.4.5 Hyperfine interaction 16

1.4.6 Intersystem crossing . . . 16
1.4.7 Triplet charge reaction . . . 17
1.5 Magnetic field effect . . . 17
1.6 Peer article review of the origin of V_{oc} in organic solar cells . . . 18
1.7 Peer article review of magnetic field effect on photocurrent change . . . 19
1.8 Outline of the dissertation . . . 21

2 Open circuit voltage in organic bulk-heterojunction photovoltaics 22
2.1 Electrode dependence of the open circuit voltage . . . 22
2.1.1 Introduction . . . 22
2.1.2 Experimental . . . 23
2.1.3 Results and Discussion . . . 23
2.1.4 Conclusion . . . 24
2.2 Thickness dependence of the open circuit voltage . . . 24
2.2.1 Introduction . . . 24
2.2.2 Experimental . . . 25
2.2.3 Results and Discussion . . . 25
2.2.4 Conclusion . . . 25
2.3 Energy level dependence of the open circuit voltage . . . 25
2.3.1 Introduction . . . 25
2.3.2 Experimental . . . 26
2.3.3 Results and Discussion . . . 27
2.3.4 Conclusion . . . 27
2.4 Dielectric effect on the open circuit voltage . . . 28
2.4.1 Introduction . . . 28
2.4.2 Experimental . . . 28
2.4.3 Results and Discussion . . . 28
2.4.4 Conclusion . . . 32
2.5 Chapter summary . . . 36

3 Determination of Open Circuit Voltage in Organic Bulk Heterojunction Photovoltaics from Photoassisted Impedance Analysis 37

3.1 Introduction . . . 37

3.2 Experimental . . . 38

3.3 Results and Discussion . . . 38

3.4 Conclusion . . . 50

4 Magnetic field effect on charge-transfer complex in P3HT:PCBM bulk-heterojunction photovoltaics 51

4.1 Introduction . . . 52

4.2 Experimental . . . 55

4.3 Results and Discussion . . . 56

4.4 Conclusion . . . 70

5 Magnetic field effect on charge-transfer complex in P3HT/TiOx double layer photovoltaics 71

5.1 Introduction . . . 72

5.2 Experimental . . . 72

5.3 Results and Discussion . . . 74

5.4 Conclusion . . . 83

6 Intra-Molecular "Donor-Acceptor" Interaction Effects on Charge Dissociation, Charge Transport, and Charge Collection in Bulk-Heterojunction Organic Photovoltaics 85

6.1 Introduction . . . 85

6.2 Experimental . . . 86

6.3 Results and Discussion . . . 87

6.4 Conclusion . . . 101

7 CONCLUSIONS 102

Bibliography 104

Vita 128

Index 129

List of Tables

2.1 Energy levels of the selected donor materials 26

List of Figures

1.1 Chemical structure of Polyacetylene polymer and p_z orbitals 3

1.2 Materials utilized for bulk heterojunction photovoltaics 5

1.3 Schematic figure of typical OPV. 6

1.4 The working principle of organic bulk-heterojunction solar cells. 1. The photon absorption; 2. Intra-molecular recombination; 3. Exciton diffusion; 3′. Hole transportation 4. Photoinduced electron transfer at donor and acceptor interface; 5. Electron transportation in acceptor; 6. Electron collection; 6′. Hole collection; 7. Geminated recombination; 8. Bimolecular recombination 7

1.5 Typical Voltage-Current characterization of solar cell under light illumination 7

1.6 Equivalent electric circuit of the organic bulk-heterojunction solar cell 8

1.7 Schematic diagram for magnetic field effect on photocurrent change setup 9

1.8 Schematic diagram of singlet and triplet states configuration. 10

1.9 Schematic diagram for exchange energy in excitonic states 11

1.10 Schematic diagram for the distance of Exciton, Polaron pair, and Charge-Transfer Complex. 12

1.11 Schematic diagram for exchange energy with the separation distance . 13

1.12 Schematic diagram of Zeeman effect 14

1.13 Schematic diagram of spin-orbit coupling 15

1.14 Schematic diagram for exchange energy in polaron pair or charge-transfer complex states 17
1.15 Schematic diagram for the magnetic field effect on resistance, photocurrent, photoluminescence and electroluminescence. 18

2.1 Work function of cathode dependence of the open circuit voltage in $P3HT : PCBM$ based bulk-heterojunction solar cells. 23
2.2 Thickness dependence of open circuit voltage in $P3HT : PCBM$ based bulk-heterojunction solar cells. 24
2.3 Effective band gap for organic bulk-heterojunction solar cells. 26
2.4 The relationship between open circuit voltage and effective energy band gap of the heterojunction solar cells. 27
2.5 Effective dielectric constant effect on open circuit voltage for thermal annealing $P3HT : PCBM$ solar cells. 30
2.6 Effective dielectric constant effect on open circuit voltage for thermally annealed $P3HT : PCBM$ solar cells. 33
2.7 AFM characterization of $P3HT : PCBM$ films before and after annealing 34
2.8 The open circuit voltage dependence on different relative $PCBM$ concentration before and after thermal annealing. 35
2.9 Effective dielectric constant effect on open circuit voltage for thermal annealed $P3HT : F8BT$ solar cells. 35

3.1 Normalized the capacitance-voltage characterization of $P3HT : PCBM$ solar cells at different light illumination intensities for as-cast device and thermally annealed device. 40
3.2 The voltage-current characterization and capacitance-voltage characterization of $P3HT : PCBM$ solar cells at 100 mW/cm^2 for as-cast device and thermally annealed device. 42

3.3 V_{oc} of $P3HT : PCBM$ solar cells at different light illumination intensities for as-cast device and thermally annealed device. 43
3.4 Short circuit current with light illumination intensity for as-cast and thermally annealed $P3HT : PCBM$ solar cells. 44
3.5 V_{peak} of $P3HT : PCBM$ solar cells at different light illumination intensities for as-cast device and thermally annealed device. 45
3.6 CV measurement at different light intensities with pristine $P3HT$, 5 wt% doping with $PCBM$, and 1:1 blend with $PCBM$ 47
3.7 Normalized CV measurement at different light intensities with pristine $P3HT$, 5 wt% and 10 wt% doping with $PCBM$ 48
3.8 $V_{oc} - V_{peak}$ versus logarithmic light illumination intensity for as-cast (Black dot) and thermally annealed (Red dot) $P3HT : PCBM$ solar cells. The solid lines are the simulation based on Equation 3.5 and Equation 3.6. 49

4.1 Photocurrent-generation channels in pristine semiconducting $P3HT$ and magnetic field effects of photocurrent MFE_{PC} in bulk-heterojunction P3HT:PCBM solar cell. 57
4.2 Electroluminescence studies for $P3HT : PCBM$ based devices at different weight ratios 59
4.3 Magnetic field effects of photocurrent (MFE_{PC}), short-circuit current-voltage ($I_{sc}-V$), and PL quenching for $P3HT/TiO_x$ and $P3HT/ZnO$ double-layer solar cells. 61
4.4 Schematic for inter-molecular CT states formed at donor-acceptor interfaces under the competition between Columbic attraction (F_A) and electrical drifting (F_D) force. The W_a and W_c are the workfunctions for anode and cathode. 62

4.5 High-field MFE_{PC} and photocurrent current-voltage ($I_{sc} - V$) characteristics for the $ITO/PEDOT/P3HT : PCBM(1 : 0.8)/Al$ device with continuous thermal annealing staring from low to high temperatures. 64
4.6 Applied electric field effects on high-field MFE_{PC} for the $ITO/PEDOT/P3HT : PCBM(1 : 0.8)/Al$ solar cells before and after annealing. 68
4.7 Light-assisted dielectric response is shown for the $P3HT : PCBM$ bulk-heterojunction solar cell before and after annealing, respectively. The capacitance is plotted as a function of light illumination intensity when the P3HT:PCBM solar cell is operated in capacitor mode. . . . 69

5.1 Schematic diagram for intra-molecular exciton in pristine polymer and inter-molecule charge-transfer complex states at donor and acceptor interface in bulk-heterojunction, respectively and Low-field and high-field MFE_{PC} in pristine polymer $P3HT$ and $P3HT : PCBM$ bulk-heterojunction solar cells. 75
5.2 Schematic dissociation processes accountable for low-field and high-field MFE_{PC} in pristine polymer $P3HT$ and $P3HT : PCBM$ bulk-heterojunction solar cells. 78
5.3 Photoexcitation-energy dependence of high-field MFE_{PC} in double-layer $ITO/PEDOT/P3HT/TiOx/Al$ device and hot electrons involved in the charge dissociation and formation of inter-molecular charge-transfer (CT) complex at the $P3HT/TiO_x$ interface 80
5.4 External electric field-dependence on high-field MFE_{PC} in double-layer $ITO/PEDOT/P3HT/TiO_x/Al$ device and MFE_{PC} versus external reverse electric field before and after thermal annealing 81

6.1 Chemical synthesis route for photovoltaic polymer $PTB2$ and $PTB4$ 90
6.2 Low-field MFE_{PC} ($< 150\ mT$): photocurrent (I_{sc}) change versus magnetic field 92
6.3 Schematic diagrams for low-field and high-field MFE_{PC} 93

6.4 High-field MFE_{PC} with applied reverse bias of - 2 V for the $P3HT$, $PTB2$, and $PTB4$ based bulk-heterojunction solar cells 97
6.5 Light-assisted dielectric response (LADR) setup and results 99
6.6 Photocurrent-voltage characteristics for $P3HT : PCBM$, $PTB2 : PCBM$ and $PTB4 : PCBM$ solar cells under the simulated sunlight illumination of 100 mW/cm^2. 101

Chapter 1

Introduction

This chapter presents the fundamental background information for the basic device physics of organic solar cells and some basic photophysics in organic materials. The motivation is trying to provide comprehensive information before the following chapters, so there would be no significantly blocks for the readers who are not working in this area.

1.1 History of solar energy conversion: photovoltaics

1.1.1 Inorganic photovoltaics

The solar cells have been extensively studied to increase the photon to electricity conversion efficiency since the first discovery of photovoltaic effect.[1] The crystalline silicon solar cell with over 6% efficiency was first developed in Bell Laboratories.[2] In 1998, the efficiency reached up to 24%,[3] which is close to the theoretical limit of 30%.[4][5] Nowadays, the Solar photovoltaics is growing rapidly, with a total global

capacity of 67,400 megawatts (MW) at the end of 2011. However, it only provides 0.5% of the worldwide electricity demand.[6] Thus, further increasing the capacity and the efficiency (for solar cell panels) of the solar photovoltaics and reducing the cost are a very critical issues in solving the energy problems in the world.

1.1.2 Organic photovoltaics

Organic photovoltaics are widely accepted as the fifth generation device of the solar energy conversion. The efficiency of the OPV has grown dramatically from 4.4 %[7]in 2004 up to 8.6 % in 2011.[8] Considering the average power efficiency of the inorganic solar cell counterparts in the market, the breakthrough of the power conversion efficiency to over 10% will make it very close to realistic application. The organic material-based solar cells have a lot of advantages that the inorganic counterparts do not have, such as flexibility, ultra-thin active layer in the hundreds nanometer scale, printing technology, wider color selection possibilities, and so on.

1.2 Organic Photovoltaic materials

1.2.1 Π-conjugated organic semiconductors

The traditional polymer were widely considered as insulator materials before 1970s; however, Alan J. Heeger, Alan G. MacDiarmid and Hideki Shirakawa have found the conductive polymers can be obtained by chemical doping, which made it possible for the polymer can be used in the application of optic and electric devices. The three scientists won the Nobel Prize for Chemistry in 2000 “for their discovery and development of conductive polymers”. Essentially, the semiconductor properties of the Π-conjugated organic materials come from the alternative single and double bond

configuration, as shown in Figure 1.1a.

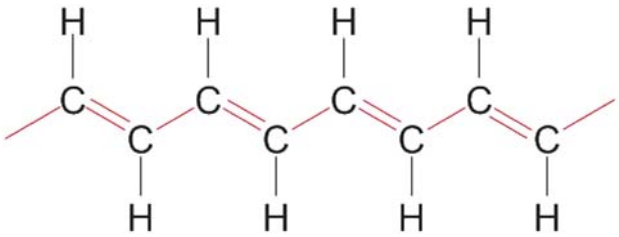

(a) Chemical structure of Polyacetylene

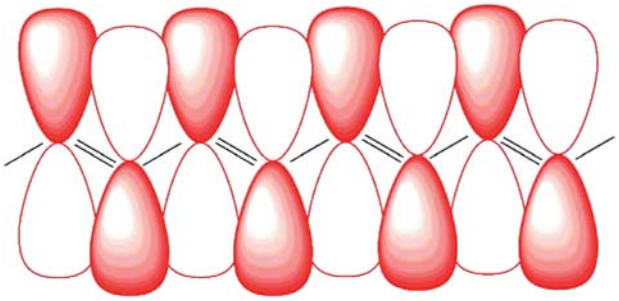

(b) The schematic diagram of p_z orbitals

Figure 1.1: (a): Chemical structure of Polyacetylene showing alternative single and double bonds; (b): The schematic diagram of p_z orbitals showing the overlap of π electron wavefunction.

Take Polyacetylene as example, the CH unite forming a quasi-one-dimensional lattice, which is because the intrachain π interaction (σ-bond or π-bond) is significantly stronger than the interchain interaction (van der Waals force or hydrogen bonding). Moreover, three of the four carbon valence electrons are sp^2 orbitals, specifically, two of the σ bonds connect with neighboring carbon atoms and the other connects with hydrogen. The fourth valence electron has a $2p_z$ orbital with the electron cloud lobes perpendicular to the plane decided by the other three.[9][10] The overlap of the p_z wavefunctions leads to the formation of π-bond, and the electrons in P_z orbitals, namely π-electrons, can then delocalize over the entire molecule. Thus the conjugated polymer can be possible to have the electric conductivity. Because the wavefunction overlap, as shown in Figure 1.1b, of π orbitals forms both bonding (π) orbitals with lower energy and antibonding (π^*) orbitals with higher energy,

the electronic structures consist of Highest Occupied Molecular Orbital ($HOMO$) and Lowest Unoccupied Molecular Orbital ($LUMO$). The concepts of $HOMO$ and $LUMO$ are similar to the concepts of the valance band and conduction band of the inorganic semiconductors. However, the band structure of organic conjugated polymer is direct band structure, and it has a much larger absorption coefficient than inorganic materials, which makes it the novel alternative material for the next generation of solar energy harvesting devices.

1.2.2 Materials for bulk heterojunction photovoltaics

The polymers used in this dissertation are $P3HT$, $PTB1$, $F8BT$, $MEH-PPV$ et al. The small molecules are $PCBM$, C_{60}, et al. The chemical structures are shown in Figure 1.2

1.3 Bulk heterojunction photovoltaics

1.3.1 Device architecture

The architecture of the OPV is typically as follows: $ITO/PEDOT:PSS/Avtivelayer/Al$. The high work function material $ITO/PEDOT:PSS$ is the anode, and the low work function metal Al is the cathode. The schematic figure is shown in Figure 1.3

1.3.2 Working principle

The working principle of OPV can be explained step by step through Figure 1.4. First, when the incident photon is absorbed by donor, an electron-hole pair is generated, leaving a hole in $HOMO$ and an electron in $LUMO$. Then, the exciton (intramolecular electron-hole pair) can move to the donor and acceptor interface if

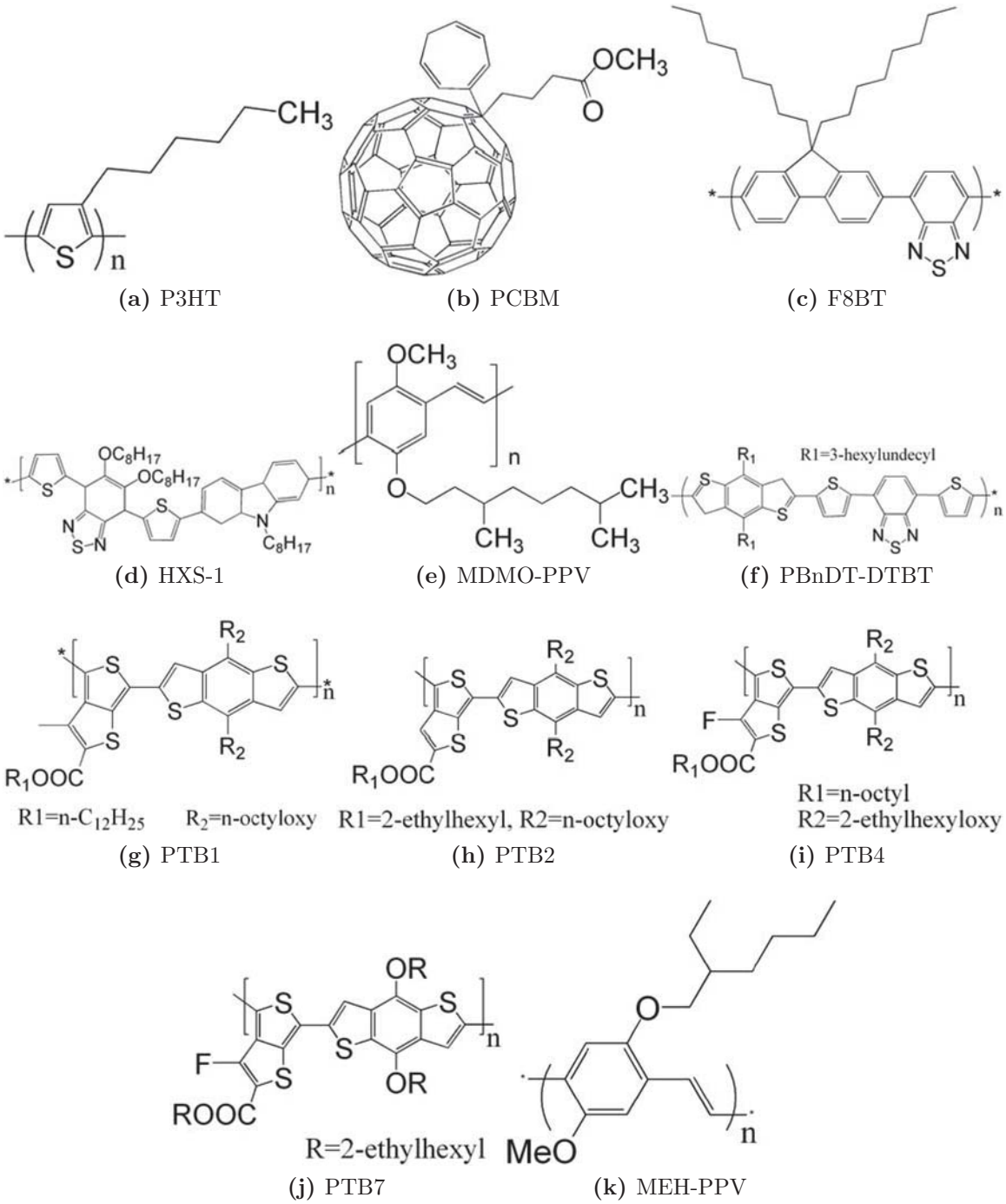

(a) P3HT **(b)** PCBM **(c)** F8BT

(d) HXS-1 **(e)** MDMO-PPV **(f)** PBnDT-DTBT

(g) PTB1 **(h)** PTB2 **(i)** PTB4

(j) PTB7 **(k)** MEH-PPV

Figure 1.2: Materials utilized in bulk heterojunctions (a): P3HT; (b): PCBM; (c): F8BT; (d): HXS-1; (e): MDMO-PPV; (f): PBnDT-DTBT; (g): PTB1; (h): PTB2; (i): PTB4; (j): PTB7; (k): MEH-PPV.

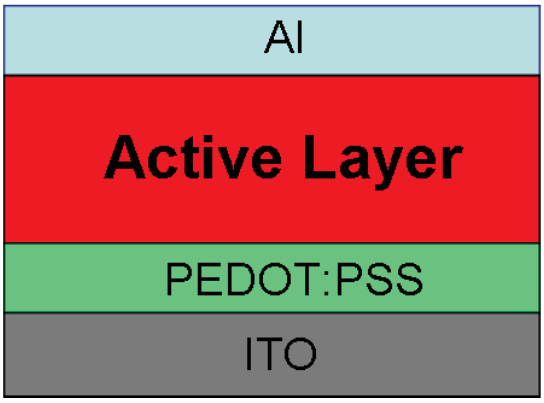

Figure 1.3: Schematic figure of typical OPV.

the exciton diffusion length is larger than the domain size of donor. Second, the photoinduced electron transfer happens in femtosecond scale at the interface. Then the electron and hole will transfer through the relative networks under the internal electric field towards the respective electrode. Finally, the electrons and holes will be collected by the anode and cathode to generate photocurrent. Moreover, it should be noted that the geminate (Process 7) and bimolecular recombination (Process 8) can occur during the photoenergy conversion process.

1.3.3 Electrical characterization

For organic photovoltaics, the efficiency can be calculated by the output power of the cell divided by the standard sunlight intensity, AM1.5 100 mW/cm^2. Mathematically, the efficiency can be obtained by Equation

$$\eta = \frac{Voc \cdot Isc \cdot FF}{P_{in}} \tag{1.1}$$

Here, the Voc is open circuit voltage, I_{sc} is short circuit current, FF refers to fill factor, P_{in} is AM1.5, 100 mW/cm^2.

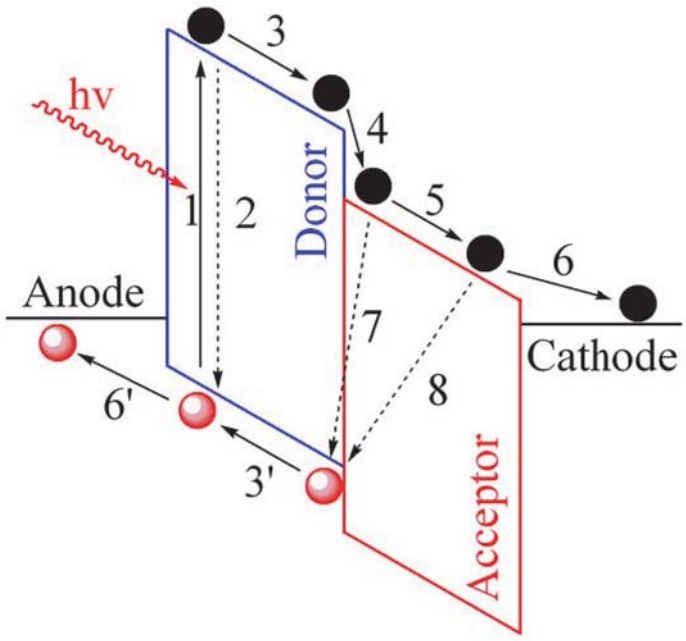

Figure 1.4: The working principle of organic bulk-heterojunction solar cells. 1. The photon absorption; 2. Intra-molecular recombination; 3. Exciton diffusion; 3′. Hole transportation 4. Photoinduced electron transfer at donor and acceptor interface; 5. Electron transportation in acceptor; 6. Electron collection; 6′. Hole collection; 7. Geminated recombination; 8. Bimolecular recombination

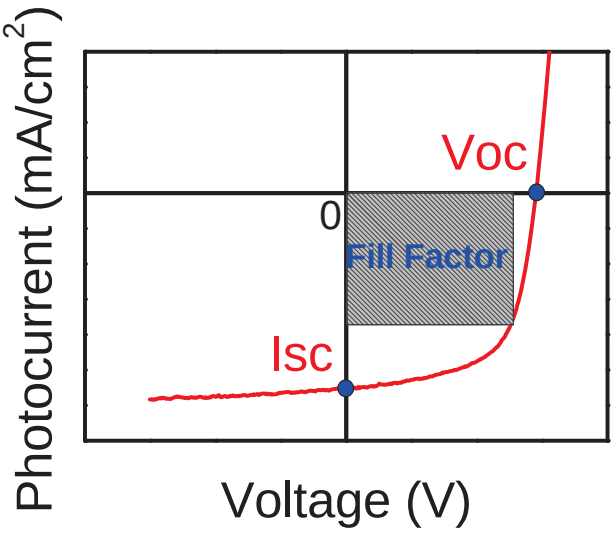

Figure 1.5: Typical Voltage-Current characterization of solar cell under light illumination

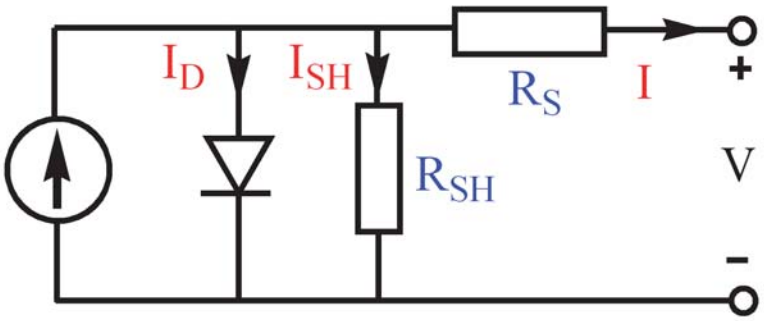

Figure 1.6: Equivalent electric circuit of the organic bulk-heterojunction solar cell

The typical current-voltage characterization of solar cell under light illumination is shown in Figure 1.5.

The equivalent electric circuit is shown in Figure 1.6. The parallel and series resistance can determine the fill factor of the solar cell.

1.3.4 Magneto-optical characterization and experimental setup

A schematic drawing of the experimental setup for the measurement of magnetic field effect on photocurrent change is shown in Figure 1.7. The sample is mounted in the middle of the electromagnet. The electric parameters are monitored by the Keithley 2400 source meter, and the magnetic field is measured by $FWBell5170$ Tesla Meter. The photocurrent change under magnetic field is defined as

$$MFE_{PC} = \frac{I_B - I_0}{I_0} \tag{1.2}$$

The maximum magnetic field can be adjusted by choosing the different gap distances between the electromagnets or by adjusting the driving current.

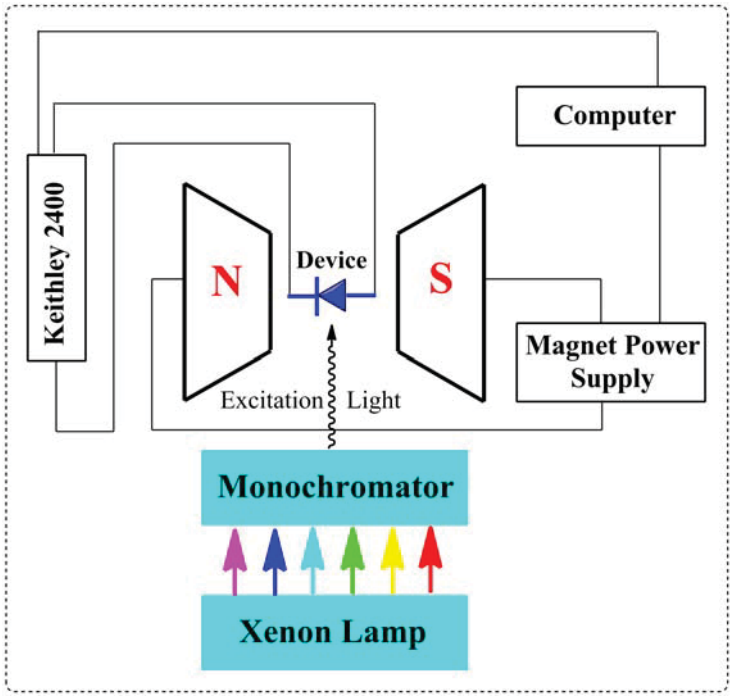

Figure 1.7: Schematic diagram for magnetic field effect on photocurrent change setup

1.4 Photophysics in organic materials and photovoltaics

1.4.1 Singlet and triplet excited states

In quantum physics, spin is the angular momentum intrinsic to the atomic length scale particles, such as individual atoms, protons, or electrons. In quantum mechanics, the spin of the particles does not have the classical feature, which is associated with the rotation of the mass; it only refers to the presence of angular momentum. For a two particle system, each of the components only has spin vector S_i quantized on values $\pm\hbar/2$. Thus, the total spin vector for the two particle system is $S = S_1 + S_2$. If the two particles are completely anti-parallel, such that $S_1 = -S_2$, then the total spin is

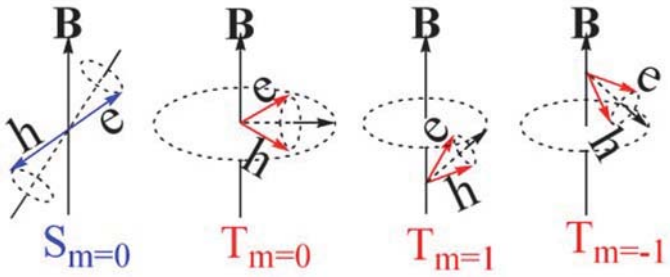

Figure 1.8: Schematic diagram of singlet and triplet states configuration.

0, and the spin multiplicity will be $m = 0$. On the other hand, if the two particles have parallel spin, then the total spin is $m = 3$ ($m = 2 \cdot S + 1$), so there are three possible combinations. Thus, the wave function of singlet and triplet state can be described as Equation 1.3 and Equation 1.4, 1.5 and 1.6. The schematic diagram of singlet state and generated triplet states can be shown in Figure 1.8.

$$\psi_s(s_1, s_2) = \frac{1}{\sqrt{2}}[\psi_\uparrow(s_1)\psi_\downarrow(s_2) - \psi_\uparrow(s_2)\psi_\downarrow(s_1)] \tag{1.3}$$

$$\psi_{t,m=1} = \psi_\uparrow(s_1)\psi_\uparrow(s_2) \tag{1.4}$$

$$\psi_{t,m=-1} = \frac{1}{\sqrt{2}}[\psi_\uparrow(s_1)\psi_\downarrow(s_2) + \psi_\uparrow(s_2)\psi_\downarrow(s_1)] \tag{1.5}$$

$$\psi_{t,m=-1} = \psi_\downarrow(s_1)\psi_\downarrow(s_2) \tag{1.6}$$

The excited state or exciton in photophysics is essentially an electron and hole pair generated by the absorption of incident photon. Because the electron hole pair is a two particle system, there are singlet excited state and triplet excited state due to the different spin configurations. In photophysics, the singlet and triple excited states are very important for the fluorescence efficiency. Due to the ultra-fast electron transition from the ground state to the excited state, excited electron-hole pair will keep the singlet spin configuration as in the ground state. The transition from singlet

excited state back to the ground state leads to the radiative emission, or non-radiative decay with phonon emission. However, the transition from triplet excited state to the ground state is spin forbidden due to the spin conservation. Thus, the triplet excited states normally have longer lifetimes and relatively longer diffusion lengths than singlet excited states. Moreover, due to spin-spin interaction, the electrons with the same spin signatures are repulsive to one another. Thus, the triplet state has a lower energy level and a larger binding energy than the corresponding singlet state. The energy difference between singlet and triplet state is called "exchange energy"; a schematic diagram is shown in Figure 1.9. Experimental results show that the exchange energy for the intramolecular excitonic states is around 0.7 eV.[11][12]

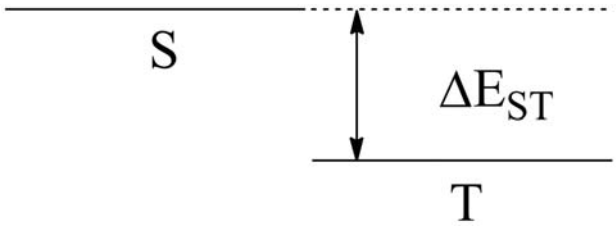

Figure 1.9: Schematic diagram for exchange energy in excitonic states

Furthermore, exchange energy dramatically depends on the separation distance between electron and hole. It should be noted that the above discussion is based on excitonic states. For the cases of polaron pair state and charge-transfer complex state, the situation will be different mainly due to the electron hole pair separation distance. The details are discussed in the next section.

1.4.2 Exciton, polaron pair, and charge-transfer complex

Essentially, exciton, polaron pair and charge-transfer complex are electron-hole pairs. The difference between them is the separation distance, which can be easily shown in Figure 1.10. It should be noted that the exciton in organic semiconductors is Frenkel type exciton which has the binding energy around $0.1 \sim 1$ eV,[13] as compared with

the inorganic counterpart with formation of Wannier-Mott exciton. The binding energy of Wannier-Mott exciton is typically on the order of 0.01 eV.[14]

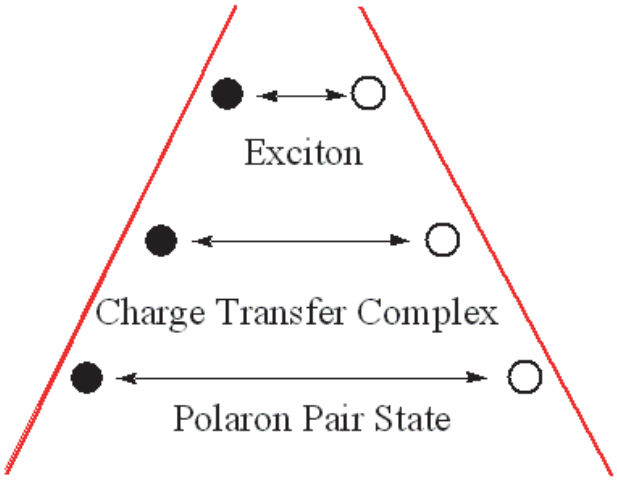

Figure 1.10: Schematic diagram for the distance of Exciton, Polaron pair, and Charge-Transfer Complex.

The distance between the electron-hole pairs is very important because it determines both the Coulomb attraction and the spin exchange energy. The Coulomb attraction energy is shown in Equation 1.7; while the exchange energy is shown in Equation 1.8.

$$U = \frac{1}{4\pi\varepsilon_0} \cdot \frac{q_1 \cdot q_2}{r} \tag{1.7}$$

$$\Delta E_{ST} = J_0 exp(-\alpha r_{e-h}) \tag{1.8}$$

The concept of exchange energy is critically important in this dissertation, because under magnetic fields of less than 1 T, as in our studies, the spin configuration only can be modified under external magnetic field in either polaron pair or charge-transfer complex states, which is due to their negligible exchange energy associated with the longer separation distance, as shown in Figure 1.11.

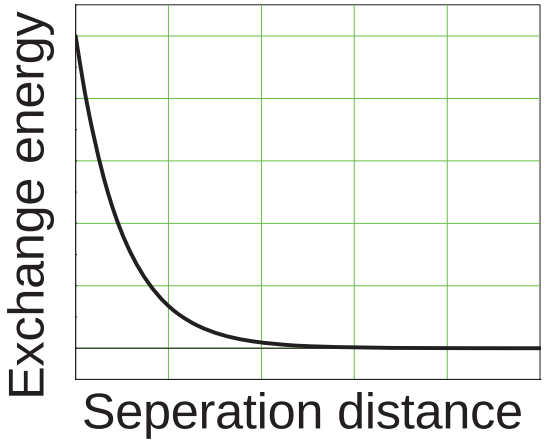

Figure 1.11: Schematic diagram for exchange energy with the separation distance

1.4.3 Zeeman effect

The energy level of an atom will be changed if the atom is placed in a static external magnetic field; this phenomenon is called the Zeeman Effect.[15] The total Hamiltonian of a single atom in a magnetic field is

$$H = H_0 + H_z \tag{1.9}$$

H_0 is the unperturbed Hamiltonian, H_z is the perturbation due to the external magnetic field B, and H_z can be determined by

$$H_z = -\vec{\mu} \cdot \vec{B} \tag{1.10}$$

$\vec{\mu}$ is the magnetic moment of the atom, which equals

$$\vec{\mu} = -\mu_B \cdot g \cdot \vec{J}/\hbar \tag{1.11}$$

$\vec{J}$ is the total electronic angular momentum including orbital angular momentum $\vec{L}$ and spin angular momentum $\vec{S}$. g is the g factor. Thus, the magnetic moment $\vec{\mu}$

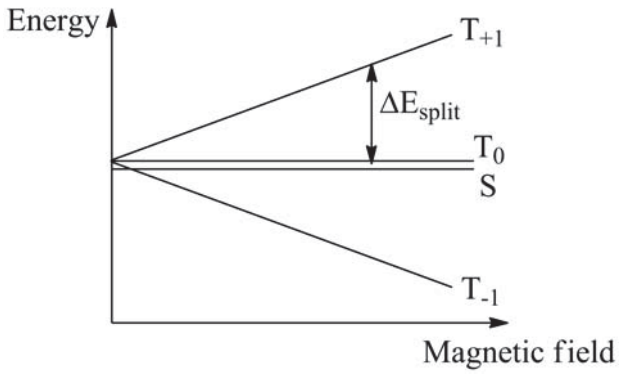

Figure 1.12: Schematic diagram of Zeeman effect

equals to

$$\vec{\mu} = -\mu_B \cdot g \cdot (g_l \cdot \vec{L} + g_s \cdot \vec{S})/\hbar \tag{1.12}$$

μ_B is the Bohr magneton, and can also be written as

$$\mu_B = \frac{e\hbar}{2m_e} \tag{1.13}$$

$g_l = 1$ and $g_s \approx 2.0023192$, which is the anomalous gyromagnetic ratio. Thus, the perturbation due to the external magnetic field can be obtained as follows:

$$H_z = \frac{e}{2m}(\vec{L} + 2\vec{S}) \cdot B_{ext} \tag{1.14}$$

It should be noted that the comparison between the *internal* field and the *external* field determines if the Zeeman splitting can happen. A schematic diagram is shown in Figure 1.12. For more information, please refers to book. [15]

1.4.4 Spin-Orbit coupling

Spin-orbit coupling is the electromagnetic interaction between the electron's spin angular momentum and the orbital momentum of this electron. This interaction can cause the shift of the electron's atomic energy levels.[16] The coupling is more pronounced in the following two situations:[17] (1) if the electron exhibits in a strong

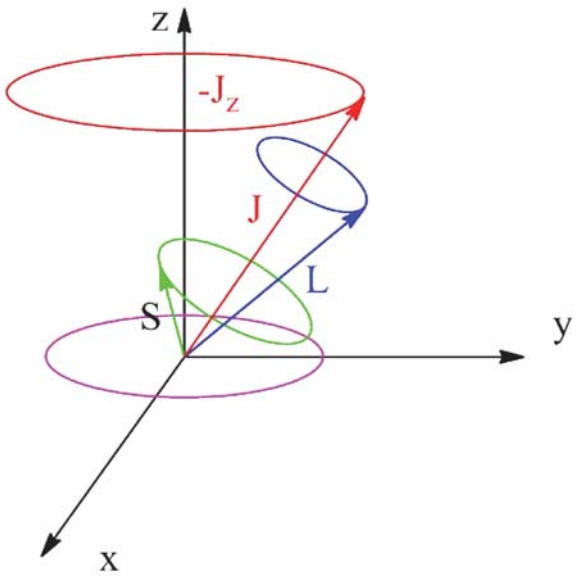

Figure 1.13: Schematic diagram of spin-orbit coupling

field, when the electron is in an orbital which is closer to the nucleus. It can be achieved when the nucleus has a high atomic number; this is called the heavy metal effect. (2) if the energies of the states being mixed are very close to each other. A schematic diagram of spin-orbit coupling is shown in Figure 1.13, and the mathematical description is given by Equation 1.15

$$H_{so} = (\frac{e^2}{8\pi\varepsilon_0})\frac{1}{m^2c^2r^3}\mathbf{S}\cdot\mathbf{L} \tag{1.15}$$

S is spin angular momentum and **L** is orbital angular momentum.

Meanwhile, the 1.15 is based on the hydrogen atom. Generally, studies have shown that the SOC constant is proportional to Z^4, where Z is the atomic number.[18][19] This is the origin of the heavy metal effect. The SOC also exponential decreases with the separation distance.[20]

1.4.5 Hyperfine interaction

The hyperfine interaction, in essence, refers to the magnetic interaction due to the nucleus spin and the electron spin; in other words, the hyperfine interaction is spin-spin interaction. Because the mass of the proton is much more heavier than the mass of the electron, so as the magnetic dipole moment, the energy shift induced by hyperfine interaction is normally orders smaller than the spin-orbit coupling.[15]

1.4.6 Intersystem crossing

The excited states only can have two spin configurations: one is the singlet configuration, in which the excited electron is anti-parallel paired with the electron in ground state; the other is the triplet configuration, in which two charges are in parallel spin. Intersystem crossing refers to the radiationless process involving the transition of the two electronic states with different spin multiplicity.[17] For instance, the excited singlet states can convert to triplet states through intersystem crossing. The probability is governed by the extent of spin-orbit coupling and the energy gap between the states involved. Normally, the transition coefficient between singlet and triplet excited states is very low because it is quantum mechanically forbidden.[16] However, when the exchange energy is small, as in the cases of polaron pair state and charge-transfer complex states, in which the electron hole separation distance is much larger than exciton, the usually forbidden of the interconversion can be partially allowed due to spin-orbit coupling or hyperfine interaction. Namely, the spin-orbit coupling and hyperfine interaction can mix the singlet and triplet wavefunctions if the exchange energy is negligible, as shown in Figure 1.14. The theoretical calculation indicates that the for the polaron pair or charge-transfer

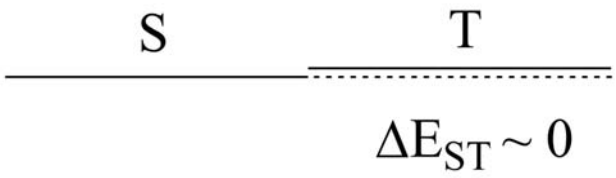

Figure 1.14: Schematic diagram for exchange energy polaron pair or charge-transfer complex states

complex states favor the singlet configuration, the singlet energy level must lie below the triplet energy level.[21]

1.4.7 Triplet charge reaction

It was found that the triplet exciton can interact with a trapped charge, and the products are a singlet exciton in ground state and a free charge. Moreover, the triplet exciton can take the energy from a free charge and then dissociate the triplet exciton. The mathematical description is shown in Equation 1.16 and 1.17

$$T + C_{trap} \rightarrow S_0 + C_{free} \tag{1.16}$$

$$T + C_{free} \rightarrow e + h + C_{free}\prime \tag{1.17}$$

1.5 Magnetic field effect

Both experimentally and theoretically, there are several parameters can be changed under magnetic field due to the spin mixing, such as resistance, photocurrent, photoluminescence and electroluminescence. The schematic diagram for the magnetic field effect is shown in Figure 1.15. When the life time of polaron pair or charge-transfer complex is shorter than the spin-lattice relaxation time, the evolution of the spin only depends on the external magnetic field. Thus, the thermal energy (which

may exceed the exchange energy by external magnetic field) cannot affect the spin motion processes.[22]

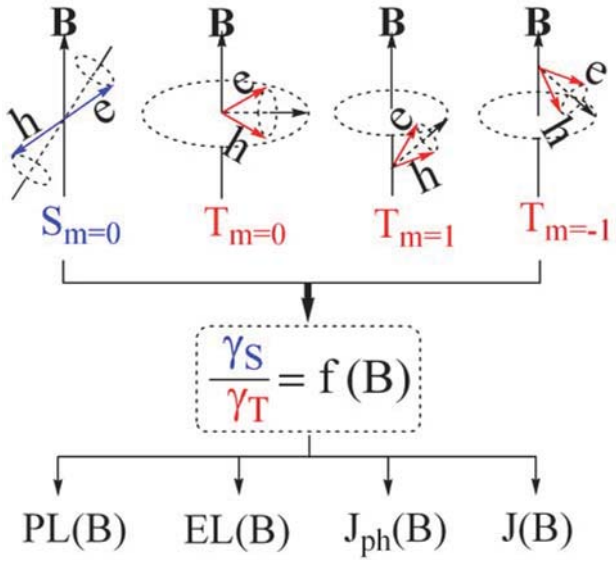

Figure 1.15: Schematic diagram for the magnetic field effect on resistance, photocurrent, photoluminescence and electroluminescence.

1.6 Peer article review of the origin of V_{oc} in organic solar cells

Since the breakthrough of the energy conversion efficiency to more than 1% in organic bulk heterojunction solar cells,[23] tremendous effort was made to further increase the solar cell efficiency and to deepen the fundamental understanding of the device physics. As one of the most important parameters, the origin of V_{oc} was investigated with different models. Here, the development of the physical understanding on the origin of V_{oc} will introduced and other possibilities that may have been missed will also be discussed. I am sorry that I cannot include every paper which has contribution on the study towards V_{oc}.

In 2001 and 2002, Brabec [24] and Ramsdale [25] et al. found that different electrodes change the V_{oc} of organic solar cells. More importantly, they claimed that the V_{oc} is more dependent on the $LUMO$ energy level of acceptors than the workfunction of electrode. Then, Deng[26] and Gadisa[27] et al. found that the V_{oc} is determined by the energy difference between $HOMO$ of donor and $LUMO$ of acceptor. In 2007 and 2008, Kim, Kinoshita and Yip et al. found that the modification of interfacial layer between active materials and the electrode can modify the V_{oc} by changing the interfacial energy diagrams.[28][29] In 2008 and 2009, Vandewal found that the V_{oc} is determined by the formation of ground state charge transfer complexes.[30][31] Although it is quite clear that the origin of V_{oc} is dominated by the energy difference between $HOMO$ of donor and $LUMO$ of acceptor, there are some other parameters that may affect the V_{oc} in organic solar cells will be explored in this dissertation.

1.7 Peer article review of magnetic field effect on photocurrent change

There has been a long history on the study of the magnetic field effect on kinetics of chemical reactions,[32] and recently, the magnetic field effect on solid state organic semiconductor devices caught great attention in the academic field. Here only the work related to the magnetic field effect on photocurrent change is reviewed.

Frankevich et al. [33][34] proposed Hyperfine interaction (HFI) mechanism to explain the low field MFE_{PC} of poly(p-phenylene vinylene) (PPV) and its derivatives. For the polaron pair states generated through photoexcitation, when the separation distance between electron and hole is long enough that the exchange energy is negligible, the singlet and triplet states are mixed by HFI. The degree of mixing is dependent on the external magnetic field. Under external magnetic field, the triplet states is degenerated and split into three energy states. When the external

magnetic field is large enough, the ISC from singlet polaron pair to triplet polaron pair will completely forbidden. With the consideration of different dissociation rates or recombination rates between singlet and triplet, the generation of photocurrent can be modified under external magnetic field. A similar explanation was also given by Kalinowski et al. [35] Tolstov and Frankevich et al. [36] also presents a triplet exciton charge reaction model to explain the negative MFE_{PC} under magnetic field. The argument is that the trapped charge can be "kick out", becoming a free charge with the interaction of triplet exciton, and the magnetic field can reduce the rate constant. As such, the TCR model can well explain the negative MFE_{PC} phenomenon.

Ito et al. [37][38] studied the MFE_{PC} of charge transfer complex based on 1,2,4,5-tetracyanobenzene (TCNB)-doped poly(N-vinylcarbazole) (PVK) film.[37] They used similar HFI to explain the positive MFE_{PC} at low field and used a level crossing mechanism to explain the dip of MFE_{PC} around 43 mT.

Gillin et al. [39][40][41] described the MFE_{PC} for Alq_3 and $P3HT : PCBM$ solar cell devices under photoexcitation around V_{oc}. Both positive and negative MFE_{PC} were found in those systems. The argument of this phenomenon is that the intersystem crossing rate will increase from the higher population density state to lower population density state under external magnetic field. For example, when the applied voltage is right below V_{oc}, the singlet state is dominated, so the ISC is from singlet to triplet, and because the triplet states has longer lifetime than singlet states, the triplet have a large possibility of dissociating and then contributing to the photocurrent, so there will be a positive MFE_{PC}. The negative MFE_{PC} also can be explained by the same mechanism.

1.8 Outline of the dissertation

In this dissertation, the magnetic, optical and dielectric effects on organic photovoltaics are studied. The dissertation includes basic concepts of polymer physics, a detailed discussion of device fabrication procedure, and device physics. In Chapter 2, the origin of open circuit voltage in organic bulk heterojunction solar cells is systematically studied. Then, the open circuit voltage is further investigated by the capacitance-voltage characterization in Chapter 3. For Chapter 4 and Chapter 5, the magnetic effect on photocurrent change in both bulk heterojunction solar cells and the polymer-inorganic double layer solar cells is studied, and it is found that the inter-molecular charge-transfer complex formation is responsible for the high-field magnetic field response. It is revealed that the control of the charge-transfer complex formation is one of the key issues to further improve the photovoltaic efficiency. In Chapter 6, the intra-molecular "donor-acceptor" interaction effect is found in the newly synthesized efficient low band gap polymers, and it is found that the intra-molecular "donor-acceptor" interaction can facilitate the electron-hole pair dissociation at the donor and acceptor interface, in another word, lower the binding energy of the inter-molecular charge-transfer complexes. Thus, the "donor-acceptor" interaction in pristine polymer forms a new way to further increase the power conversion efficiency in organic photovoltaic devices.

Chapter 2

Open circuit voltage in organic bulk-heterojunction photovoltaics

2.1 Electrode dependence of the open circuit voltage

2.1.1 Introduction

For the Metal-insulator-Metal model (MIM), the open circuit voltage depends, in first order, on the work function difference between the cathode and anode. However, for the organic bulk-heterojunction solar cells, the V_{oc} is only weakly dependent upon the work function difference, which indicates that the MIM is not fit in bulk-heterojunction solar cells. It has also been studied that the energy level pinning of the electrode is responsible for the weakly dependence upon work function difference.[42]

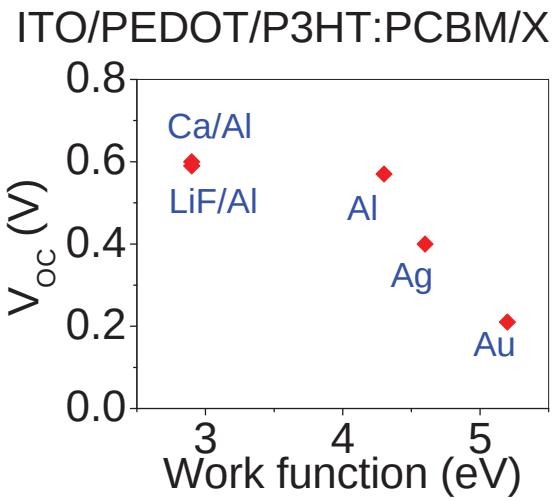

Figure 2.1: Work function of cathode dependence of the open circuit voltage in $P3HT : PCBM$ based bulk-heterojunction solar cells.

2.1.2 Experimental

For the fabrication of solar cell devices, at first, ITO glass was cleaned in ultrasonic bath in the following sequence: detergent, deionized water, acetone, isopropanol, and chloroform. Then, approximately 40 nm polyethylenedioxythiophene/polystyrenesulphonate ($PEDOT/PSS$) was spin-casted on the top of UV treatment ITO glass. After baking the substrates at 140 °C for one hour and spin-coating the active layer, the appropriate cathode was thermally deposited under the vacuum of 7×10^{-7} $Torr$. The current-voltage characteristics were measured utilizing Keithley 2400 source meter, and light source of photon response was measured using Thermal Oriel 96000 300 W solar simulator from $Newport$.

2.1.3 Results and Discussion

The Figure 2.1 shows that the workfunction change of the cathode in $ITO/PEDOT/P3HT : PCBM/X$ solar cell by 2.3 eV can only change the V_{oc} by around 0.4 V,

thus, it can be concluded that the work function difference is not the first parameter to determine the V_{oc} in organic bulk-heterojunction solar cells. (*Hint: See Figure 2.4*)

2.1.4 Conclusion

It can be seen from Figure 2.1 that the work function of the electrode is not the first order parameter to determine the open circuit voltage for organic bulk-heterojunction solar cells. Thus, more work needs to be done to clarify the origin of V_{oc} in organic bulk-heterojunction solar cells.

2.2 Thickness dependence of the open circuit voltage

2.2.1 Introduction

In this section, the thickness dependence of the active layer on V_{oc} is studies, and it is found that the V_{oc} is independent with the thickness of the active layer.

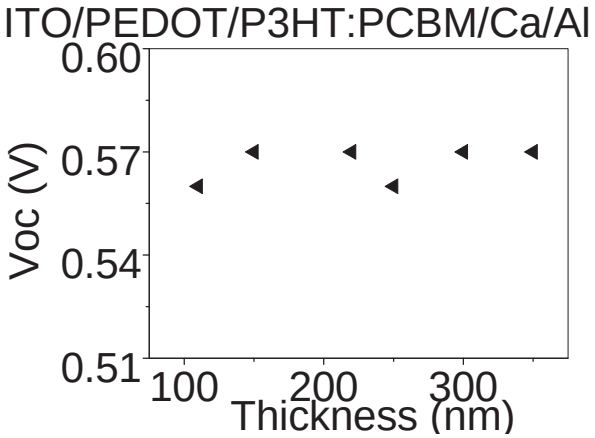

Figure 2.2: Thickness dependence of open circuit voltage in $P3HT : PCBM$ based bulk-heterojunction solar cells.

2.2.2 Experimental

The fabrication procedure of $P3HT : PCBM$ solar cell devices is the same as the procedure in 2.1.2. The thickness can be controlled by adjusting total weight of the materials or by changing the spin coating speed. All of the solar cells with different film thickness in this section are made up by $P3HT$ and $PCBM$ at $1 : 1$ weight ratio without further treatment. The solvent is dichlorobenzene.

2.2.3 Results and Discussion

It can be seen from Figure 2.2 that the open circuit voltage does not change with the thickness of the active layer thickness.

2.2.4 Conclusion

The independence of open circuit voltage on the active layer thickness indicates that the open circuit voltage in organic bulk heterojunction solar cells is not dimension related but determined by the intrinsic properties of the materials themselves in a selected electrode combination.

2.3 Energy level dependence of the open circuit voltage

2.3.1 Introduction

It has been studied that the V_{oc} of the bulk heterojunction is proportional to the energy difference between $HOMO$ of the donor and the $LUMO$ of the acceptor.[43]

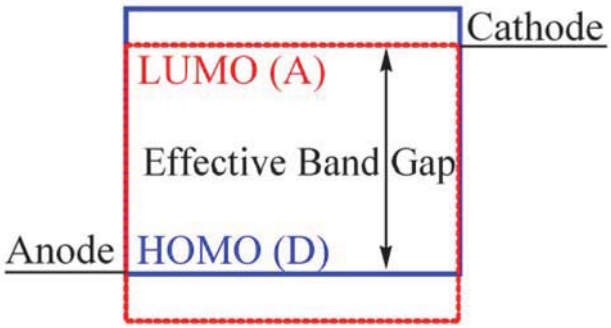

Figure 2.3: Effective band gap for organic bulk-heterojunction solar cells.

It can be also treated as the effective energy band gap of the bulk-heterojunction if compared with the counterpart of the inorganic semiconductor solar cell. Moreover, it should be noted that the V_{oc} is essentially smaller than the effective energy band gap, due to the Coulomb energy loss. The schematic description of the effective energy band gap is shows in Figure 2.3.

2.3.2 Experimental

There are eight polymers used in this section, they are $PTB1$, $PTB2$, $PTB4$, $PTB7$, $HXS-1$, $MEH-PPV$, $MDMO-PPV$ and $P3HT$. The chosen acceptor is $PCBM$. The weight ratio between donor and acceptor $PCBM$ is 1:1 for $PTB1$, $PTB2$, $PTB4$, $PTB7$, $HXS-1$; 1:4 for $MEH-PPV$, $MDMO-PPV$; and 1:2 for $P3HT$. The chemical structures of the polymers are shown in Figure 1.2. The energy levels of the materials are shown in Table 2.1. Moreover, the HOMO and LUMO for $PCBM$ is 3.7 eV and 6.2 eV, respectively.

Table 2.1: Energy levels of the selected donor materials

(eV)	PTB1	PTB2	PTB4	PTB7	HXS-1	MEH-PPV	MDMO-PPV	P3HT
LUMO	3.20	3.22	3.31	3.31	3.35	2.70	3.00	3.53
HOMO	4.90	4.94	5.12	5.15	5.21	5.11	5.30	5.30

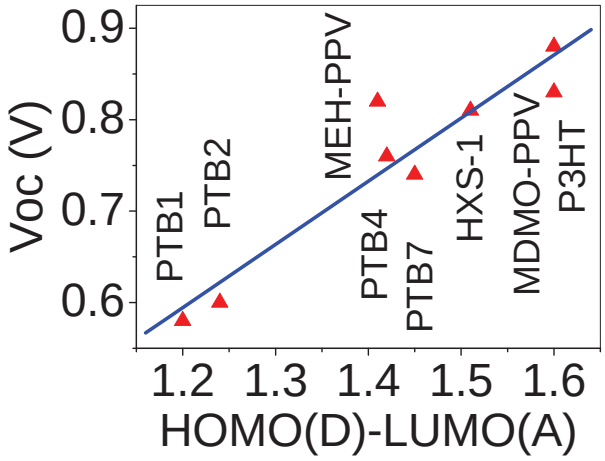

Figure 2.4: The relationship between open circuit voltage and effective energy band gap of the heterojunction solar cells.

2.3.3 Results and Discussion

Figure 2.4 shows the relationship between V_{oc} and the effective energy band gap, the difference between the $HOMO$ of donor and the $LUMO$ of acceptor. It can be seen that the V_{oc} of the solar cell is proportional to the effective energy gap. This has also been studied by other groups. It should be noted that the relative weight ratio of the donor and acceptor can also affect the V_{oc} of the solar cell. This dependence is essentially related to the effective dielectric constant of the medium or the free energy of the charge-transfer complex. The detailed study of this part is presented in Section 2.4.

2.3.4 Conclusion

In conclusion, by selecting different energy band gap of the donor materials, or by adjusting the $HOMO$ of the donor materials, the effective energy band gap can be changed. It can be seen from the experimental results that the V_{oc} is proportional to the effective energy band gap of the bulk heterojunction solar cells.

2.4 Dielectric effect on the open circuit voltage

2.4.1 Introduction

The energy conversion from photoexcited states at donor-acceptor interface to electrical potential determines the maximum open-circuit voltage (V_{oc}) in bulk heterojunction organic solar cells. However, the V_{oc} is always smaller than the theoretical prediction due to the energy loss in the photon-electron conversion process. This section reports the experimental studies on the effects of dielectric constant on V_{oc} based on $P3HT : PCBM$ solar cells. Our experimental results suggest that the dielectric constant of the bulk heterojunction can control the V_{oc} in the non-thermal annealing treatment solar cells. Therefore, our experimental studies indicate that controlling the medium dielectric constant forms a new mechanism to reduce the V_{oc} loss toward device efficiency improvement in organic solar cells.

2.4.2 Experimental

The fabrication procedure is the same as that described in 2.1.2. The solvent for the solution is chlorobenzene. Thermal annealing treatment is only performed on the organic heterojunction films without cathode. The thermal annealing temperature is 155 °C for 5 min.

2.4.3 Results and Discussion

Figure 2.5a shows the current-voltage characteristics for the $P3HT : PCBM$ bulk-heterojunction solar cells with different donor:acceptor compositions. It can be clearly seen that the V_{oc} changes from 0.60 V to 0.86 V with the increase of $PCBM$

concentration.

It is noted that the obtained V_{oc} is much smaller than the energy difference (1.5 eV) between the $HOMO$ of $P3HT$ (5.3 eV)[44] and the $LUMO$ of $PCBM$ (3.7 eV),[45] which indicates a significant V_{oc} loss in the $P3HT:PCBM$ solar cells. We know that changing donor:acceptor composition can change both charge transport channels, due to binary morphological development, and average bulk dielectric constant, due to their different dielectric constants. The charge transport channels can directly affect the dissociated electrons and holes, causing them to be transported to electrode interfaces. We further characterized the effects of average dielectric constant on V_{oc} at different donor:acceptor compositions. We can see from Figure 2.5b that the average dielectric constant of the $P3HT:PCBM$ film decreases with increasing the $PCBM$ concentration. The decrease in average dielectric constant can be attributed to the mixing of relative high and low dielectric $P3HT$ ($\varepsilon = 6.5$)[46] and $PCBM$ ($\varepsilon = 3.9$).[47] More importantly, we can see from Figure 2.5c that the V_{oc} is inversely proportional to the average dielectric constant ε_r. This means that the compositional dependence of V_{oc} is essentially related to the effective dielectric constant for the bulk medium, in other words, the real V_{oc} increases with the decrease of effective dielectric constant.

It has been reported by Veldman etc. al.[48] that the V_{oc} is proportional to the energy of the CT states E_{CT}, which can be calculated via Equation 2.1 from the Gibbs free energy of photoinduced electron transfer,

$$E_{CT} = e[E_{OX}(D) - E_{RED}(A)] - \frac{e^2}{8\pi\varepsilon_0 r}(\frac{1}{\varepsilon_{ref}} - \frac{1}{\langle\varepsilon_r\rangle}) - \frac{e^2}{8\pi\varepsilon_0\varepsilon_r}(\frac{2}{R_{CC}}) \tag{2.1}$$

It is straightforward to get the relationship between V_{oc} and E_{CT} with the consideration of complete separation of electron and hole, which is corresponding to $R_{CC} = \infty$,[48] shown in Equation 2.2

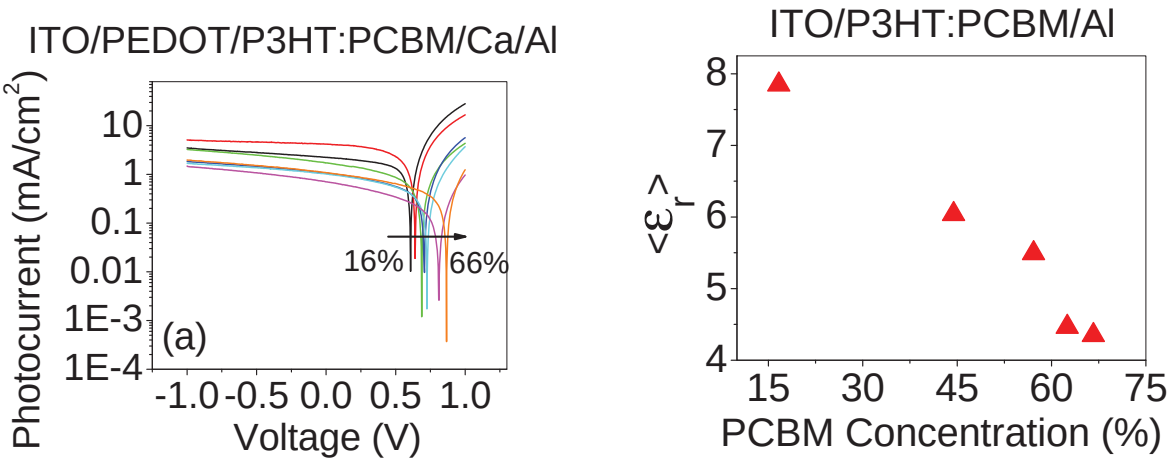

(a) Current-Voltage characteristics before thermal annealing under illumination

(b) Effective dielectric constant dependence on the concentration of $PCBM$

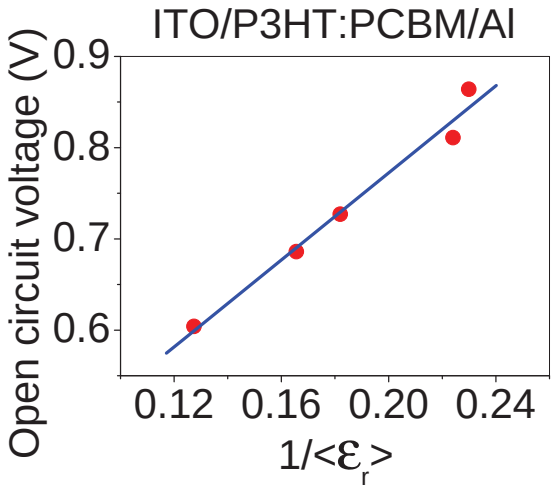

(c) Open circuit voltage versus reciprocal of the effective dielectric constant

Figure 2.5: (a) Current-Voltage characteristics before annealing under illumination (100 mW/cm^2) from Thermal Oriel 96000 300 W solar simulator for $P3HT$ and $PCBM$ blend heterojunction. The arrow shows that the weight ratio of $PCBM$ corresponding to the total weight of the blend from 16% to 66%. (b) Effective dielectric constant dependence on the concentration of $PCBM$. (c) Open circuit voltage versus reciprocal of the effective dielectric constant.

$$V_{oc} = k \cdot \{[E_{OX}(D) - E_{RED}(A)] - \frac{e^2}{8\pi\varepsilon_0}(\frac{1}{\varepsilon_{ref}} - \frac{1}{\langle\varepsilon_r\rangle})\frac{1}{r}\} \tag{2.2}$$

It should be pointed out that k in Equation 2.2 equals to 1 only when V_{oc} becomes saturated with strong light, because the V_{oc} can be turned by changing illumination intensity. Here, e and ε_0 refer to electron charge and vacuum permittivity, respectively; r stands for average ionic radius, ε_r is the effective dielectric constant of the blend materials. Besides $E_{OX}(D)$ and $E_{RED}(A)$, the average dielectric constant ε_r will affect the V_{oc}. Our study on the dielectric measurement on V_{oc} for the un-annealed devices demonstrates that the local electrical polarization will weaken the Gibbs free energy. Thus, with higher average dielectric constant in the bulk heterojunction, a relatively low free energy of the complex was tuned. This is responsible for the decrease of V_{oc} with increasing of effective dielectric constant of the active medium.

Now we discuss the decrease of V_{oc} due to the morphology change of the heterojunction film after thermal annealing. It is noticed from Figure 2.6a that after the devices were baked at 155 °C for 5 min, the V_{oc} of all the devices decrease, the V_{oc} dropped to around 0.6 V which is the typical number appearing in most publications[49][50][51] except for the first one. The effective dielectric constant was also measured (under dark condition) of the thermally annealed films, as reported in Figure 2.6b. It was found that there is almost no change on the effective dielectric constant, although it should be noticed that the interfacial dipole between $P3HT$ and $PCBM$ can be different due to the local morphology change. Considering the open circuit voltage dependence upon the $PCBM$ concentration, as shown in Figure 2.6c, it can be seen that the V_{oc} lose the linear dependence on the reciprocal of effective dielectric constant after the thermal annealing induced morphology change. This indicates that after thermal annealing, the local electrical polarization is not the primary parameter for the compositional dependence of V_{oc}. In other words, the Gibbs free energy expression of V_{oc} is not capable of explaining the V_{oc} loss after thermal annealing. It is widely

known that thermal annealing on $P3HT$ and $PCBM$ blended film would form a nanoscale interpenetrating network with crystalline order.[52] Moreover, long and thin conduction nanowires were formed in a rather homogeneous, nanocrystalline $PCBM$ film. The newly developed $PCBM$ rich domains were also generated. Thus, the thermal annealing changes the local morphology of the bulk film, destroying the relative uniform mixing of $P3HT$ and $PCBM$ and forming a more binary structure after thermal annealing. Furthermore, the AFM description of the $P3HT$ and $PCBM$ films before and after thermal annealing is presented in Figure 2.7(*Here, just one weight ratio* $P3HT : PCBM = 1 : 0.8$ *is given*). From the figures, it can be seen that after thermal annealing under 155 °C for 5min, the area RMS goes from 0.2537 nm to 0.5322 nm, which indicates that the strong material aggregation happens. It is also well reasonable to argue that the material domain size is bigger than the un-annealed film.[50][51] Figure 2.8 presents the $PCBM$ compositional dependence of V_{oc} for both non-annealed devices and the annealed ones. More importantly, the V_{oc} loss due to thermal annealing was found for all the combinations, and the detailed analysis about the V_{oc} loss at a typical weight ratio will be discussed by photo-induce impedance measurement in Chapter 3.

To further prove the argument of effective dielectric constant effect on V_{oc} for the organic bulk heterojunction solar cells, the $P3HT : F8BT$ solar cells were fabricated. Here, the $F8BT$ is acceptor material. It can be seen from Figure 2.9 that the dependence of the effective dielectric constant of V_{oc} is the same as that of $P3HT : PCBM$ solar cells.

2.4.4 Conclusion

In conclusion, our studies shows the effective dielectric constant effect on the Gibbs free energy of the $P3HT : PCBM$ solar cells with different weight combination; it reveals that the average dielectric constant of the active medium is a control

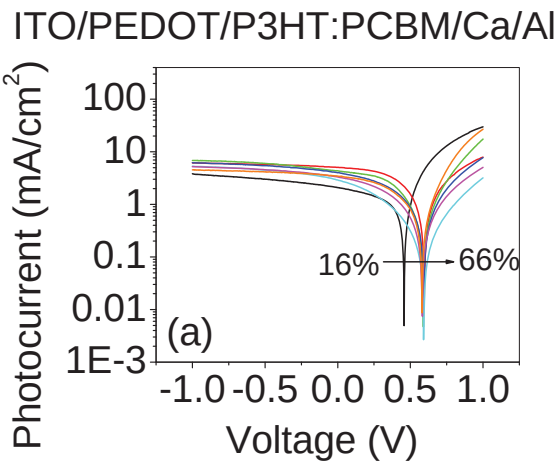

(a) Current-Voltage characteristics for thermally annealed solar cell under illumination

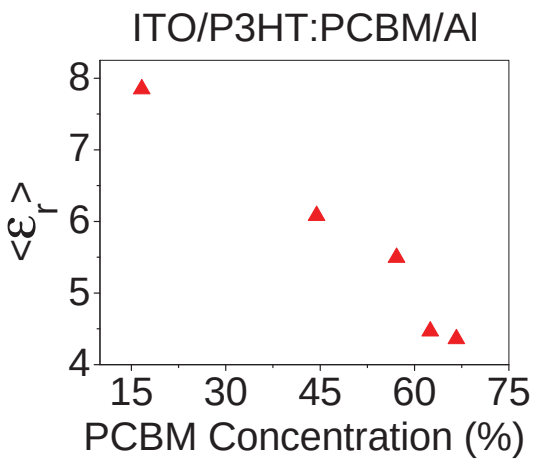

(b) Effective dielectric constant dependence on the concentration of $PCBM$

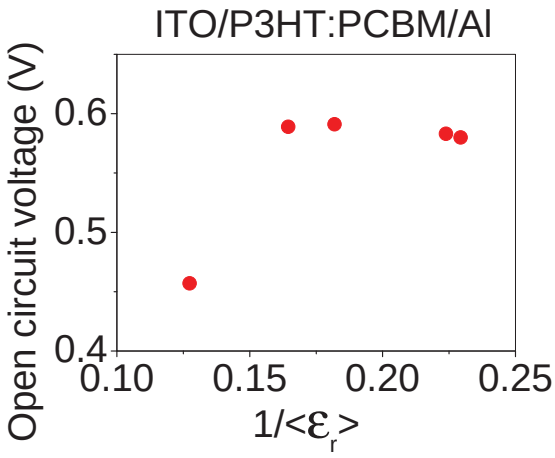

(c) Open circuit voltage versus reciprocal of the effective dielectric constant

Figure 2.6: (a) Current-Voltage characteristics after thermal annealing under illumination (100 mW/cm^2) from Thermal Oriel 96000 300 W solar simulator for $P3HT$ and $PCBM$ blend heterojunction. The arrow shows that the weight ratio of $PCBM$ corresponding to the total weight of the blend from 16% to 66%. (b) Effective dielectric constant dependence on the concentration of $PCBM$ after thermal annealing. (c) Open circuit voltage versus reciprocal of the effective dielectric constant.

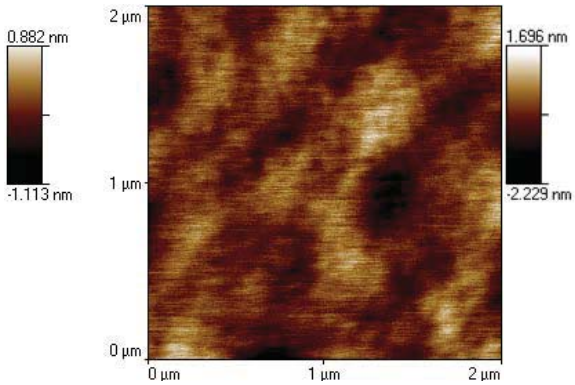

(a) Before annealing

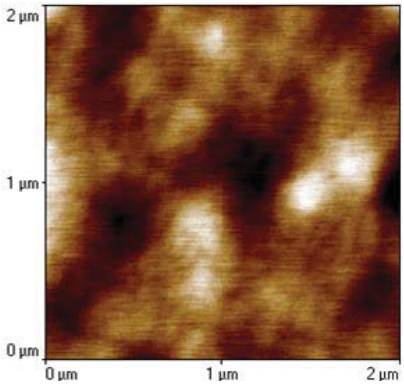

(b) After annealing

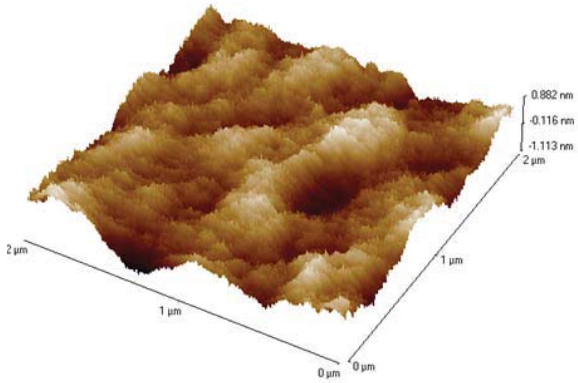

(c) Before annealing in 3D

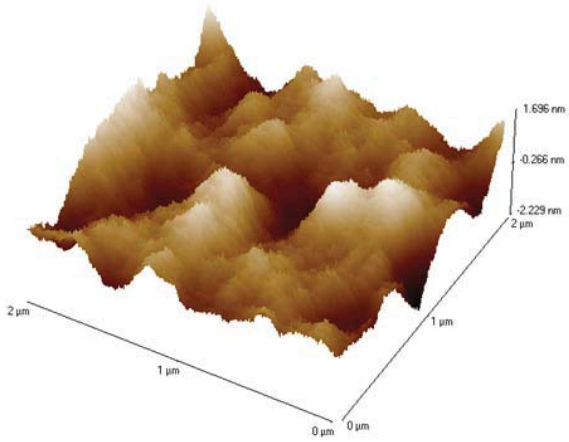

(d) After annealing in 3D

Figure 2.7: AFM characterization of $P3HT : PCBM$ films before (a), (c) and after (c), (d) thermal annealing under 155 °C in nitrogen gas atmosphere.

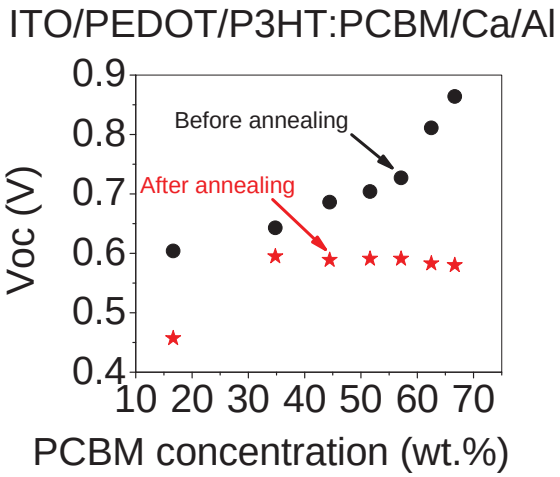

Figure 2.8: The open circuit voltage dependence on different relative $PCBM$ concentration before and after thermal annealing.

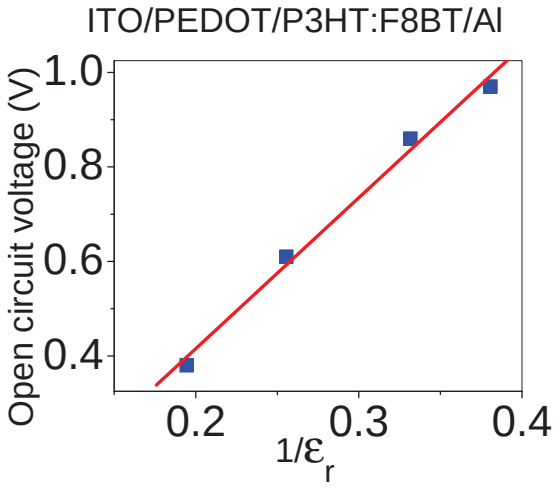

Figure 2.9: Effective dielectric constant effect on open circuit voltage for thermal annealed $P3HT : F8BT$ solar cells.

parameter of V_{oc} for the non-annealed solar cells. However, for the films with more pronounced phase separation and the molecular aggregation by thermal annealing, the average dielectric constant lost the control of V_{oc} due to the significantly changed local morphology.

2.5 Chapter summary

In this chapter, the origin of V_{oc} for the organic bulk heterojunction solar cells was systemically studied. It was found that the V_{oc} is weakly dependent on the work function of the electrode and the active layer thickness. However, the V_{oc} is strongly dependent on the effective dielectric constant of the active layer and the effective dielectric constant. Essentially, the V_{oc} is determined by the Gibbs free energy of the photoinduced electron transfer. It should be also pointed out that in the classical metal-insulator-metal (MIM) architecture, the V_{oc} is only proportional to the work function difference of the anode and cathode. More importantly, the MIM model only works for the situation in which the work function of the electrode is located between the $LUMO$ and $HOMO$ of the active layer.[42] However, for the organic bulk heterojunction solar cells, the electrode work function will be pinned to the $LUMO$ or $HOMO$ of the semiconductor. Thus, the change of the electrode with different work function can only slightly change the V_{oc} in organic bulk heterojunction solar cells.

Chapter 3

Determination of Open Circuit Voltage in Organic Bulk Heterojunction Photovoltaics from Photoassisted Impedance Analysis

3.1 Introduction

The open circuit voltage of $P3HT : PCBM$ based organic bulk heterojunction photovoltaics was studied by capacitance-voltage analysis under different light illumination intensities. It was found that the peak position of the capacitance-voltage (CV) plots for the photovoltaics is essentially related to the dark current injection barrier at the interface between organic medium and the electrode. Moreover, the charge injection barrier can be determined by the surface charge density at the interface. It was revealed that the open circuit voltage can be decided by the capability of dark current injection due to the matching of photon generated

current and the dark injection current at open circuit voltage. The open circuit voltage loss due to the local morphology change by thermally annealing can also be explained by the decrease of the dark injection barrier. This chapter further presents understanding of the determination of open circuit voltage for organic bulk heterojunction photovoltaics.

3.2 Experimental

The materials used in this cshapter are the regioregular poly(3-methylthiophene) ($P3HT$) and fullerene derivative 1-(3-methyloxycarbonyl)-propyl-1-phenyl (6,6) C61 ($PCBM$), which were purchased from Rieke Metal, Inc. and Nano-C, Inc., respectively. The average molecular weight of $P3HT$ is 50,000. The chlorobenzene purchased from Sigma Aldrich Inc. was taken as the solvent for the mixture solution, and the weight ratio of $P3HT$: $PCBM$ was 1 : 0.8. The device fabrication procedure is similar to that described in 2.1.2. Thermal annealing was carried out in a nitrogen atmosphere by heating the films at 155 °C for 5 min. The bulk-heterojunction OPV was then fabricated by the vacuum deposition of calcium (Ca) and aluminum (Al) electrode with the device architecture of ITO/PEDOT/P3HT:PCBM/Ca/Al. The CV measurements were performed by using dielectric spectrometer ($Agilent, E4980A$) with different light illumination intensities.

3.3 Results and Discussion

Figure 3.1a and 3.1b show the CV plots for the OPV at different light illumination intensities. It was found that the CV plots including both increasing component and decrease component. Moreover, it is interesting to find that the CV peak shifted from high voltage to low voltage regime with the increase of light illumination intensity. The shift was found for both the as-cast and the thermally annealed devices. From

the CV plots, four conclusions can be drawn. First, the capacitance of CV plot at certain light illumination intensity increases with the forward bias, because the capacitance essentially reflects the capability of storage of charges. Thus, the increase of the capacitance can be explained by the charge accumulation at the interface. The larger capacitance indicates that the more charge accumulated at the interface. Second, the capacitance will decrease with further increase the bias voltage after certain voltage, defined as V_{peak}. Based our understanding, we can argue that the decrease component is due to the charge injection from the electrode, which caused the charge recombination. Third, it is worthy to note that the V_{peak} is smaller than the V_{oc} at any light illumination intensities, the V_{peak} can be attributed to the dark current injection barrier in OPV. Fourth, as shown in Figure 3.1a and 3.1b, the V_{peak} will shift to low voltage regime with the increase of light illumination intensity, for both as-cast and thermally annealed devices. The decrease of V_{peak} was due to the photo-illumination induced dark injection barrier reduction, which will be discussed later.

Now we discuss the V_{peak} shift in Figure 3.1. In the metal-semiconductor contact, the dark injection barrier can be described by the following Equation[53]

$$n_i = N_t exp(-\frac{\phi_i}{k_B T}) \tag{3.1}$$

where the n_i is the surface charge density, N_t is the volume density of molecular sites, and ϕ_i is the energy barrier at the interface between active medium and the electrode. This shows that higher surface charge density leads to reduction of energy barrier ϕ_i Without an applied field, the thermionically injected current is determined by

$$J_{inj} = Cexp(-\frac{\phi}{k_B T}) \tag{3.2}$$

where ϕ is the Schottky barrier and C is constant. Obviously, with the higher light illumination intensity, there is more surface charge density at the metal-semiconductor

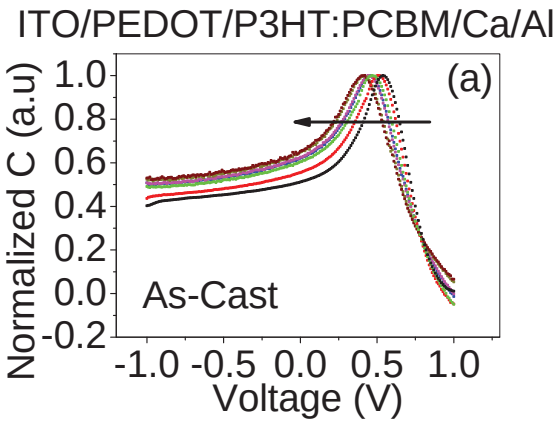

(a) As-cast device

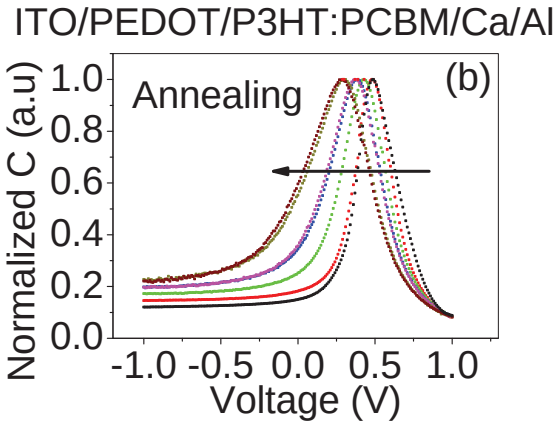

(b) Thermally annealed device

Figure 3.1: Normalized the capacitance-voltage characterization of $P3HT : PCBM$ solar cells at different light illumination intensities for: (a) as-cast device; and (b) thermally annealed device. The solid arrow bar indicates the light illumination intensity increase.

interface. The energy barrier ϕ_i will decrease with the higher light illumination intensity, which is essentially the larger dark injection current. The exponential expression of ϕ in Equation 3.2 also indicates that the V_{peak} is an energy related parameter in the energy diagram of OPV.

It has been intensively studied that the thermal annealing can greatly enhance the $P3HT : PCBM$ cell power conversion efficiency. Figure 3.2a shows the voltage-current characterization of $P3HT : PCBM$ devices for as-cast and thermally annealed condition. The I_{sc} increases from 6.2 mA/cm^2 to 10.8 mA/cm^2, and the power conversion efficiency η increases from 2.2% to 3.7%. However, it was found that the V_{oc} decreases from 0.63 V to 0.58 V, which corresponds to the findings of other groups.[54][55][56] The V_{oc} loss due to thermal annealing will decrease the overall power conversion efficiency. Moreover, the V_{oc} loss was found in different light illumination intensities as shown in Figure 3.3.

Our studies indicate that the V_{oc} loss after thermal annealing can be explained by the following arguments: (i). Better charge transport channels can be formed after thermal annealing, which leads to the higher charge density at the interface between the active medium and the electrode. (ii). The dark current injection barrier is essentially related to the surface charge density state both in dark and light conditions. (iii). The dark current injection barrier decreases after thermal annealing. Figure 3.1 shows the CV plots for both as-cast and thermally annealed OPV under 100 mW/cm^2; it was found the V_{peak} shifts to low voltage after thermal annealing. The capacitance increases under zero bias for the thermally annealed OPV shown in Figure 3.2b further supporting our argument about the morphological induced surface charge density increasing by thermal annealing.

The dark injection current with an applied field can be modified, based on Equation 3.2, as follows

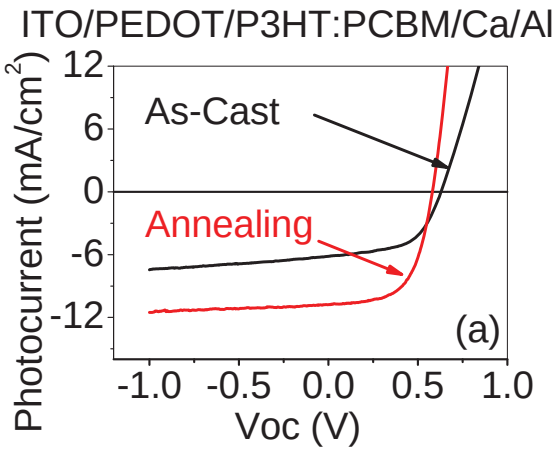

(a) The voltage-current characterization

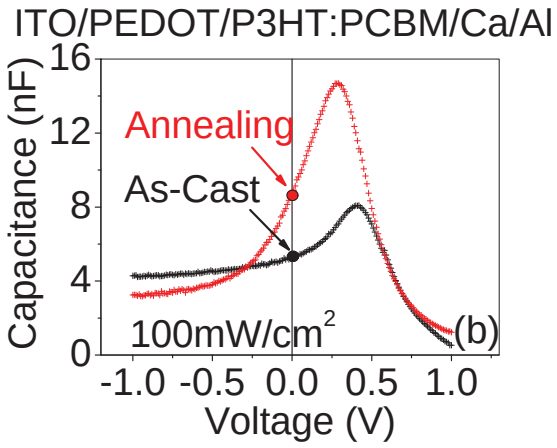

(b) The capacitance-voltage characterization

Figure 3.2: The voltage-current characterization (a) and capacitance-voltage characterization (b) of $P3HT : PCBM$ solar cells at 100 mW/cm^2 for as-cast device and thermally annealed device.

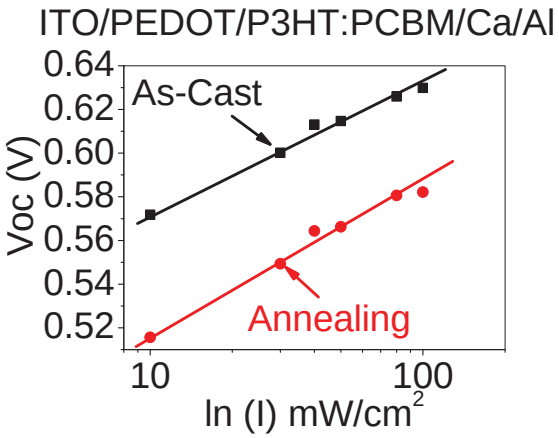

Figure 3.3: V_{oc} of $P3HT : PCBM$ solar cells at different light illumination intensities for as-cast device and thermally annealed device.

$$J_{inj} = C' exp(\frac{(V_{app} - \phi)}{k_B T}) \tag{3.3}$$

V_{app} is the applied bias. It should be noted that $V_{app} = V_{oc}$ when $J_{inj} = -J_{ph}$.[57] Thus, the reduction of energy barrier will affect the V_{oc} (Or can be seen as V_{app}), which is responsible for the matching of photocurrent under light illumination. It was also found that the V_{peak} for the thermally annealed device is smaller than the as-cast one at different light intensities. Moreover, the reduction of V_{oc} is also found with high boiling point, 1-2 dichlorobenzene as solvent, which functions in a similar way to thermal annealing, which increase the crystallinity of the bulk films.[7]

Figure 3.4 shows the short circuit current versus the light illumination intensity for both as-cast and thermally annealed devices in double logarithmic plot. The slope of the curve can be obtained by the power law $J_{sc} = I^{\alpha}$, where $\alpha = 0.94$ for the as-cast device and $\alpha = 0.92$ for the thermally annealed device. I_{sc} is short circuit current, and I is the light illumination intensity. The sublinear dependence of the short circuit current and the light intensity for both as-cast and thermally annealed device indicates that the bimolecular recombination is not sufficient reason for the

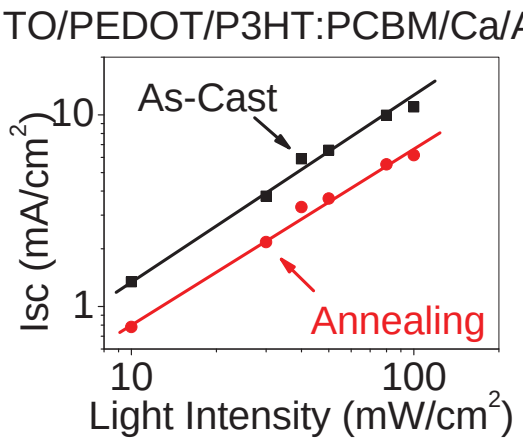

Figure 3.4: Short circuit current with light illumination intensity for as-cast and thermally annealed $P3HT : PCBM$ solar cells.

current increase by thermal annealing.[58]

Now we discuss whether electron or hole accumulation leads to the dark injection barrier reduction due to thermal annealing or the stronger light illumination intensities. It should be noted from the energy diagram of the OPV under architecture $ITO/PEDOT : PSS/P3HT : PCBM/Ca/Al$ that the work function of Ca is 2.9 eV. However, the $LUMO$ of $P3HT$ and $PCBM$ are 3.5 eV[59] and 3.7 eV,[60] respectively. Thus, there is no dark injection barrier from the cathode. As for anode, the work function of $ITO/PEDOT : PSS$ is around 5.2 eV, and the $HOMO$ of $P3HT$ and $PCBM$ are 5.3 eV [59] and 6.1 eV,[60] respectively. With the consideration of the bulk heterojunction of $P3HT : PCBM$ cell, the active layer essentially the mixture of donor and acceptor material, so with the strict consideration, three components are coexist at the contact between ITO/PEDOT:PSS and active layer, namely, $PEDOT : PSS$, $P3HT$ and $PCBM$. Thus, more holes have a larger chance of being accumulated at the interface. This argument can also be supported by Figure 3.5; it is known that thermally annealing can dramatic increase the hole's mobility by three orders,[61] while only limitedly enhance on electron's

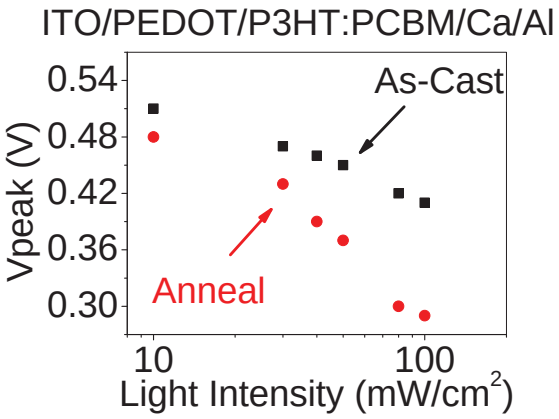

Figure 3.5: V_{peak} of $P3HT$: $PCBM$ solar cells at different light illumination intensities for as-cast device and thermally annealed device.

mobility.[30][61] Thus, for the thermally annealed device, more holes can transport and accumulate to the interface, as compared to the devices not receiving annealing treatment; this leads to the reduction of the dark injection barrier for the thermally annealed device. It can be shown in Figure 3.5 that at all light intensity ranges measured, the V_{peak} after thermally annealing is smaller than that corresponding to the as-cast devices.

The identification of what type of charge carriers accumulated at which interface can be further studied by changing the doping level of the electron acceptor $PCBM$, and essentially, it has the similar function as the thermal annealing and increase the light illumination intensities which all can increase the generation of free charge carriers in the photovoltaic devices. Figure 3.6 shows the capacitance-voltage results for pristine $P3HT$, 5 wt% doping with $PCBM$, and $P3HT$ with $PCBM$ in 1:1 weight ratio. It was clearly shown that in Figure 3.6a, the increase of light intensity does not change the CV peak position; this is because most of the photogenerated excitons are quenched by radiative emission in pristine form of $P3HT$. There are few dissociated charge carriers in this type of device. Thus, the charge density at the interface did not significantly changed, so the current injection barrier which is essentially related

to CV peaks position also did not change. From Figure 3.6b, with the 5 wt% $PCBM$ doping in $P3HT$, it can be clearly seen that the increase of illumination does not significantly change the position of CV peaks either. This is because the formation of photogenerated current is limited by the the $PCBM$ transport channel. In other words, with small $PCBM$ doping level, the increase of photo illumination cannot significantly change the charge carrier density at the interface. More importantly, because the low level doping of $PCBM$ cannot form efficient $PCBM$ networks in the heterojunction, the transportation of electron is limited. As such, the accumulation of holes at the anode and active layer will dominate. However, this hole accumulation is not pronounced enough to significantly change the CV peak position. Finally, when the $P3HT$ is heavily doped with $PCBM$ to form real organic solar cells, both the $P3HT$ and $PCBM$ charge transport channels are formed due the the high level doping. From Figure 3.6c, it can be seen for the heterojunction with both efficient $P3HT$ and $PCBM$ networks, the holes and electrons transportation are very efficient. Thus the increase of light illumination intensity can shift the CV peaks, which are related to the dark current injection in this device. It should be noted that the high work function of cathode Ca/Al cannot form an electron injection barrier in this device due to the ohmic contact formation because the energy level pinning effect. Thus, the dark current injection barrier is coming from the hole's injection at the anode.

To further identify our argument, the CV peaks for pristine $P3HT$, 5 wt% $PCBM$ doping in $P3HT$ and 10 wt% $PCBM$ doping $P3HT$ are studied. It can be clearly seen in the Figure 3.7 that the CV peaks shift significantly. As discussed above, the 5 wt% $PCBM$ doping in $P3HT$ cannot form efficient $PCBM$ networks, so the capability of electron transportation is limited. However, the holes have a very good transport channel due to the richness of $P3HT$ in the bulk heterojunction. Thus, the holes have more change to accumulate between the anode and active layer. So the

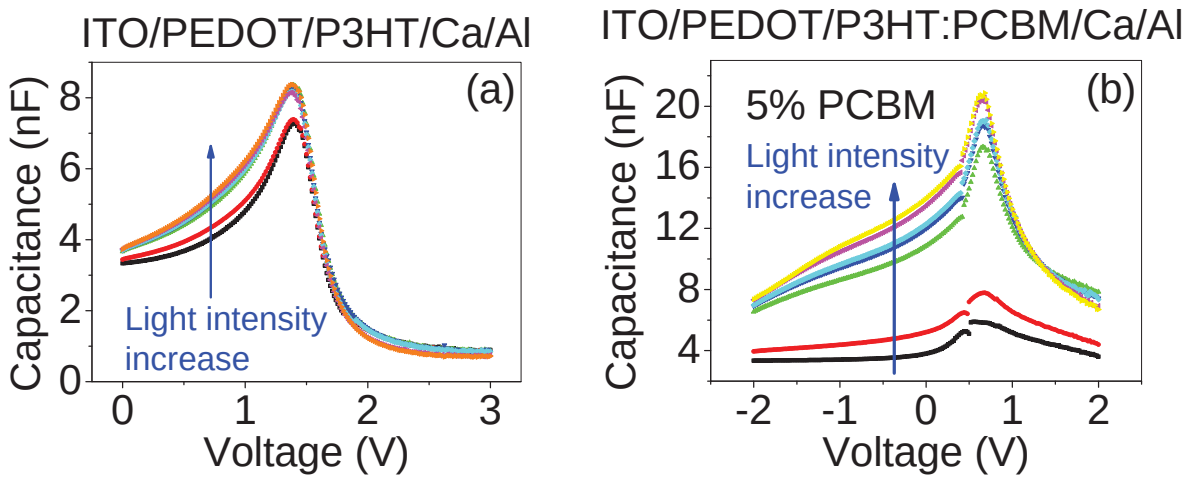

(a) Pristine $P3HT$

(b) $P3HT$ with 5 wt% doping of $PCBM$

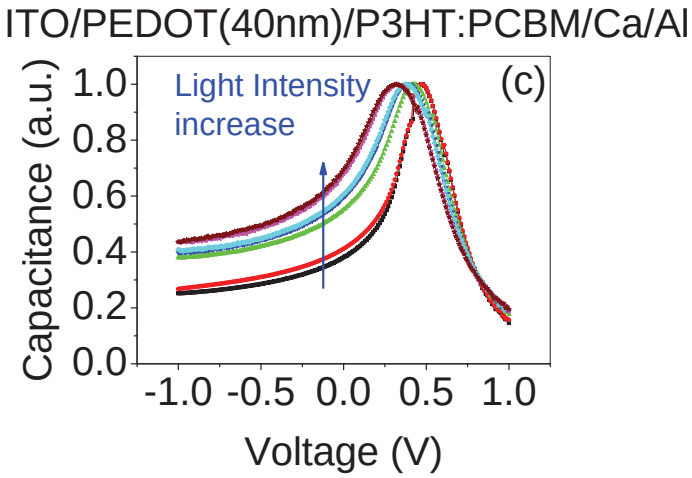

(c) $P3HT$ with $PCBM$ in 1:1 weight ratio

Figure 3.6: CV measurement at different light intensities with pristine $P3HT$, 5 wt% doping with $PCBM$, and 1:1 blend with $PCBM$; (a): pristine $P3HT$; (b): $P3HT$ with 5 wt% doping of $PCBM$; and (c): $P3HT$ and $PCBM$ with 1:1 weight ratio.

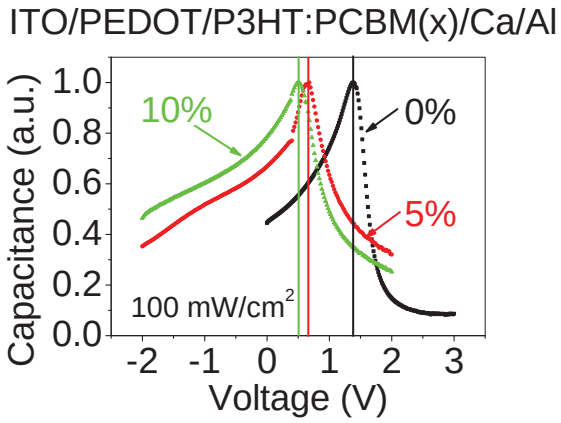

Figure 3.7: CV measurement at different light intensities with pristine $P3HT$, 5 wt% and 10 wt% doping with $PCBM$.

shift of CV peaks here is due to the holes accumulation.

Moreover, it was confirmed by both experimental and theoretical studies that the energy level pinning occurs between the cathode and the LUMO of $PCBM$. That is why changing the cathode to metals with different work functions cannot significantly change the V_{oc} of the organic solar cells.[42][62]

Figure 3.8 shows the $V_{oc} - V_{peak}$ versus the light illumination intensity at the range from 10 mW/cm^2 to 100 mW/cm^2. It is found that the difference between V_{oc} and V_{peak} is linearly depended on the logarithmic light intensity. This indicates that V_{peak} is an energy potential related parameter. Based on our studies, the following equations were obtained by combine both the CV and voltage-current behavior under light illumination.

$$V_{oc} - V_{peak} = \frac{nKT}{e} \cdot \ln \frac{J_{sc}}{J_{00}} \tag{3.4}$$

Where, V_{peak} refers to the charge carriers injection barrier, V_{oc} is the open circuit voltage, n is the morphology related factor, K is the Boltzmann constant, T is the absolute temperature, and J_{00} is the characteristic current. Thus, for the as-cast and

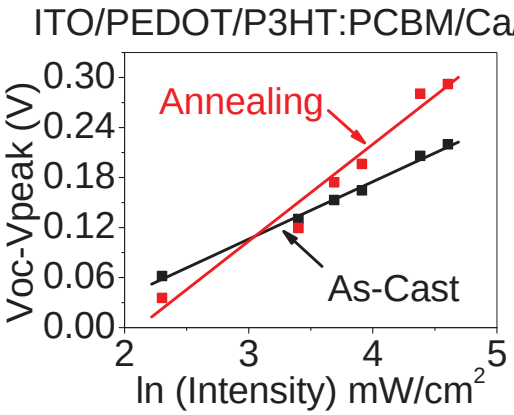

Figure 3.8: $V_{oc} - V_{peak}$ versus logarithmic light illumination intensity for as-cast (Black dot) and thermally annealed (Red dot) $P3HT : PCBM$ solar cells. The solid lines are the simulation based on Equation 3.5 and Equation 3.6.

thermally annealed devices, V_{oc} , J_{sc} , and V_{peak} can be described through 3.5 and 3.6, respectively.

$$V_{oc} - V_{peak} = \frac{2.9068KT}{e} \cdot \ln \frac{J_{sc}}{0.3779} \tag{3.5}$$

$$V_{oc} - V_{peak} = \frac{4.7983KT}{e} \cdot \ln \frac{J_{sc}}{1.17} \tag{3.6}$$

Moreover, by using the J_{sc} at different light illumination intensities into Equation 3.5 and 3.6, it can be shown in Figure 3.8 that the simulated value of $V_{oc} - V_{peak}$ versus light intensity agrees with the experimental data. Essentially, this equation describes the dark injection current density at $V_{app} = V_{oc}$, stating that it is equal to the photogenerated current J_{sc}. Thus, this also supports the argument that the V_{peak} can be seen as the dark current injection barrier at the metal-semiconductor interface.

3.4 Conclusion

In conclusion, our capacitance-voltage study on $P3HT:PCBM$ photovoltaics shows that the CV peak is essentially determined by the dark current injection barrier, and the surface charge density induced by either higher light illumination intensity or the formation of better charge transport channels due to thermal annealing can reduce the interfacial potential energy barrier. Essentially, the total current density of $P3HT:PCBM$ photovoltaics is zero at bias voltage V_{oc}. Thus, the value of V_{oc} can be determined by the dark injection capability, which matches the photo-generated current. In this chapter, an empirical equation was presented to describe both the capacitance-voltage and voltage-current characterization. The V_{oc} loss due to thermal annealing was also explained by the shift of CV peak under light illumination. Our study on the CV analysis reveals an alternative description on the determination of V_{oc} in $P3HT:PCBM$ bulk heterojunction photovoltaic devices.

Chapter 4

Magnetic field effect on charge-transfer complex in P3HT:PCBM bulk-heterojunction photovoltaics

The electron-hole pairs can be formed in inter-molecular charge-transfer (CT) states between two adjacent molecules due to Coulomb interaction in organic semiconducting materials. In general, the exciton dissociation can experience the intermediate states: inter-molecular CT states at donor-acceptor interfaces to generate photocurrent in organic solar cells. This chapter focuses on the magneto-optical studies on inter-molecular CT states in the generation of photocurrent by using magnetic field effects of photocurrent (MFE_{PC}) and light-assisted dielectric response ($LADR$). The MFE_{PC} and $LADR$ studies reveal that internal electrical drifting and local Coulomb interaction can largely change the formation and dissociation of CT states by changing internal charge-transport channels and local Coulomb interaction through morphological development upon thermal annealing. Therefore, the MFE_{PC}

and $LADR$ can be used as effective magneto-optical tools to investigate charge recombination, separation, and transport in organic solar cells.

4.1 Introduction

Organic semiconducting polymers have become promising photovoltaic materials with large optical absorption coefficients, efficient formation of photoexcited states, and morphologically controllable charge-transport channels.[7][23][63][64][65][66][67][68][69] It has been experimentally found that the light absorption leads to the formation of Coulombically bound intra-molecular electron-hole pairs, namely Frenkel excitons with large binding energies in organic semiconducting polymers.[13][43][70][71][72] Therefore, sufficient donor-acceptor interaction is necessarily required to dissociate the photoexcited excitons for the generation of photocurrent in organic solar cells. In general, the dissociated electrons and holes can form electron-hole pairs at CT states at donor-acceptor interfaces due to inter-charge Coulomb attraction.[73][74][75][76][77] As a result, dissociating electron-hole pairs at CT states is an important issue in improving photocurrent in organic solar cells.[78][79][80][81][82] In this chapter, we use magnetic field effects of photocurrent: MFE_{PC} and light-assisted dielectric response: $LADR$ as new experimental tools to detect the electron-hole pairs at inter-molecular CT states at the donor-acceptor interfaces. In particular, we investigate the effects of internal electrical drifting and local Coulomb interaction on the formation and dissociation of inter-molecular CT states by adjusting morphological structures upon thermal annealing in the generation of photocurrent. It is noted that the MFE_{PC} can be divided into low ($<$ 150 mT) and high ($>$ 150 mT) field regimes corresponding to the dissociation processes in pristine polymers[38][41][83] and donor-acceptor bulk-heterojunctions, respectively.[37][84][85][86] In general, the low-field MFE_{PC} from pristine polymers can show positive and negative components.[33][34][36][85][87] We have observed in our previous study that $MEH-PPV$, which has a nearly 100% singlets under

photoexcitation, only shows a positive MFE_{PC} in low-field regime. However, the $P3HT$, which has both significant singlet and triplet states under photoexcitation, gives both positive and negative components in the low-field MFE_{PC}. Therefore, we suggest that the positive and negative components in low-field MFE_{PC} are due to singlets and triplets, respectively. It can be further suggested that the positive and negative components arise from the dissociation in polaron-pair states[33][34] and the charge reaction in excitonic states,[32][36][88][89] respectively. The positive MFE_{PC} generated by the dissociation of polaron pairs comes from the following two arguments. First, a low magnetic field can increase the singlet ratio in polaron-pair states through intersystem crossing by disturbing the spin momentum conservation involved in the intersystem crossing. Second, the singlets have stronger ionic natures in wavefunctions relative to the triplets due to different spin configurations and can therefore exhibit larger dissociation rates through Onsager process in pristine conjugated polymers.[32][90][91] As a result, the dissociation in polaron-pair states can generate a positive component in low-field MFE_{PC} (Figure 4.1a). Indeed, the photoexcited excitons can Coulombically interact with charge carriers, generating exciton-charge reaction. It can be suggested from the photophysics studies of radical pairs that the relevant outcome of exciton-charge reaction is the separation of excitons to generate free charge carriers[36][92][93][94][95][96] (Figure 4.1a). Furthermore, magnetic field effects of electroluminescence have also suggested that the excitons can react with charge carriers, with the consequence of generating free charges in organic light-emitting diodes.[97][98] It is noted that an external magnetic field can reduce the exciton-charge reaction rate constant,[36][99] leading to a negative magnetic field effect in the generation of free charge carriers. Nevertheless, the negative low-field MFE_{PC} can indicate the existence of exciton-charge reaction. It should be noted that the singlet and triplet excitons can dominate the dissociation of polaron pairs and the exciton-charge reaction, respectively, due to their different ionic natures and lifetimes. On the other hand, the high-field MFE_{PC} can be used as a new experimental tool to detect the electron-hole pairs formed in inter-molecular

CT states at donor-acceptor interfaces, based on the following three fundamental arguments. First, photophysics studies have suggested that the inter-molecular CT states are formed with both singlet and triplet states through geminate and non-geminate capture of dissociated electrons and holes at donor-acceptor interfaces when electron spin multiplicities are considered.[100] Second, an external magnetic field can change the singlet and triplet ratios in the inter-molecular CT states by perturbing the intersystem crossing[32][33][101] through spin momentum conservation. Third, the singlet and triplet inter-molecular CT states can have high and low dissociation rates in bulk-heterojunctions,[35][91] respectively, similar to polaron pairs in pristine polymers, due to their different ionic natures involved in dissociation driven by Onsager process.[90] Therefore, applying an adequate magnetic field can change the photocurrent by altering the singlet and triplet ratios in CT states, generating high-field MFE_{PC} in bulk-heterojunction organic solar cells.[85][86][102] Furthermore, we found that light-assisted dielectric response, $LADR$, can provide experimental information on charge generation, transport, and collection in donor and acceptor interpenetrating networks when an organic solar cell is operated in capacitor mode under photoexcitation. Specifically, the measurement of device capacitance under light illumination can essentially reflect the following three pieces of information. First, the local electrical polarizabilities from Coulomb interaction can be given under dark condition when light illumination is off. Second, at a given light illumination, the capacitance change caused by light illumination can be related to the generation of charge carriers. Third, the measurement of device capacitance with light illumination can describe the transport of generated charge carriers. Therefore, the use of MFE_{PC} and $LADR$ can reveal the internal photovoltaic processes in bulk-heterojunction organic solar cells.

4.2 Experimental

The regioregular Poly(3-hexylthiophene) ($P3HT$) and fullerene derivative 1-(3-methyloxycarbonyl)-propyl-1-phenyl (6,6) C61 ($PCBM$) were purchased from Aldrich and American Dye Sources, Inc., respectively. The number-average molecular weight of $P3HT$ is 87,000. The $P3HT$: $PCBM$ composite films were spin-coated from chrolobenzene solutions on indium-tin-oxide (ITO) glass substrates pre-coated with 40 nm thin layer of poly(3,4-ethylenedioxythiophene): poly(styrene sulfonate) ($PEDOT$: PSS) (Baytron P 4083) in nitrogen atmosphere. The $P3HT$: $PCBM$ compositions are given by their relative weight ratios. The bulk-heterojunction organic solar cells were then fabricated by the vacuum deposition of aluminum (Al) electrode with the device architecture of $ITO/PEDOT/P3HT$: $PCBM/Al$. Thermal annealing was carried out in nitrogen atmosphere by thermally heating the devices with selected temperature and time period. The MFE_{PC} and $LADR$ measurements were performed based on a single device with continuous thermal annealing starting from low to high temperatures to remove experimental errors. The double-layer solar cells were also fabricated by using TiO_x and ZnO films, as more and less polar materials, with a $P3HT$ layer. The TiO_x and ZnO films were prepared by spin casting with the thickness of 60 nm from their respective solutions based on published procedures.[103][104] The thickness of $P3HT$ layer was controlled at 80 nm in the double-layer devices. The photocurrent-voltage characteristics were measured by using Keithley 2400 source meter and the photoillumination of AM1.5G 100 mW/cm^2 from Thermal Oriel 96000 300 W solar simulator for the fabricated solar cells. The MFE_{PC} was measured from the solar cells placed in magnetic field under the light illumination with central wavelength of 500 nm selected by monochromator and transported through a liquid light waveguide fiber. The magnetic field was applied parallel to the device plane during measurements.

However, the MFE_{PC} does not show appreciable angle dependence with magnetic field direction in the $P3HT : PCBM$ bulk-heterojunction solar cells. The MFE_{PC} is determined by the relative change in photocurrent at short-circuit condition, as shown in Equation 1.2. The light-assisted dielectric response $LADR$ was recorded by using a dielectric spectrometer $(Agilent, E4980A)$ to measure the capacitance of bulk-heterojunction organic solar cells. Specifically, the capacitance measurement was performed for organic solar cells under the light illumination from a sunlight simulator. The light illumination intensity was changed by using different neutral optical filters. The $LADR$ results were obtained by measuring the capacitance of bulk-heterojunction solar cell with light illumination intensity. The photoluminescence (PL) was characterized by using a SPEX Florolog 3 spectrometer. All measurements were performed in nitrogen gas atmosphere at room temperature.

4.3 Results and Discussion

Figure 4.1b shows the MFE_{PC} for the $P3HT : PCBM$ bulk-heterojunction solar cell when the short-circuit photocurrent was measured as a function of magnetic field. Clearly, the $P3HT : PCBM$ bulk-heterojunction solar cell lacks a low-field MFE_{PC} ($< 150\ mT$) but shows considerable a high-field MFE_{PC} ($> 150\ mT$). Specifically, the MFE_{PC} remains flat at low field ($0 \sim 150\ mT$) but has a positive component at a high field ($150\ mT \sim 1$ T). In contrast, the pristine $P3HT$ device shows significant low-field MFE_{PC} with typical rapid increase and slow decrease components based on short-circuit photocurrent. However, the pristine $P3HT$ does not exhibit positive high-field MFE_{PC}. Therefore, we can suggest that low-field and high-field MFE_{PC} can be attributed to pristine organic semiconducting materials and bulk-heterojunctions, respectively. In the pristine $P3HT$ device the positive and negative low-field MFE_{PC} indicates that the photocurrent is generated by two processes: the dissociation of polaron pairs and the charge reaction in excitonic states. In contrast, the lack of low-field MFE_{PC} implies that the strong donor-acceptor interaction can

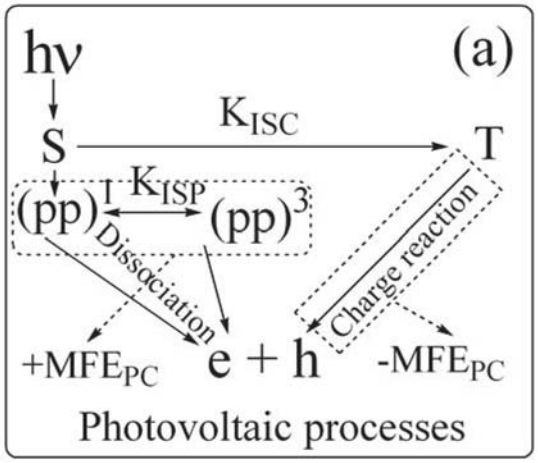

(a) Photocurrent-generation channels

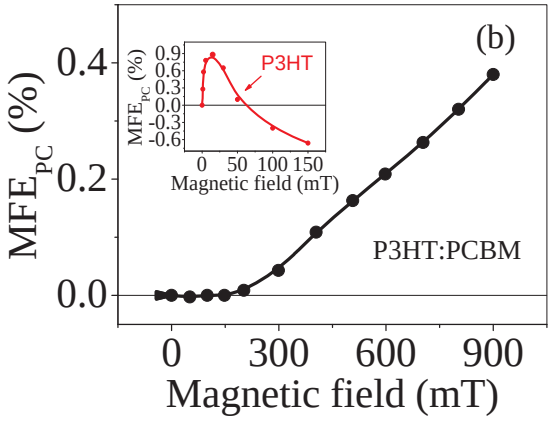

(b) MFE_{PC} for $ITO/PEDOT/P3HT:PCBM/Al$ solar cell

Figure 4.1: Photocurrent-generation channels in pristine semiconducting $P3HT$ and magnetic field effects of photocurrent MFE_{PC} in bulk-heterojunction P3HT:PCBM solar cell. (a): Photocurrent-generation channels: dissociation of polaron pairs, dominated by singlet excitons, and exciton-charge reaction, dominated by triplet excitons. S and T represent photoexcited singlet and triplet excitons. (PP)1 and (PP)3 are inter-molecular singlet and triplet polaron pairs in pristine P3HT. $K_(ISC)$ and $K_(ISP)$ are intersystem crossing in excitonic and polaron-pair states. $+MFE_{PC}$ and $-MFE_{PC}$ are positive and negative components in magnetic field effects of photocurrent in low-field regimes. (b): MFE_{PC} for $ITO/PEDOT/P3HT:PCBM/Al$ solar cell. The weight ratio of P3HT:PCBM is 1 : 0.8. The MFE_{PC} for pristine $P3HT$ device ($ITO/PEDOT/P3HT/Al$) is shown as an inset.

directly dissociate both singlet and triplet excitons without going through polaron-pair states and exciton-charge reaction process, and consequently removes the low-field MFE_{PC} in $P3HT : PCBM$ solar cell. In particular, the positive high-field MFE_{PC} implies that the exciton dissociation undergoes significant CT states at donor-acceptor interfaces in bulk-heterojunctions.[88] Because it is difficult to get the CT states signature from the photoluminescence spectrum due to the weak light emission from the complexes formed at the donor-acceptor interface, we use the electroluminescence studies to prove for $P3HT : PCBM$ based bulk-heterojunction devices. The alternative detection of the CT formation by electroluminescence other than photoluminescence in the bulk-heterojunction film is based on the following two arguments: first, the optical spectrum of the photoluminescence and electroluminescence in conjugated organic semiconductors relatively have the same spectrum characteristic such as the spectrum peak position; and second, due to the formation of the interpenetrate networks for both electrons and holes, and the significant mobility difference at the donor acceptor interface, it is possible to accumulate abundant charge carriers at the interface at high injection condition. Figure 4.2 shows the the electroluminescence spectrum for $P3HT : PCBM$ film at different weight ratios at $15mg : 3mg$, $15mg : 12mg$, and $15mg : 30mg$. It was found that a new peak exists for all different combinations at approximately 830 nm, and the peaks at 666 nm and 720 nm comes from the pristine form of $P3HT$ and $PCBM$, respectively.

The dissociation of CT states generates a positive signal in high-field MFE_{PC}. This positive high-field MFE_{PC} generated by the CT states is similar to the positive low-field MFE_{PC} generated by the polaron pairs. This similarity can be attributed to the fact that both polaron pairs and CT states are electron-hole pairs. Specifically, a polaron pair is formed when electron and hole are captured in different molecules in pristine polymers, while a CT state is generated when electron and hole are captured at donor and acceptor interface in bulk-heterojunctions. Therefore, both polaron

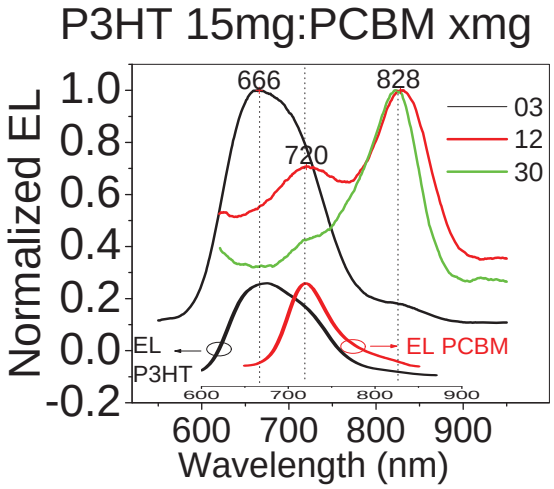

Figure 4.2: Electroluminescence studies for $P3HT : PCBM$ based devices at different weight ratios.

pairs and CT states are essentially electron-hole pairs. However, the electron-hole separation distance in CT states is usually shorter than that in polaron pairs due the close contact between donor and acceptor domains in bulk-heterojunctions. Due to the shorter electron-hole separation distance CT states can have larger binding energies and exchange energies relative to polaron pairs. We should note that bulk-heterojunctions are still more efficient to generate photocurrent although the CT states have larger binding energies. This is because (i) almost every exciton undergo dissociation, (ii) the donor and acceptor interpenetrating networks can largely facilitate the charge collection at respective electrodes, and (iii) only a portion of dissociated charge carriers forms the CT states at donor and acceptor interfaces in bulk-heterojunctions. In contrast, only small portion of excitons undergo dissociation to form polaron pairs in pristine polymers. In addition, pristine polymers lack sufficient donor and acceptor interpenetrating networks for the collection of dissociated charge carriers. As a consequence, pristine polymers do not efficiently to generate photocurrent although the polaron pairs have lower binding energies. We further examined the relationship between positive high-field MFE_{PC} and CT

states by using double-layer design with different dielectric materials: TiO_x and ZnO, respectively. The TiO_x and ZnO have different dielectric constants ($\varepsilon = 86$ for TiO_x and $\varepsilon = 8$ for ZnO)[105] but similar electronic levels ($LUMO = 4.4\ eV$ and $HOMO = 8.1\ eV$ for TiO_x;[68] $LUMO = 4.3\ eV$ and $HOMO = 7.7\ eV$ for ZnO).[106] In particular, the TiO_x and ZnO can be used as more and less polar materials to form the double-layer solar cells with the $P3HT$. Figure 4.3a shows that the use of more polar TiO_x layer causes a positive high-field MFE_{PC}. In contrast, the less polar ZnO layer does not appreciably change the MFE_{PC} from the $P3HT$, lacking high-field MFE_{PC}.

In addition, the $P3HT/TiO_x$ solar cell shows a larger photocurrent and photoluminescence (PL) quenching relative to the $P3HT/ZnO$ device (Figure 4.3b). The larger PL quenching caused by the TiO_x film can be attributed to the stronger Coulomb interaction between the $P3HT$ and TiO_x at the interface due to the larger dielectric constant of TiO_x. Nevertheless, these experimental results imply that (i) more polar TiO_x can enhance the exciton dissociation through local Coulomb interaction and (ii) the dissociated electrons and holes form CT states at the $P3HT/TiO_x$ interface in the generation of photocurrent in the double-layer organic solar cell. Therefore, the comparison between more and less polar effects in MFE_{PC} further indicates that the high-field MFE_{PC} can be attributed to the electron-hole pairs formed in CT states at the donor-acceptor interfaces in organic solar cells. We should note that the MFE_{PC} signal from the CT states in the $P3HT/TiO_x$ covers both low and high-field regimes, while the MFE_{PC} signal from the CT states in the $P3HT : PCBM$ bulk-heterojunctions only exists in high-field regimes. This is because the MFE_{PC} signal consists of the contributions from both bulk and interface in the $P3HT/TiO_x$ device, and the combination of bulk (low-field positive and negative components) and interface (high-field positive component) contributions can produce a positive MFE_{PC} covering low and high-field regimes. For the $P3HT : PCBM$ bulk-heterojunctions the MFE_{PC} signal only consists of the contribution from the CT

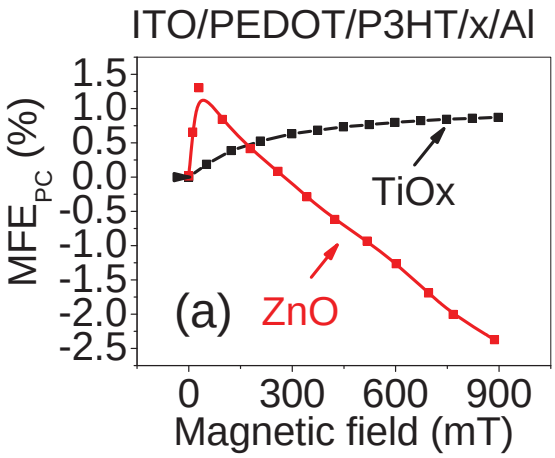

(a)

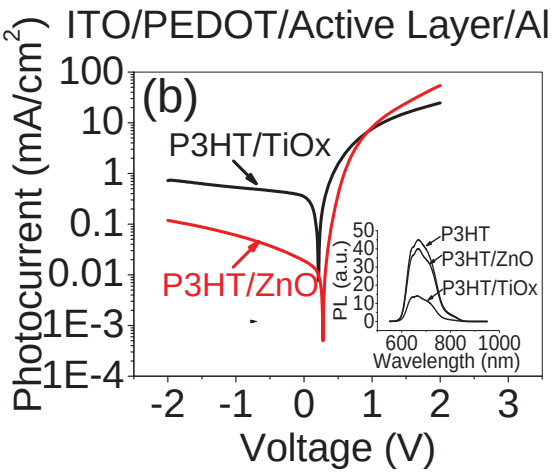

(b)

Figure 4.3: Magnetic field effects of photocurrent (MFE_{PC}), short-circuit current-voltage ($I_{sc} - V$), and PL quenching for $P3HT/TiO_x$ and $P3HT/ZnO$ double-layer solar cells. (a): MFE_{PC} for $ITO/PEDOT/P3HT/TiO_x/Al$ and $ITO/PEDOT/P3HT/ZnO/Al$ solar cells. (b): $I_{sc} - V$ for $P3HT/TiO_x$ and $P3HT/ZnO$ double-layer solar cells insert: PL quenching for $P3HT$ with TiO_x and ZnO dielectric films, respectively, in double-layer design.

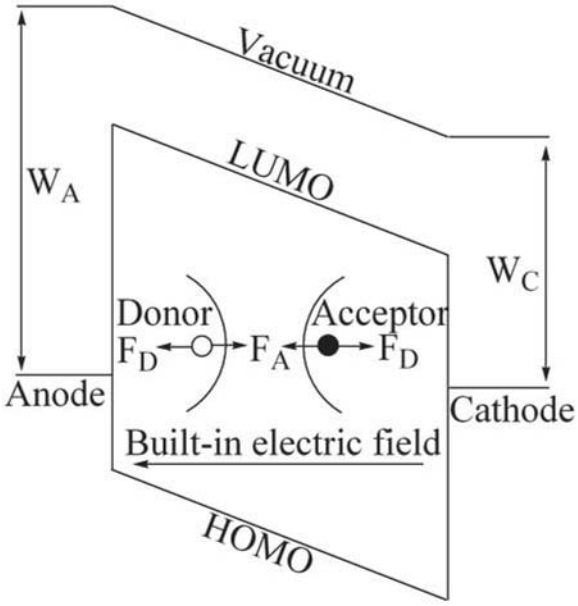

Figure 4.4: Schematic for inter-molecular CT states formed at donor-acceptor interfaces under the competition between Columbic attraction (F_A) and electrical drifting (F_D) force. The W_a and W_c are the workfunctions for anode and cathode.

states formed at the donor and acceptor interfaces and consequently gives rise to a positive component at high field. The experimental studies from transient absorption measurements have suggested that the formation of an electron-hole pair in CT states is determined by the competition between the free energy of charge separation and the Coulomb binding energy.[78] Based on this experimental finding, we can consider the electrically attractive force F_A, due to the Coulomb interaction, and the electrical drifting force FD, due to built-in electric field in the formation of electron-hole pairs in CT states, as schematically shown in Figure 4.4.

The Coulomb interaction depends on both the dielectric constant in the medium and the electron-hole separation distance at donor-acceptor interfaces. The built-in electric field can be estimated by the open-circuit voltage V_{oc}, given by $E = \frac{V_{oc}}{d}$, where d is the photovoltaic film thickness. The total energy U of a CT state can therefore consist of electronic energy associated with donor and acceptor electronic levels,

potential energy from the Coulomb attraction, and kinetic energy from electrical drifting, shown in Equation (4.1).

$$U = |E_D(HOMO) - E_A(LUMO)| - \frac{1}{4\pi\varepsilon}\frac{e^2}{r} + \frac{1}{2}m_e V_e^2 + \frac{1}{2}m_h V_h^2 \qquad (4.1)$$

Where $E_D(HOMO)$ and $E_A(LUMO)$ are the $HOMO$ for donor and the $LUMO$ for acceptor, e and h are the electron and hole drifting velocities, m_e and m_h are the masses for electron and hole, r is the separation distance between electron and hole at donor-acceptor interface, and ε is the medium dielectric constant. It can be seen from Equation 4.1 that increasing the kinetic energy can reduce the stability of charge-transfer complexes and consequently enhance the dissociation of CT states. However, increasing the Coulomb potential energy can stabilize the CT states and thus weaken the dissociation of CT states. In principle, changing the potential energy, through Coulomb interaction, and the kinetic energy, through electrical drifting, forms a mechanism to control the formation and dissociation of CT states at the donor-acceptor interfaces in organic solar cells. In potential energy, the medium dielectric constant and donor-acceptor interfacial distance essentially determine the electron-hole capture probability in the formation of CT states through Coulomb interaction. In kinetic energy, the built-in electric field and charge mobility control the probability for dissociated electrons and holes to completely escape from their mutual Coulomb attraction towards the generation of photocurrent. Therefore, adjusting kinetic and potential energies through electrical drifting and Coulomb interaction can essentially change the density of inter-molecular CT states. Figure 4.5a shows that the morphological adjustment through thermal annealing can reduce the high-field MFE_{PC} signal strength in the $P3HT:PCBM$ (1:0.8) solar cell.

According to the high-field signal amplitude at 900 mT, the optimized thermal annealing (five-minute heating at 155 °C) can largely decrease the density of CT states by at least 61 % in the $ITO/PEDOT/P3HT:PCBM/Al$ solar cell (Figure

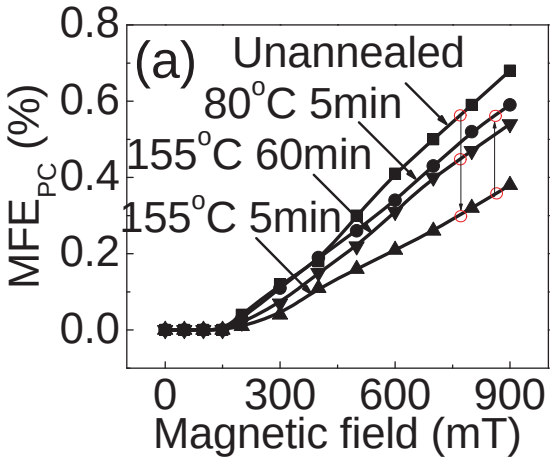

(a) High-field MFE_{PC}

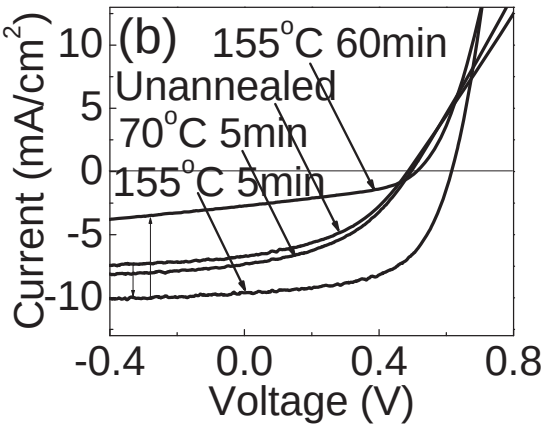

(b) $I_{sc} - V$ characteristics

Figure 4.5: High-field MFE_{PC} and photocurrent current-voltage ($I_{sc} - V$) characteristics for the $ITO/PEDOT/P3HT : PCBM(1 : 0.8)/Al$ device with continuous thermal annealing staring from low to high temperatures. (a): High-field MFE_{PC}; (b): $I_{sc} - V$ characteristics.

4.5a). The transient spectroscopy measurements have found that thermal annealing can significantly increase the yield of dissociated charge carriers by increasing the free energy of charge separation.[58] Our studies of high-field MFE_{PC} have further shown that the thermal annealing can also reduce the density of CT states in $P3HT:PCBM$ bulk-heterojunction solar cells through morphological development. We note in the formation of CT states that the electron and hole drifting velocities μ_e and μ_h involved in the kinetic energy depend on both charge mobility and built-in electric field, given by

$$\nu_e = \mu_e \cdot E \tag{4.2}$$

$$\nu_h = \mu_h \cdot E \tag{4.3}$$

where μ_e and μ_h are the electron and hole mobilities, and E is the built-in electric field. It has been experimentally found that thermal annealing can substantially improve the interpenetrating networks for charge transport[51][52][107] and consequently increase charge mobilities.[58][61][108][109][110] It can be therefore suggested from Equation 4.2 and 4.3 that the increase in charge mobilities upon annealing can lead to a reduction in the density of CT states through increasing the kinetic energies of dissociated electrons and holes in organic solar cells. In addition, earlier experimental studies have already found that thermal annealing can significantly improve photovoltaic efficiencies of the $P3HT:PCBM$ solar cells[7][107][111][112][113] due to the improvements of optical absorption and charge mobilities induced by morphological change through $PCBM$ aggregation and $P3HT$ chain packing.[52][61][113][114][115][116] Figure 4.5b indicates that the power conversion efficiency (PCE) was improved from 1.4% for the un-annealed device (I_{sc}=6.5 mA/cm2, V_{oc}=0.49V, FF=0.42) to 3.5% for the optimally annealed device (I_{sc})=9.6 mA/cm2, V_{oc}=0.61V, FF=0.60) under the simulated sunlight illumination of 100 mw/cm^2 ($AM1.5$). Our MFE_{PC} results suggest that the reduction in the density of CT states can also contribute to the improvement of photovoltaic efficiencies

upon thermal annealing. Now we discuss the binding energy and dissociation of CT states formed at donor-acceptor interfaces in organic solar cells based on the experimental measurements of electrical field dependence of MFE_{PC}. It was observed that the MFE_{PC} can be significantly increased in organic solar cells by reducing the dissociation of photoexcited states around open-circuit condition when a forward electric field is applied to cancel internal electric field.[41] This experimental result implies that the density of photoexcited states responsible for MFE_{PC} can be modulated by the external electric field through dissociation process. Here, we apply a reverse electric field to enhance the dissociation of CT states and consequently to decrease the MFE_{PC} amplitude. We should note that the measurement of MFE_{PC} versus reverse electric field can provide the information on the binding energy of CT states. Figure 4.6a shows that an applied reverse electric field can decrease the high-field MFE_{PC} signal in the annealed $P3HT : PCBM$ (1 : 0.8) solar cell. The amplitude reduction of high-field MFE_{PC} at 900 mT shows that the applied electric field of 2.0 V reverse bias reduces the density of CT states by 18% in the annealed $P3HT : PCBM$ solar cell. This experimental result indicates that the applied external electric field can compete with the electron-hole Coulomb attraction in the CT states and consequently decrease the density of CT states by enhancing the dissociation of CT states at the donor-acceptor interfaces. It should be further noted that the un-annealed $P3HT : PCBM$ solar cell shows a much larger reduction ($\sim$ 65%) in high-field MFE_{PC} signal amplitude under the influence of an equivalent applied electric field (1.8 V reverse bias) (Figure 4.6b). This experimental result implies that thermal annealing can indeed destroy the CT states of lower binding energy. However, the CT states with higher binding energy still exist after thermal annealing. In addition, it can also be seen that the annealed device shows a higher threshold ($\sim$ 300 mT) in the MFE_{PC} as compared to the un-annealed device (threshold $\sim$ 180 mT). This implies that the remaining CT states have larger exchange energies in the annealed $P3HT : PCBM$ solar cell. It can be suggested from the larger exchange energies that thermal annealing enhances the donor and acceptor

interfacial contacts and consequently reduces the donor and acceptor separation distance for more efficient dissociation. Clearly, the thermal annealing can dissociate low binding-energy CT states and significantly reduce the total density of CT states by enhancing the kinetic energies of dissociated charge carriers (4.1). However, the remaining CT states have higher binding energies at the donor and acceptor interfaces in the annealed $P3HT : PCBM$ solar cell. On the other hand, the un-annealed $P3HT : PCBM$ solar cell has lower binding energies but a higher density of CT states. Therefore, completely removing the CT states is an important issue in the generation of photocurrent in bulk-heterojunction solar cells. It can be suggested from Equation 4.1 that the internal charge transport and local Coulomb interaction are two critical parameters that control the formation of CT states at donor-acceptor interfaces. Here, we use light-assisted dielectric response: $LADR$ to investigate the charge transport and local Coulomb interaction upon thermal annealing when the $P3HT : PCBM$ solar cell is operated in capacitor mode under photoexcitation. Figure 4.7 shows the capacitance of the $P3HT : PCBM$ solar cell as a function of light illumination intensity before and after annealing. It is known that the capacitance is essentially related to the internal electrical polarization of $P3HT : PCBM$ blend film and the amount of photogenerated charge carriers stored in the electrodes in the $P3HT : PCBM$ solar cell.

It can be seen from Figure 4.7 that the thermal annealing causes three changes in the dielectric response. First, under dark condition the device capacitance slightly increases with thermal annealing in the $P3HT : PCBM$ solar cell. This indicates that the thermal annealing increases the electrical polarizabilities of local morphological structures through $P3HT$ chain packing and $PCBM$ aggregation and consequently enhances the overall dielectric constant of $P3HT : PCBM$ film. It should be also noted that our experimental result of enhanced dielectric constant can explain the early published result: the increase of absorbance for $P3HT : PCBM$ film after thermal annealing.[61][110] Moreover, this morphology-dependent polarizability can

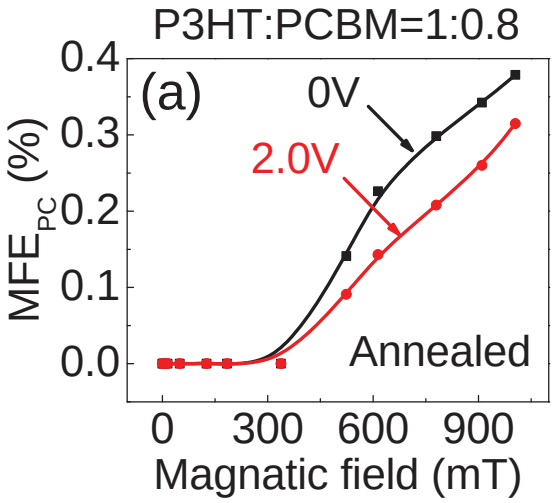

(a) Annealed solar cell

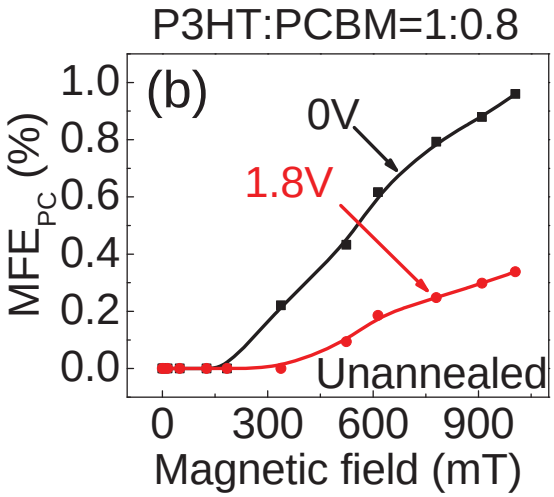

(b) Un-annealed solar cell

Figure 4.6: Applied electric field effects on high-field MFE_{PC} for the $ITO/PEDOT/P3HT : PCBM(1 : 0.8)/Al$ solar cells before and after annealing: (a): Annealed solar cell; (b): Un-annealed solar cell. The equivalent electric fields were applied by using reverse biases of 2.0 V (after annealing) and 1.8 V (before annealing).

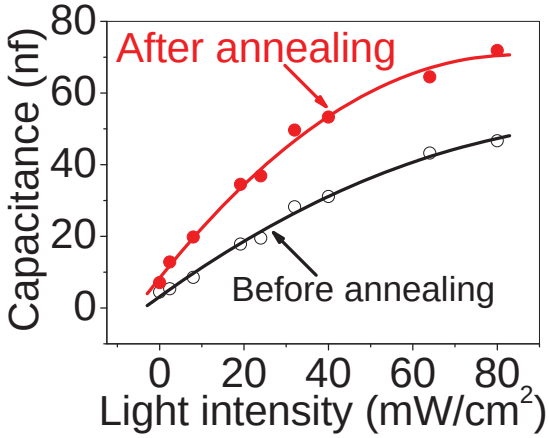

Figure 4.7: Light-assisted dielectric response is shown for the $P3HT : PCBM$ bulk-heterojunction solar cell before and after annealing, respectively. The capacitance is plotted as a function of light illumination intensity when the P3HT:PCBM solar cell is operated in capacitor mode.

be backed by nanosize-dependent dielectric interaction in nanomaterials.[117][118] It has been suggested that the increased electrical polarizabilities can increase the donor-acceptor interaction and thus reduce the formation of CT states.[119] Second, at a given light illumination intensity the thermal annealing increases the device capacitance in the $P3HT : PCBM$ solar cell. This result implies that the thermal annealing can indeed increase the exciton dissociation and consequently the amount of photocharge carriers stored in the respective electrodes through morphological development. Third, the larger increase rate of device capacitance with light illumination intensity implies that the thermal annealing enhances the charge-transport channels for dissociated electrons and holes to drift to respective electrodes. It is noted that the enhancement of charge-transport channels can essentially decrease the stability of CT states by increasing the kinetic energies of dissociated electrons and holes at the donor-acceptor interfaces. Nevertheless, the light-assisted dielectric studies reveal that morphological development generates three outcomes upon thermal annealing: (i) the increase of electrical polarizations of local

$P3HT$ and $PCBM$ morphological structures, (ii) the increase in effective donor-acceptor interaction and exciton dissociation, and (iii) the enhancement of charge-transport channels.

4.4 Conclusion

In summary, our magneto-optical studies indicate that MFE_{PC} and $LADR$ can be presented as new experimental tools to investigate the inter-molecular CT states at donor-acceptor interfaces during exciton dissociation in the generation of photocurrent in bulk-heterojunction organic solar cells. The MFE_{PC} and $LADR$ measurements have shown that morphological development can change the internal electrical drifting and local Coulomb interaction and consequently affect the formation and dissociation of CT states at the donor-acceptor interfaces in the generation of photocurrent in bulk-heterojunction organic solar cells. Specifically, the competition between electrical drifting force and Coulomb attraction determines the formation and dissociation probabilities of electron-hole pairs in the CT states at the donor-acceptor interfaces. As a result, adjusting internal electrical drifting and local Coulomb interaction through materials design and film-morphological development presents a fundamental pathway to improve the photocurrent by controlling the formation and dissociation of inter-molecular CT states at the donor-acceptor interfaces in bulk-heterojunction organic solar cells.

Chapter 5

Magnetic field effect on charge-transfer complex in P3HT/TiOx double layer photovoltaics

In this chapter, we use the magnetic field effects of photocurrent (MFE_{PC}) to study the photovoltaic processes in pristine conjugated polymer, bulk-heterojunction, and double-layer solar cells based on poly(3-alkylthiophene) ($P3HT$). The MFE_{PC} reveals that the photocurrent generation undergoes dissociation in polaron-pair states and the charge reaction in excitonic states in pristine conjugated polymers. As for the bulk-heterojunction solar cells consisting of the electron donor: $P3HT$ and electron acceptor: [6,6]-phenyl C61-butyric acid methyl ester ($PCBM$), the MFE_{PC} indicates that the dissociated electrons and holes inevitably form the inter-molecular charge-transfer complexes at donor and acceptor interfaces. Essentially, the photocurrent generation relies on the further dissociation of inter-molecular charge-transfer complexes. Moreover, we use double-layer solar cell to further study the inter-molecular charge-transfer complexes with well-controlled donor-acceptor

interfaces based on double-layer $P3HT/TiO_x$ design. We find that the increase in free energies can significantly reduce the density of charge-transfer complexes upon thermal annealing.

5.1 Introduction

It has been found that photoexcitation generates intra-molecular electron-hole pairs, namely Frenkel excitons.[13][43][70][71][72] Therefore, the photocurrent generation requires sufficient donor-acceptor interaction[23][63] to dissociate the photoexcited excitons in organic solar cells. However, it has been found that the dissociated electrons and holes can inevitably form the inter-molecular charge-transfer complexes at donor and acceptor interfaces.[73][76][77][78][79][80][81][82][120][121][122] Generally, the charge-transfer complexes have two pathways to release their energies: one is the direct dissociation into free charge carriers and followed by the charge transportation through the respective networks to generate photocurrent, and the other is the bimolecular recombination of the electrons and holes generating radiative or non-radiative emission. Due to the large binding energies occurring in both excitonic and charge-transfer complex states,[123][124][125] dissociating the photoexcited excitons and charge-transfer complexes is a critical issue in the generation of photocurrent in organic solar cells, as schematically shown in Figure 5.1a. In this work, we use MFE_{PC} as an effective tool to study the electron-hole pair dissociation processes in pristine conjugated polymer, bulk-heterojunction, and double-layer systems. Clearly, the MFE_{PC} can elucidate the dissociation in polaron-pair states, the charge reaction in excitonic states, and the dissociation in charge-transfer complex states.

5.2 Experimental

The photovoltaic materials of $P3HT$ and $PCBM$ were purchased from Reiki Metals Inc., and American Dye Source Inc., respectively. The TiO_x was prepared

by the method based on published procedures.[103] Here, the bulk-heterojunction organic solar cells were fabricated by mixing the $P3HT$, as electron donor, and the low molecular-weight molecules $PCBM$, as electron acceptor. Chlorobenzene (anhydrous, 99.8%) from Sigma-Aldrich was used to prepare blend solution of $P3HT$ and $PCBM$ for the spin-cast $P3HT : PCBM$ thin films with the weight ratio of 1:0.8. For the fabrication of solar cells, ITO glass was first cleaned in ultrasonic bath by using detergent, deionized water, acetone, isopropanol, and chloroform. Then, the polyethylenedioxythiophene/polystyrenesulphonate (PEDOT/PSS) (Baytron P 4083) was spin cast on the top of UV treatment ITO glasses with the film thickness of 40 nm. After baking the PEDOT films in vacuum at 140 °C for one hour, the photovoltaic layer $P3HT : PCBM$ was then coated with the film thickness of 150 nm on the previously thermally treated PEDOT. The aluminum (Al) was thermally deposited to form bulk-heterojunction solar cells. The double-layer solar cell was prepared with the architecture of $P3HT/TiO_x$ with the thickness of 75 nm/15 nm, where the TiO_x functions as electron acceptor. The film thicknesses were measured by utilizing Veeco diCaliber (004-1001-000) Atomic Force Microscope (AFM). Both bulk-heterojunction and double-layer solar cells were thermally annealed at 155 °C for 5 min on a digitally controlled hot plate under nitrogen atmosphere to maximize device performance. The current-voltage characteristics were measured utilizing Keithley 2400 source meter under the photoexcitation provide by Thermal Oriel 96000 300 W solar simulator from Newport. The MFE_{PC} was measured from the solar cells placed in magnetic field under the light illumination with central wavelength of 500 nm selected by monochromator and transported through a liquid light waveguide fiber. The MFE_{PC} is determined by the relative change in photocurrent at short-circuit condition, as shown in Equation 1.2. The magnetic field was applied parallel to the device plane during measurements. Moreover, the MFE_{PC} does not show appreciable angle dependence with magnetic field direction in the fabricated solar cells.

5.3 Results and Discussion

Figure 5.1b shows the MFE_{PC} at short-circuit condition for both pristine polymer and bulk-heterojunction solar cells. It is noted that the pristine $P3HT$ device shows considerable low-field MFE_{PC} with typical rapid increase and slowly decreasing components. However, the $P3HT : PCBM$ bulk-heterojunction solar cell lacks a low-field MFE_{PC} ($< 150\ mT$) and shows a significant positive component at high-field regime ($150\ mT \sim 900\ mT$). Therefore, we can suggest that low-field and high-field MFE_{PC} correspond to the photovoltaic processes in the pristine organic semiconducting materials and bulk heterojunction, respectively. At low field, we have observed that singlet polymers such as polyfluorene only exhibit a positive MFE_{PC} but gives rise to both positive and negative MFE_{PC} when the triplet excitons are introduced by using heavy-metal complexes.[85] Therefore, it can be therefore suggested that the singlet and triplet excitons are responsible for positive and negative MFE_{PC}, respectively. Specifically, the positive MFE_{PC} component is generated by the dissociation in the polaron-pair states, while the negative MFE_{PC} component is due to the exciton-charge reaction in pristine conjugated polymer devices, schematically shown in Figure 5.2a.

It can be noted that the polaron pairs are mainly generated by singlet excitons through charge separation process driven by Onsager process[90] due to strong ionic natures in singlet wavefunctions. It has been experimentally found that an external magnetic field can change the singlet and triplet ratios in polaron-pair states through spin-dependent intersystem crossing.[35][38][126] It is noted that the spin-dependent intersystem crossing requires both energy and spin-momentum conservations. The energy conservation can be satisfied by thermal vibration. The spin-momentum conservation must be satisfied by internal magnetic field from spin-orbital coupling or hyperfine interaction to flip spin polarizations during the intersystem crossing.

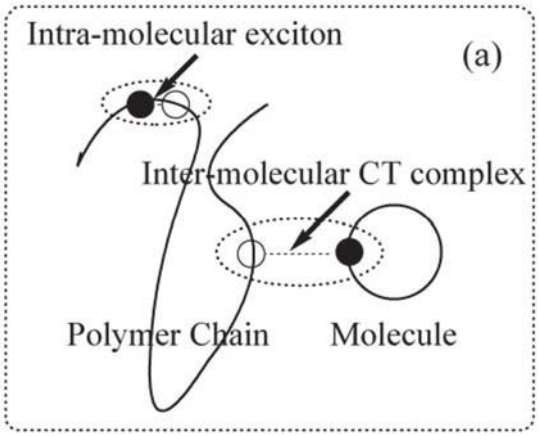

(a) Intra-molecular exciton and inter-molecule charge-transfer complex

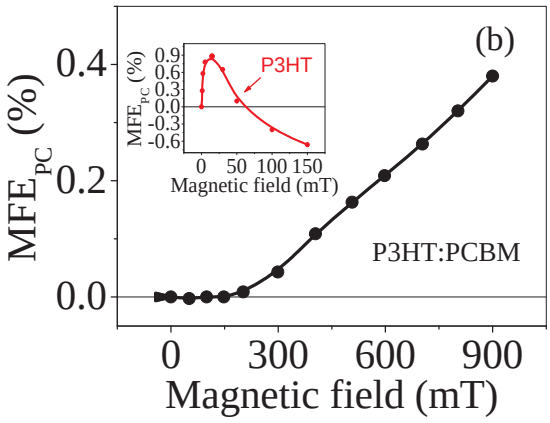

(b) Low-field and high-field MFE_{PC}

Figure 5.1: (a): Schematic diagram for intra-molecular exciton in pristine polymer and inter-molecule charge-transfer complex states at donor and acceptor interface in bulk-heterojunction, respectively and (b) Low-field and high-field MFE_{PC} in pristine polymer $P3HT$ and $P3HT : PCBM$ bulk-heterojunction solar cells.

When an external magnetic field is comparable to internal magnetic field, the spin-momentum conservation can be partially broken, leading to a modification on the singlet and triplet ratios in polaron-pair states.[35][38][126] It has been found that the increase in singlet-to-triplet ratio in polaron-pair states can lead to a positive MFE_{PC} at low field in pristine polymers due to the higher dissociation rates of singlet polaron pairs.[32][91] The exciton-charge reaction is usually dominated by triplet excitons due to the long lifetimes involved in Coulomb exciton-charge contacts. The relevant outcome of triplet exciton-charge reaction is the generation of free charge carriers by Coulombically breaking the triplet excitons.[94] Photophysics studies have found that a low magnetic field can reduce the triplet exciton-charge reaction rate constant[32][34][36] by disturbing the spin-spin interaction between a triplet exciton and a charge. As a consequence, the triplet exciton-charge reaction generates a negative MFE_{PC} at low field in pristine polymers. On the other hand, we noticed that the triplet excitons can form trions, a complex consisting of a free charge and a triplet exciton, which can cause a temporary trapping of mobile charges.[39][127] There is a possibility that an external magnetic field may affect the trions and then changes the photocurrent. However, the magnetic field dependence of photoluminescence has indicated that an external magnetic field does not appreciably change the singlet and triplet exciton ratios under photoexcitation due to strong spin interaction and large exchange energy in excitonic states.[85] This implies that an external magnetic field does not change the trions through triplet density. It should be also noted that an external magnetic field can reduce the formation rate constant of trions when the spin interaction between a triplet exciton and a charge is perturbed. However, this perturbation would generate a positive MFE_{PC} instead of a negative MFE_{PC}. Therefore, we can suggest that the trions do not play a significant role in the MFE_{PC}. Nevertheless, the typical rapidly increase and slowly decrease components in the MFE_{PC} indicate that the pristine $P3HT$ experiences the dissociation in polaron-pair states and the charge reaction in excitonic states in the generation of free charge carriers. More importantly, the lack of low-field MFE_{PC} in $P3HT:PCBM$ solar cell

implies that the strong donor-acceptor interaction can directly dissociate both singlet and triplet excitons without going through polaron-pair states and exciton-charge reaction process, and consequently removes the low-field MFE_{PC} in $P3HT:PCBM$ bulk-heterojunction solar cell. However, the $P3HT:PCBM$ solar cell shows a clear high-field MFE_{PC} with a positive component. This high-field MFE_{PC} has been found as evidence that the dissociated electrons and holes form inter-molecular charge-transfer complexes at donor and acceptor interfaces in the generation of free charge carriers in donor-acceptor bulk-heterojunction solar cells, as shown in Figure 5.2b.[85][86] Furthermore, the high-field required for the MFE_{PC} suggests that the electron-hole pairs in charge-transfer complex states formed at donor-acceptor interfaces have relatively larger exchange energies in bulk-heterojunctions as compared to the polaron pairs in pristine organic semiconducting polymers.

We further study the formation and dissociation of inter-molecular charge-transfer complexes by using the double-layer $P3HT/TiO_x$ solar cell with a well-controlled interface. Figure 5.3a shows the high-field MFE_{PC} at different photoexcitation energies for the $P3HT/TiO_x$ device up to 900 mT. The high-field MFE_{PC} confirms the formation of inter-molecular charge-transfer complexes at the $P3HT$ and TiO_x interfaces in the double-layer $P3HT/TiO_x$ system. We find that the magnitude of MFE_{PC} signal gradually decreases with increasing photoexcitation energy. Particularly, when the excitation energy reaches to 4.13 eV, no high-field MFE_{PC} signal is observed in the double-layer $P3HT/TiO_x$ device. This means that higher photoexcitation can lead to a significant reduction in the formation of inter-molecular charge-transfer complexes. It has been observed that the photoexcitation with energy greater than the $S_0 - S_1$ transition energy can generate hot electrons in higher energy levels and consequently reduce the exciton formation in conjugated polymers.[128][129][130] Figure 5.3b schematically shows that the very hot electrons with very high energies generated in the donor $P3HT$ can adiabatically transfer to the acceptor TiO_x and then directly dissociate to the electrode without forming

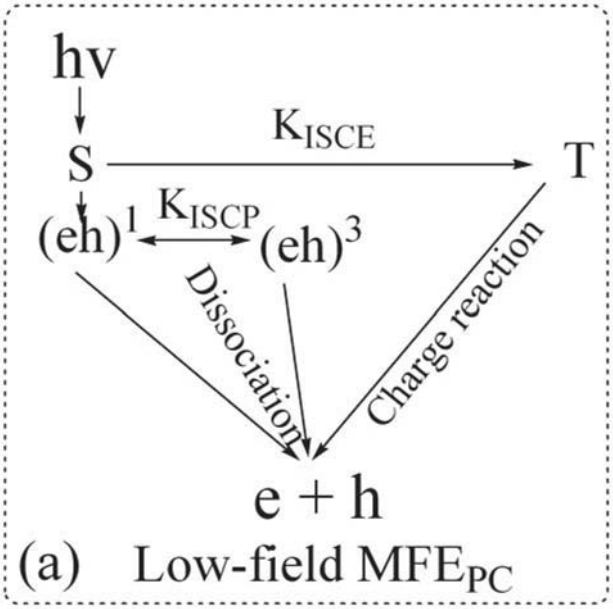

(a) Low-field

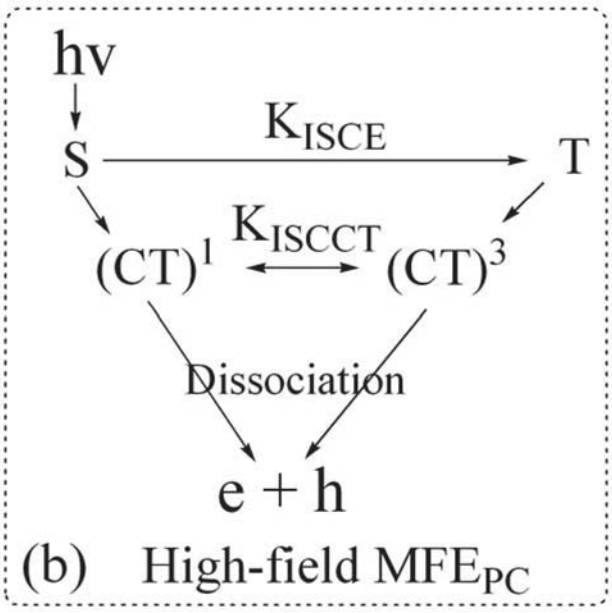

(b) High-field

Figure 5.2: Schematic dissociation processes accountable for (a) low-field and (b) high-field MFE_{PC} in pristine polymer $P3HT$ and $P3HT : PCBM$ bulk-heterojunction solar cells, respectively.

the charge-transfer complexes (labeled as process 1 in Figure 5.3b), as indicated by the MFE_{PC} result at the photoexcitation energy of 4.13 eV in Figure 5.3a. Moreover, the hot electrons can adiabatically transfer to the acceptor TiO_x at the $P3HT/TiO_x$ interface (labeled as process 2 in Figure 5.3b). A portion of transferred hot electrons can directly dissociate and transfer to the electrode. The other portion of transferred electrons can intra-molecularly relax to the lowest excited state (S1) within the acceptor TiO_x and then inter-molecularly form charge-transfer complexes at the $P3HT/TiO_x$ interface (labeled as process $2'$ in Figure 5.3b). Second, the photoexcited hot electrons with intermediate energies can intra-molecularly release their energies and relax to the lowest excited state (S1) within the donor $P3HT$ and then transfer to the acceptor TiO_x at the $P3HT/TiO_x$ interface to form charge-transfer complexes (labeled as processes 3 and $3'$ in Figure 5.3b). Clearly, changing photoexcitation energy relative to the $S_1 - S_0$ energy difference can change the ratio between direct dissociation and formation of charge-transfer complexes in organic solar cells, as shown in the MFE_{PC} resulting with different photoexcitation energies in Figure 5.3a. This experimental finding implies that reducing the energy gap relative to the photoexcitation energy presents a new pathway to control the formation and dissociation of inter-molecular charge-transfer complexes in the generation of photocurrent in organic solar cells. We further study the binding energies of inter-molecular charge-transfer complexes based on the double-layer $P3HT/TiO_x$ solar cell by combining applied reverse electric field and MFE_{PC}. It has been found that applying external electric field can largely reduce the density of charge-transfer complexes and consequently decrease the amplitude of high-field MFE_{PC}.[41]

Figure 5.4a and 5.4b shows the high-field MFE_{PC} for both thermally annealed and un-annealed devices under external reverse electric field. In particular, the high-field MFE_{PC} results reflect two important phenomena. First, at zero bias the thermal annealing clearly reduces the MFE_{PC} amplitude. This means that the thermal annealing decreases the densities of charge-transfer complexes at the $P3HT/TiO_x$

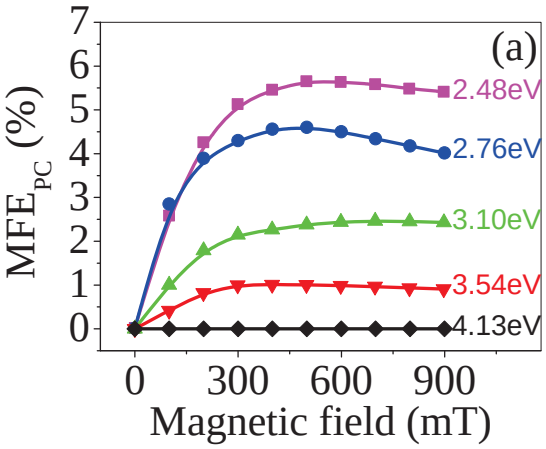

(a) Photoexcitation energy dependence of high-field MFE_{PC} in double-layer $ITO/PEDOT/P3HT/TiOx/Al$ device

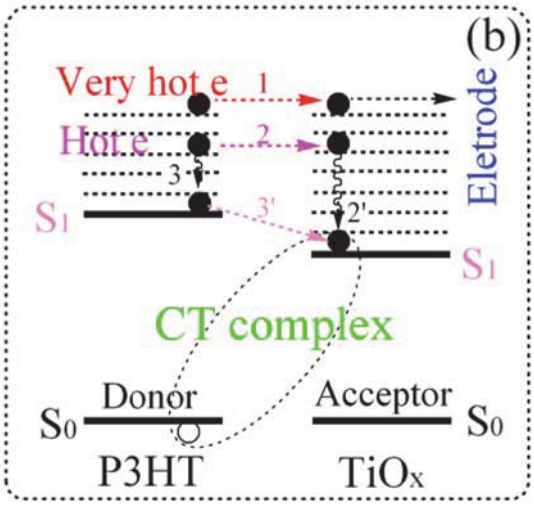

(b) Hot electrons involved in the charge dissociation and formation of inter-molecular charge-transfer (CT) complex at the $P3HT/TiO_x$ interface

Figure 5.3: (a): Photoexcitation-energy dependence of high-field MFE_{PC} in double-layer $ITO/PEDOT/P3HT/TiOx/Al$ device; (b): hot electrons involved in the charge dissociation and formation of inter-molecular charge-transfer (CT) complex at the $P3HT/TiO_x$ interface, 1: Very hot electron with high energy generated in electron donor $P3HT$ can directly transport to cathode through electron acceptor TiO_x. 2: Hot electron with intermediate energy can transport from donor $P3HT$ to acceptor TiO_x across $P3HT/TiO_x$ interface. 2′: Transferred hot electron intra-molecularly relaxes within acceptor TiO_x. 3: Photoexcited hot electron intra-molecularly relaxes within donor $P3HT$. 3′: Relaxed electron can transfer from donor $P3HT$ to acceptor TiO_x and then forms CT complex.

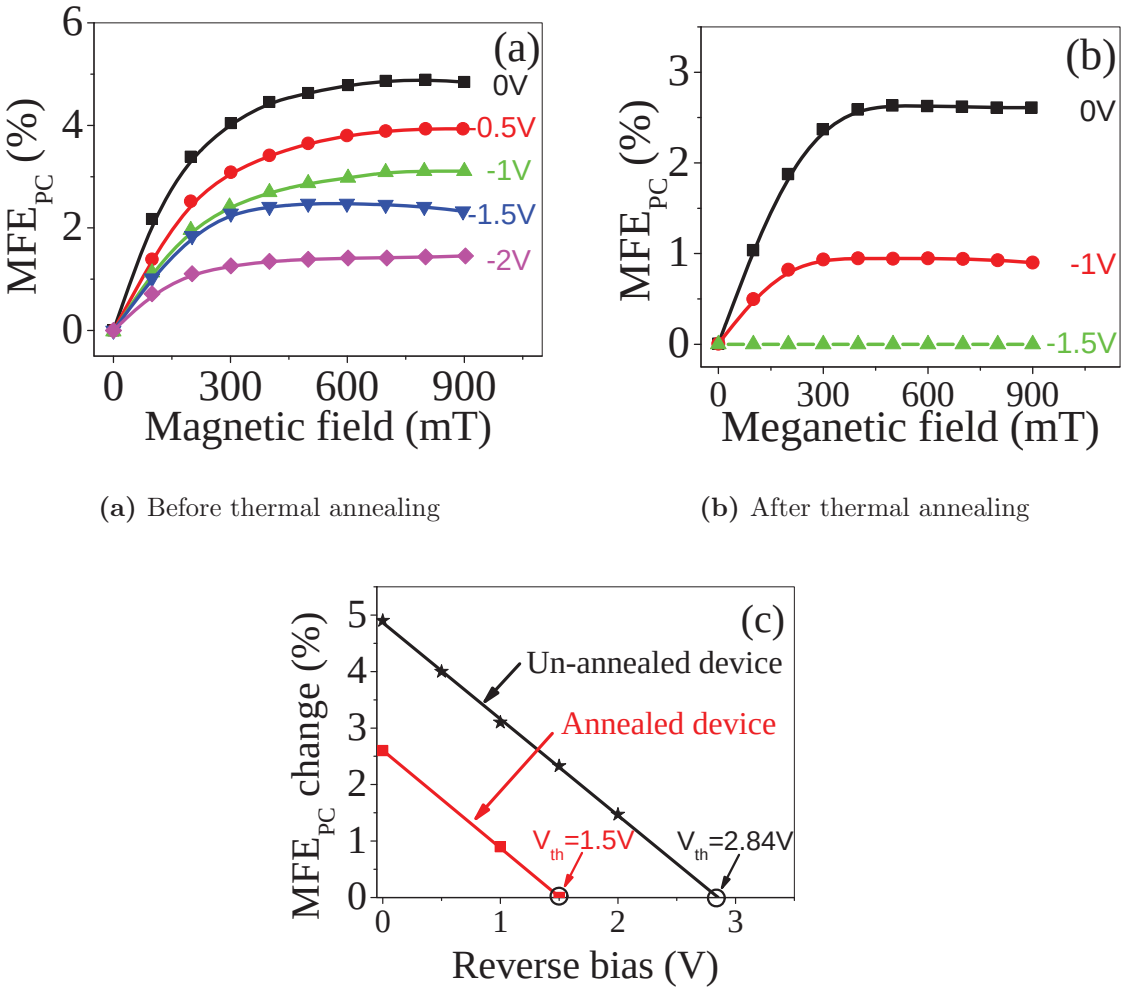

(a) Before thermal annealing

(b) After thermal annealing

(c) MFE_{PC} versus external reverse electric field before and after thermal annealing

Figure 5.4: External electric field-dependence on high-field MFE_{PC} in double-layer $ITO/PEDOT/P3HT/TiO_x/Al$ device (a): before thermal annealing. (b): after thermal annealing. (c): MFE_{PC} versus external reverse electric field before and after thermal annealing. The linear lines are curve fitting for visual guidance. V_{th} is the threshold voltage to remove the charge-transfer complexes.

interface. Second, applying reverse electric field can largely reduce the high-field MFE_{PC} magnitude in both annealed and un-annealed $P3HT/TiO_x$ solar cells. The comparison of electric field-dependent MFE_{PC} between annealed and un-annealed $P3HT/TiO_x$ solar cells clearly indicates that the thermal annealing reduces the binding energies of charge-transfer complexes at the donor/acceptor interface. For the densities of charge-transfer complexes, we note that the total energy U of a charge-transfer complex can consists of both potential energy from the Coulomb attraction and kinetic energy from electrical drifting,

$$U = |E_D(HOMO) - E_A(LUMO)| - \frac{1}{4\pi\varepsilon}\frac{e^2}{r} + \frac{1}{2}m_e V_e^2 + \frac{1}{2}m_h V_h^2 \qquad (5.1)$$

where $E_D(HOMO)$ and $E_A(LUMO)$ are the $HOMO$ for donor and the $LUMO$ for acceptor, V_e and V_h are the electron and hole drifting velocities, m_e and m_h are the masses for electron and hole, r is the separation distance between electron and hole at donor-acceptor interface, and ε is the medium dielectric constant. Experimentally, increasing free energies of dissociated charge carriers can largely decrease the binding energies of charge-transfer complexes towards charge dissociation.[58] As a result, the reduction in the densities of charge-transfer complexes can be attributed to the following experimental arguments. It has been found that the thermal annealing can increase the charge mobilities in the $P3HT$.[61][108][110] We can suggest that the increase in charge mobilities can then increase the kinetic energies of dissociated charge carriers and decrease the contact time between dissociated charge carriers at the $P3HT/TiO_x$ interface. Therefore, the thermal annealing can reduce the formation of charge-transfer complexes at the donor/acceptor interface. In regards to the reduction in the binding energies of charge-transfer complexes, we note that applied electric field can compete with the electron-hole Coulomb attraction in inter-molecular charge-transfer complexes and therefore decrease the densities of charge-transfer complexes through electric field-assisted dissociation. More importantly, by plotting the amplitude of high-field MFE_{PC} with the different applied reverse voltages, we can

see from Figure 5.4c that in the thermally annealed $P3HT/TiO_x$ device the threshold voltage (V_th) of 1.5 V can completely remove the high-field MFE_{PC}. However, the un-annealed $P3HT/TiO_x$ device requires a much higher threshold voltage of 2.84 V to completely remove the inter-molecular charge-transfer complexes. The comparison of electric field-dependent MFE_{PC} between annealed and un-annealed $P3HT/TiO_x$ solar cells clearly indicates that the thermal annealing can largely reduce the binding energies of charge-transfer complexes. It has been found that the thermal annealing can enhance the dielectric constant of TiO_x.[131] In particular, increasing of dielectric constant can cause an increase in the local electrical polarizations and consequently reduce the Coulomb attraction between dissociated charge carriers. Nevertheless, our MFE_{PC} results suggest that the thermal annealing can decrease the formation and binding energies of charge-transfer complexes by increasing the free energy of dissociated charge carriers and by weakening the Coulomb attraction between dissociated charge carriers through the modification of local dielectric constant in organic solar cells.

5.4 Conclusion

In summary, we found that the MFE_{PC} can show photovoltaic processes in pristine, bulk-heterojunction, and double-layer solar cells. Specifically, the low-field MFE_{PC} reveals that the generation of free charge carriers can undergo dissociation in polaron-pair states and the charge reaction in excitonic states in pristine polymers. In the $P3HT : PCBM$ bulk-heterojunctions, the high-field MFE_{PC} indicates that the dissociated electrons and holes inevitably form inter-molecular charge-transfer complexes at donor/acceptor interfaces. It also indicates that the generation of free charge carriers requires the further dissociation of charge-transfer complexes. In the $P3HT/TiO_x$ double-layer solar cells, we find that thermal annealing can reduce the density and binding energies of charge-transfer complexes at the $P3HT/TiO_x$ interfaces towards the charge dissociation in the generation of photocurrent. Moreover, the photoexcitation-energy dependence of high-field

MFE_{PC} shows that high photoexcitation energy can lead to a significant reduction in the formation of inter-molecular charge-transfer complexes towards the generation of photocurrent in the double-layer $P3HT/TiO_x$ solar cell. This experimental result suggests that engineering the energy band gap can lead to a reduction in the formation of inter-molecular charge-transfer complexes to enhance photocurrent generation. Nevertheless, our MFE_{PC} results indicate that internal charge transport, potential energy, and local electrical polarization can largely affect the densities and binding of charge-transfer complexes in the generation of photocurrent in organic solar cells.

Chapter 6

Intra-Molecular "Donor-Acceptor" Interaction Effects on Charge Dissociation, Charge Transport, and Charge Collection in Bulk-Heterojunction Organic Photovoltaics

6.1 Introduction

This chapter reports experimental studies on internal photovoltaic processes: charge dissociation, transport, and collection by using magnetic field effects of photocurrent (MFE_{PC}) and light-assisted dielectric response (LADR) in highly-efficient organic solar cells based on newly synthesized photovoltaic polymer CT and $PTB4$ with

intra-molecular "Donor-Acceptor" interactions. The low-field MFE_{PC} (< 150 mT) indicates that the intra-molecular "Donor-Acceptor" interactions generate charge dissociation in pristine $PTB2$ and $PTB4$ films, which is similar to that in lightly doped Poly(3-hexylthiophene) with 5 wt% $PCBM$ (fullerene derivative 1-(3-methyloxycarbonyl)-propyl-1-phenyl (6,6) C61). After the CT and $PTB4$ are mixed with electron acceptor $PCBM$ to form bulk-heterojunctions, the high-field MFE_{PC} (> 150 mT) reveals that the charge-transfer (CT) complexes formed at the $PTB2 : PCBM$ and $PTB4 : PCBM$ interfaces have much lower binding energies due to stronger electron-withdrawing abilities, as compared to the $P3HT : PCBM$ device, towards the generation of photocurrent. Furthermore, the light-assisted dielectric response: LADR indicates that the $PTB2$ and $PTB4$ based solar cells exhibit much larger capacitances relative to $P3HT : PCBM$ device under photoexcitation. The photoinduced capacitances suggest that the $PTB2 : PCBM$ and $PTB4 : PCBM$ bulk heterojunctions have more effective charge transport and collection than their $P3HT : PCBM$ counterpart. As a result, our experimental results indicate that the intra-molecular "Donor-Acceptor" interaction plays an important role to enhance charge dissociation, transport, and collection in bulk-heterojunction organic solar cells.

6.2 Experimental

The bulk-heterojunction photovoltaic systems were formulated by the photovoltaic polymer CT and $PTB4$ and commercially available regioregular $P3HT$ with electron acceptor $PCBM$. The compositions were prepared with the weight ratio of 1:0.8 for $P3HT : PCBM$ and 1:1 for both $PTB2 : PCBM$ and $PTB4 : PCBM$. The respective photovoltaic films were spin cast with the thickness of 120 nm for $P3HT : PCBM$ and 100 nm for both $PTB2 : PCBM$ and $PTB4 : PCBM$ films on indium-tin-oxide (ITO) glass substrates pre-coated with 40 nm thin layer of poly(3,4-ethylenedioxythiophene): poly(styrene sulfonate) (PEDOT:PSS) (Baytron P 4083)

in nitrogen atmosphere. The bulk-heterojunction solar cells were fabricated with the architecture of $ITO/PEDOT/polymer : PCBM/Ca/Al$. The $P3HT : PCBM$ was dissolved in chlorobenzene and thermally annealed at 155 °C for 5 min to optimize the efficiency, while 1,2 dichlorobenzene was used for $PTB2$ and $PTB4$ based solar cells without further treatment. The photocurrent-voltage characteristics were measured by using Keithley 2400 source meter under photoillumination of AM1.5G 100 mW/cm^2 from Thermal Oriel 96000 300 W solar simulator. The MFE_{PC} was characterized by measuring the change in short-circuit photocurrent as a function of applied magnetic field under the photoexcitation with the central wavelength of 500 nm selected from the monochromator and transported through a liquid light waveguide fiber. The light-assisted dielectric response: LADR was measured by using dielectric spectrometer $(Agilent, E4980A)$ with alternating voltage of 50 mV at 1 KHz under light illumination from a sunlight simulator at 100 mW/cm^2 when an organic solar cell was operated at short-circuit condition. In the LADR measurement, the dielectric spectrometer essentially measures the impedance of organic solar cell as a function of light illumination intensity. In particular, the impedance measurement can show the dielectric constant, the generation of charge carriers at electrodes, and the transport of charge carriers to electrodes under photoexcitation in organic solar cells. All measurements were performed in nitrogen gas atmosphere at room temperature.

6.3 Results and Discussion

The recently synthesized photovoltaic polymers have led to remarkable enhancement in photovoltaic efficiencies when mixed with fullurene-type electron acceptors in bulk-heterojunction organic solar cells.[132][133][134][135] The highest efficiencies of organic photovoltaic devices have reached over 8%.[8] However, it demands further investigations to elucidate the internal photovoltaic processes occurring in those highly-efficient organic solar cells for the development of advanced photovoltaic

materials. In this work we use magnetic field effects of photocurrent and light-assisted dielectric measurements to investigate the charge dissociation, transport, and collection in bulk-heterojunction organic solar cells based on efficient photovoltaic polymers $PTB2$ and $PTB4$, which have intra-molecular "Donor-Acceptor" interactions due to electron-withdrawing side-groups, compared with the commonly used polymer $P3HT$. It is known that the light absorption results in the formation of intra-molecular strongly-bound electron-hole pairs, namely excitons, in organic semiconducting polymers due to low dielectric constants and direct band structures.[13][70][136][137] The photocurrent can be consequently generated by exciton dissociation followed by charge transport in organic solar cells. In general, the photoexcitation-generated excitons can dissociate into charge carriers in both pristine semiconducting polymers,[138][139] and bulk-heterojunctions.[52][63] In pristine semiconducting polymers, the dissociated charge carriers can form electron-hole pairs at chain-chain interfaces, generating polaron pairs.[33][136][140][141][142] The polaron pairs can re-dissociate into charge carriers, when local electric fields can overcome the inter-chain electron-hole Coulomb attraction, to generate the photocurrent in organic materials. In bulk-heterojunction solar cells, the dissociated charge carriers can form inter-molecular charge-transfer (CT) complexes at donor-acceptor interfaces.[73][76][77][120][125] Furthermore, the CT complexes can re-dissociate into charge carriers, when their free energies can compete with the Coulomb attraction at the donor and acceptor interfaces,[58][143] towards the generation of photocurrent in donor-acceptor bulk-heterojunction systems. Nevertheless, the polaron pairs and CT complexes play an important role in the generation of photocurrent in pristine polymers and bulk-heterojunctions, respectively. Early experimental studies have shown that the photocurrent is sensitive to an external magnetic field in organic materials, leading to magnetic field effects of photocurrent.[37][84][144][145][146][147] The magnetic field effects of photocurrent originate from following two facts. First, an external magnetic field can change singlet and triplet ratios by changing intersystem crossing through spin-momentum conservation due to magnetic scattering

or through energy conservation due to Zeeman splitting.[35][36][85][148][149] Second, singlets and triplets have different contributions to the generation of photocurrent through dissociation and charge reaction due to their different ionic properties and lifetimes.[41][91] In particular, magnetic field effects of photocurrent can form an effective tool to elucidate charge dissociation processes. We recently found that the polaron pairs and CT complexes generate magnetic field effects of photocurrent at low-field and high-field regimes,[85][88] namely low-field MFE_{PC} ($< 150\ mT$) and high-field ($> 150\ mT$) MFE_{PC}, respectively. As a result, using low-field and high-field MFE_{PC} can elucidate the dissociation in polaron pairs and CT complexes. Furthermore, we know that an external electric field can interact with internal electrical polarizations to compete with the binding energies of electron-hole pairs, enhancing the charge dissociation in the polaron pairs and CT complexes[150] through Onsager process,[90] reducing the densities of polaron pairs and CT complexes. As a consequence, applying an electric field can lead to a reduction in low-field and high-field MFE_{PC} generated by polaron pairs and CT complexes in pristine and bulk-heterojunctions, respectively. As a result, measuring MFE_{PC} in an external electric field can form a new experimental tool: $V - MFE_{PC}$ to estimate the binding energies of polaron pairs and CT complexes. It is further noted that the interpenetrating donor-acceptor networks can form necessary charge-transport channels to collect the dissociated charge carriers at the cathode and anode to generate photocurrent in bulk-heterojunction organic solar cells.[52][151] Here, we use light-assisted dielectric response: $LADR$ to study the charge transport and collection in the $PTB2 : PCBM$ and $PTB4 : PCBM$ solar cells as compared to $P3HT : PCBM$ device based on impedance measurement.[143][152] In particular, we combine the MFE_{PC} and LADR measurements to elucidate internal charge dissociation, transport, and collection in $PTB2 : PCBM$ and $PTB4 : PCBM$ solar cells.

The photovoltaic polymer PTB derivatives were synthesized by using the procedure shown in Figure 6.1.[153] *(The synthesis is done by Dr. Liang in University of*

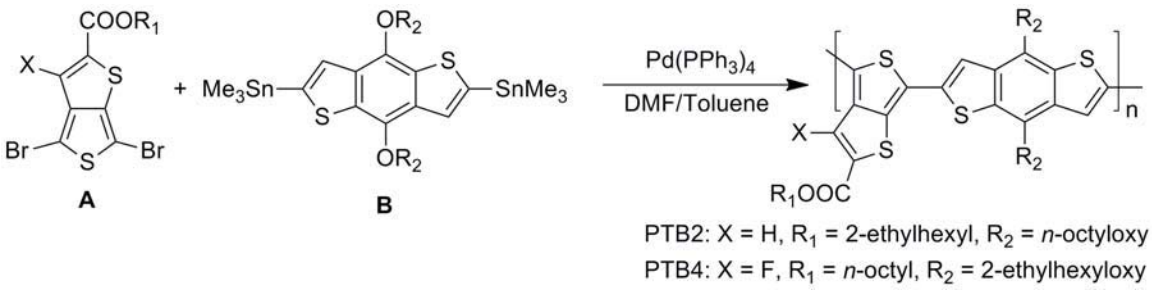

Figure 6.1: Chemical synthesis route for photovoltaic polymer $PTB2$ and $PTB4$.

Chicago) The monomer A (0.50 $mmol$) was weighted into a 25 mL round-bottom flask. 2,6-Bis(trimethyltin)-4,8-Bis(n-octyloxy)benzo[1,2-b:4,5-b']dithiophene (0.50 $mmol$) and Pd(PPh3)4 (25 mg) were added. The flask was subjected to three successive cycles of vacuum followed by refilling with argon. Then, anhydrous DMF (2 mL) and anhydrous toluene (8 mL) were added via a syringe. The polymerization was carried out at 120 °C for 12 h under nitrogen. The polymer was precipitated into methanol and collected by filtration. The precipitate was dissolved in chloroform and filtered through Celite to remove the metal catalyst. The final polymers were obtained by precipitating in hexanes and drying in vacuum for 12 h, yielding $PTB2$ and $PTB4$ (Figure 6.1). The electron-withdrawing ester group in both $PTB2$ and $PTB4$ is introduced to stabilize the electron-rich thieno[3,4-b]thiophene moiety.[45][154][155] The benzo[1,2-b:4,5-b']dithiophene unit can provide extended conjugated system and enhanced solubility due to its proper side chain pattern. Previous studies have revealed high power conversion efficiency based on theses polymers.[133] It should be noted in Scheme 6.1 that the A and B structures can exhibit intra-molecular "Donor-Acceptor" interaction caused by electron-withdrawing side-groups which can enhance exciton dissociation and charge transport by affecting the development of interpenetrating bulk-heterojunction morphological structures when mixing with electron acceptor $PCBM$. Moreover, the strong electron withdrawing fluorine side-group in $PTB4$ can further enhance the intra-molecular "Donor-Acceptor" interaction due to its high electronegativity.

Figure 6.2a shows the low-field MFE_{PC} ($< 150\ mT$) for the pristine $P3HT$, $PTB2$, and $PTB4$ devices with the ITO/PEDOT/Polymer/Ca/Al architecture. The $P3HT$ device shows both positive and negative components in low-field MFE_{PC}. Interestingly, the $PTB2$ and $PTB4$ devices only exhibit a flat low-field MFE_{PC}. It should be particularly pointed out that the pristine $PTB2$ and $PTB4$ are equivalent to 5 wt% $PCBM$ doped $P3HT$ in the low-field regime with flat MFE_{PC} (Figure 6.2b). We know that the low-field MFE_{PC} can, in general, include both positive and negative components through dissociation and charge reaction in pristine polymers.[85][86] Figure 6.2a schematically shows that the positive component at low-field MFE_{PC} arises from the dissociation of polaron pairs in pristine polymers[33][34][85] based on the following three experimental arguments.

First, an external magnetic field can change the singlet-triplet intersystem crossing in polaron-pair states by perturbing the spin momentum conservation and consequently modifying the singlet and triplet ratios[33][35][85][126][148][149] when applied magnetic field is comparable to the internal magnetic interaction generated from hyperfine interaction or from spin-orbital coupling in polaron-pair states. Second, magnetic field dependence of photoluminescence (MFE_{PL}) in exciplexes has suggested that changing the intersystem crossing can lead to an increase in singlet ratio in polaron-pair states.[38][88] Third, increasing singlet ratio in polaron-pair states can increase the photocurrent and consequently generate a positive low-field MFE_{PC}, because singlets and triplets have relatively high and low dissociation rates through Onsager process[90] due to their different ionic natures in their wavefunctions.[32][91] Therefore, increasing the singlet ratio in polaron-pair states can increase the photocurrent, leading to a positive component in low-field MFE_{PC}.

On the other hand, the negative component in low-field MFE_{PC} can also be generated when photoexcited excitons react with charge carriers through Coulomb interaction, generating exciton-charge reaction with the consequence of separating excitons into

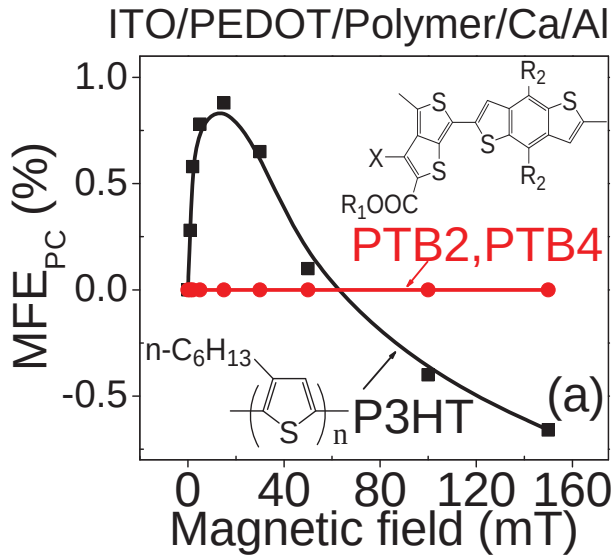

(a) Low-field MFE_{PC} in pristine forms

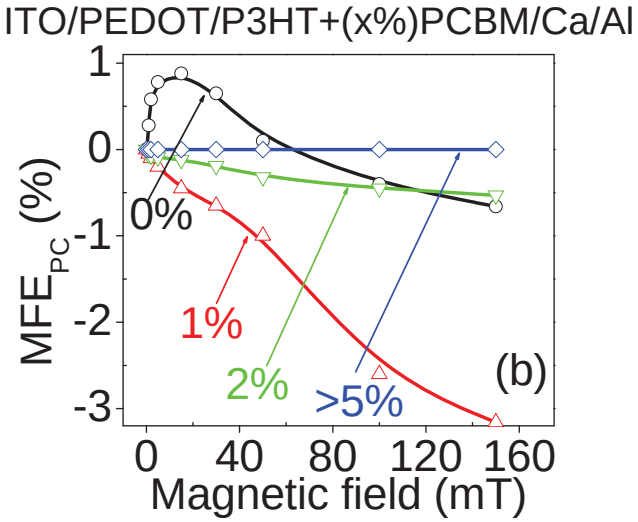

(b) Low-field MFE_{PC} for $P3HT$ with doped $PCBM$

Figure 6.2: (a): low-field MFE_{PC} for the $P3HT$, $PTB2$, and $PTB4$ in their pristine forms with the device structure of $ITO/PEDOT/Polymer/Ca/Al$. The inset shows the chemical structures for the $P3HT$, $PTB2$, and $PTB4$. The side groups are $X = H$, $R1 = 2-ethylhexyl$, $R2 = n-octyloxy$ for the $PTB2$, and $X = F$, $R1 = n-octyl$, $R2 = 2-ethylhexyloxy$ for $PTB4$. (b): Low-field MFE_{PC} for lightly doped $P3HT$ with different $PCBM$ concentrations. The doping concentrations were given by weight percent.

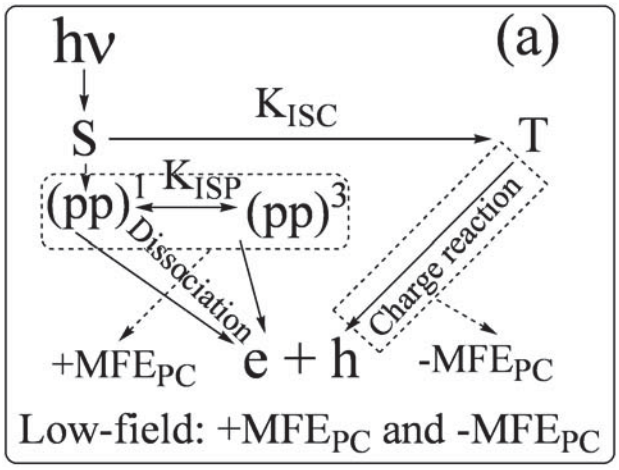

(a) Singlet dissociation and triplet-charge reaction generate + MFE_{PC} and - MFE_{PC}

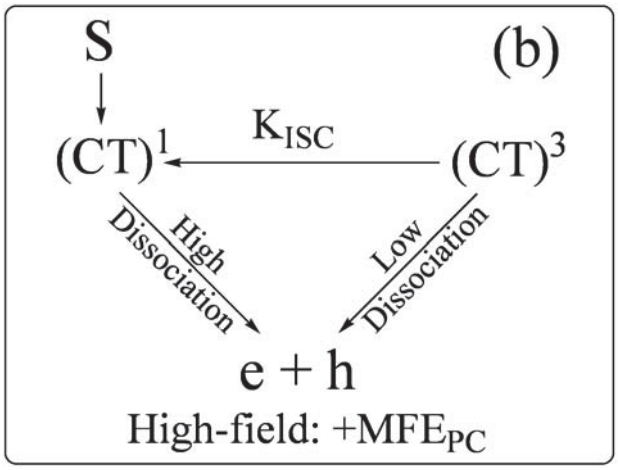

(b) Dissociation of CT complexes generates + MFE_{PC}

Figure 6.3: Schematic diagrams for low-field and high-field MFE_{PC}: (a): Singlet dissociation and triplet-charge reaction generate + MFE_{PC} and - MFE_{PC} at low field ($< 150\ mT$). (b): Dissociation of CT complexes generates + MFE_{PC} at high field ($> 150\ mT$).

free charge carriers.[34][36][85][89] Indeed, the exciton-charge reaction can occur with free carriers,[94][127] or with trapped carriers,[94][145] or with the electrode.[94] In essence, the exciton-charge reaction is determined by the contact probabilities between an exciton and a charge. Although both singlet and triplet excitons can react with charge carriers through Coulomb interaction, the triplet excitons can dominate the exciton-charge reaction in organic materials due to their long lifetimes.[40][94][99] In particular, a magnetic field can reduce the triplet exciton-charge reaction-rate constants by perturbing the spin-spin interaction between a triplet exciton and a charge, consequently leading to a reduction in photocurrent and generating a negative component in low-field MFE_{PC} in pristine polymers.[32][85] Therefore, positive and negative components in low-field MFE_{PC} can reflect the dissociation in polaron-pair states and the charge reaction in excitonic states in the generation of photocurrent in pristine polymers. We note in Figure 6.2b that lightly doped $P3HT$ with the $PCBM$ at 1 wt% concentration can remove the positive MFE_{PC} but keeps the negative MFE_{PC} at low field. This indicates that the weak donor-acceptor interaction introduced by low $PCBM$ doping can dissociate the polaron pairs but leaves the triplet exciton-charge reaction unchanged in the $P3HT$. However, increasing the $PCBM$ concentration to 5 wt% can lead to a flat MFE_{PC} by removing both positive and negative components. In addition, it has been found that 5 wt% $PCBM$ doping can largely quench the photoluminescence (PL) from the $P3HT$ by 78% in solid films.[156] This PL quenching suggests that the 5 wt% $PCBM$ doping can significantly dissociate excitons in the $P3HT$. Therefore, the flat low-field MFE_{PC} at low field implies that the $P3HT : PCBM$ composite with 5 wt% $PCBM$ doping can destroy both the polaron pairs and exciton-charge reaction. This experimental result confirms that the 5 wt% $PCBM$ doping can generate significant charge dissociation in the $P3HT$. By comparing the pristine $PTB2$ and $PTB4$ with the 5 wt% $PCBM$ doped $P3HT$, we can clearly see in Figure 6.2a and 6.2b that the pristine $PBT2$ and $PTB4$ exhibit considerable intra-molecular "Donor-Acceptor" interaction, which is similar to the externally introduced donor-acceptor

interaction in the 5 wt% $PCBM$ doped $P3HT$. Our studies on MFE_{PC} at low field ($< 150\ mT$) reveal that the pristine $PTB2$ and $PTB4$ can generate significant charge dissociation due to the intra-molecular "Donor-Acceptor" interaction, similar to the 5 wt% $PCBM$ doped $P3HT$. On one hand, this intra-molecular "Donor-Acceptor" interaction yields a flat low-field MFE_{PC} in their pristine forms. On the other hand, this intra-molecular "Donor-Acceptor" may reduce the binding energies of CT states, shown in high-field MFE_{PC}, when the $PTB2$ and $PTB4$ are mixed with the $PCBM$ to form heterojunction solar cells. We should note that the enhanced intra-molecular electrical polarization has been used to shift electronic levels towards the improvement of photovoltaic responses based on "push-pull" donor and acceptor blocks.[157][158][159][160][161] In addition, early experimental results have also indicated that intra-molecular "Donor-Acceptor" interaction can enhance charge dissociation to generate photoconduction in organic materials.[162][163] Now we discuss the effects of intra-molecular "Donor-Acceptor" interaction on the dissociation of CT complexes when the $PTB2$ and $PTB4$ are mixed with $PCBM$ to form bulk-heterojunction solar cells. The experimental results on photoinduced absorption, photoluminescence, and electroluminescence have shown that in bulk-heterojunction solar cells the dissociated electrons and holes undergo inter-molecular CT complexes to generate photocurrent.[73][76][77][120][164][165][166] Our theoretical consideration shows that the dissociation is essentially determined by the kinetic energy and Coulomb attraction of electrons and holes at donor-acceptor interfaces. More importantly, we found that the dissociation of CT complexes can generate high-field MFE_{PC}.[85][86] Figure 6.3b schematically indicates that the generation of high-field MFE_{PC} is based on the following three experimental evidences. First, photophysics studies have suggested that the CT complexes are formed with both singlet and triplet states through geminate and non-geminate capture of dissociated electrons and holes at donor-acceptor interfaces when electron spin multiplicities are considered.[100][167] Second, an external magnetic field can change the singlet and triplet ratios in the CT complexes by perturbing the intersystem crossing[101][151] through spin momentum

conservation in competition with internal magnetic field generated from spin-orbital coupling or hyperfine interaction, similar to magnetic field-dependent intersystem crossing in polaron-pair states. Third, the singlet and triplet CT complexes can have high and low dissociation rates in bulk-heterojunctions, respectively, similar to the phenomenon occurring in polaron pairs in pristine polymers,[88][91][151] due to their different ionic natures involved in Onsager process-driven dissociation.[90] Here, we combine MFE_{PC} and electric field, namely $V - MFE_{PC}$, to characterize the binding energies of CT complexes formed at donor:acceptor interfaces in the $PTB2 : PCBM$ and $PTB4 : PCBM$ solar cells as compared to the $P3HT : PCBM$ device.

Figure 6.4a and 6.4b indicate that both $PTB2 : PCBM$ and $P3HT : PCBM$ bulk-heterojunction solar cells show strong positive signals in high-field MFE_{PC}. This confirms that the dissociated charge carriers form the CT complexes at the donor:acceptor interfaces towards the generation of photocurrent in bulk-heterojunction organic solar cells. However, it can be seen in Figure 6.4b that the applied reverse bias of 2 V can completely remove the high-field MFE_{PC} in the $PTB2 : PCBM$ solar cell. On contrast, this reverse bias of -2 V can only quench the high-field MFE_{PC} by 26% in the $P3HT : PCBM$ solar cell (Figure 6.4a). The $V - MFE_{PC}$ result clearly suggests that the CT complexes in $PTB2 : PCBM$ device have lower binding energies than that in the $P3HT : PCBM$ device. The lower binding energies of CT complexes suggest that the intra-molecular "Donor-Acceptor" interaction can form strong local electric fields with the electron acceptor $PCBM$ molecules to overcome the Coulomb attraction at $PTB2 : PCBM$ interfaces for charge dissociation. We should note in Figure 6.4c that the $PTB4 : PCBM$ solar cell shows un-appreciable high-field MFE_{PC}.

This un-appreciable MFE_{PC} indicates that the electrons and holes do not form considerable CT complexes at $PTB4 : PCBM$ interfaces. This result implies that the CT complexes have much lower binding energies at $PTB4 : PCBM$ interfaces

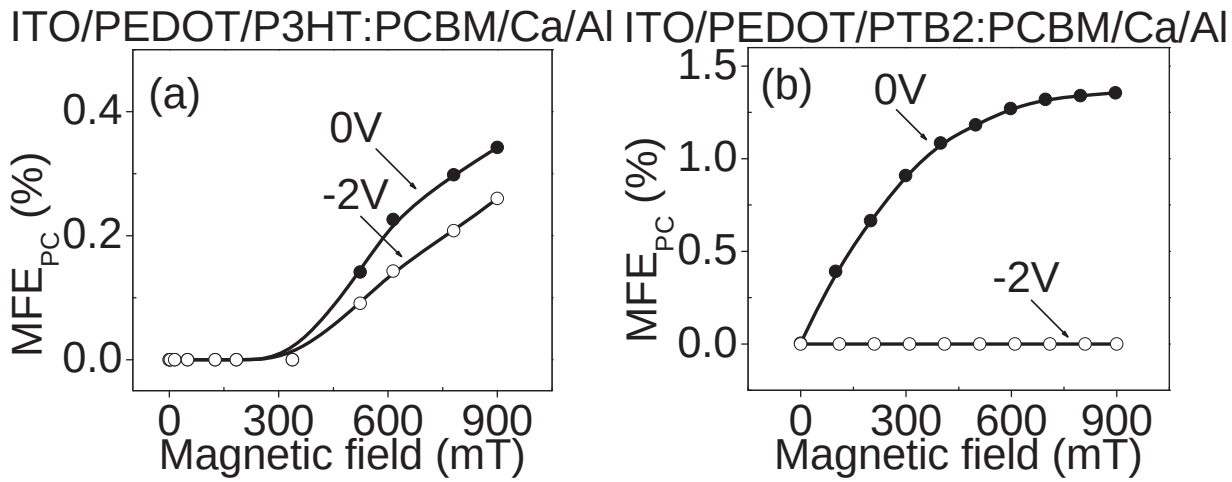

(a) High-field MFE_{PC} for $P3HT : PCBM$ solar cell**(b)** High-field MFE_{PC} for $PTB2 : PCBM$ solar cell

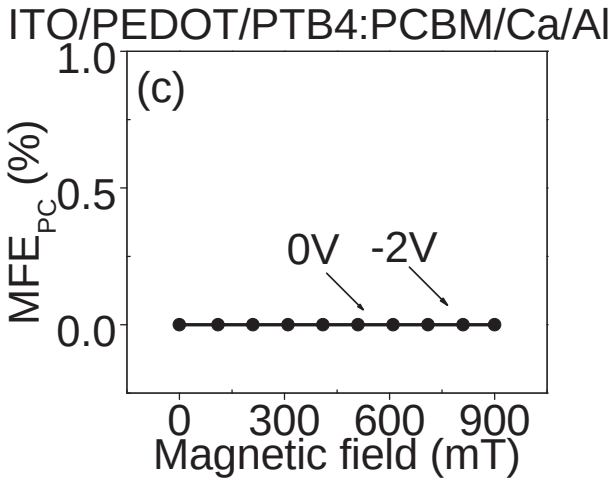

(c) High-field MFE_{PC} for $PTB4 : PCBM$ solar cell

Figure 6.4: High-field MFE_{PC} with applied reverse bias of - 2 V for the $P3HT$, $PTB2$, and $PTB4$ based bulk-heterojunction solar cells: (a): $P3HT : PCBM$ solar cell. (b): $PTB2 : PCBM$ solar cell. (c): $PTB4 : PCBM$ solar cell.

and consequently lead to higher photovoltaic efficiency in the $PTB4:PCBM$ solar cell. Here, we suggest that the strong electron-withdrawing fluorine side-group is responsible for the reduced binding energies of CT complexes at the $PTB4:PCBM$ interfaces. Photovoltaic studies have also found that the incorporation of fluorine in the polymer backbone can play an important role for the high-performance organic solar cells.[168][169] Nevertheless, our $V-MFE_{PC}$ results indicate that intra-molecular "Donor-Acceptor" interaction can reduce the binding energies of CT complexes when photovoltaic PTB derivatives are mixed with electron acceptor $PCBM$ to form bulk-heterojunction solar cells. Now we discuss the charge transport and collection through donor and acceptor interpenetrating networks in the $PTB2:PCBM$ and $PTB4:PCBM$ solar cells. It is known from polymer thermodynamics that the formation of morphological interpenetrating networks is mainly driven by the intermolecular interaction in polymer blends.[170][171] Therefore, the intra-molecular "Donor-Acceptor" interaction may enhance the formation of PTB derivative and $PCBM$ interpenetrating morphological structures, when the PTB derivative and $PCBM$ are mixed to form bulk heterojunction solar cells, and consequently increasing the charge transport. Here, we use light-assisted dielectric response: LADR, where the capacitance is measured at the frequency of 1 KHz under photoexcitation (Figure 6.5a), to characterize the charge transport through PTB derivative and $PCBM$ interpenetrating networks in the $PTB2$ and $PTB4$ based solar cells as compared to the $P3HT:PCBM$ device.

It should be noted that this frequency of 1 KHz is largely below the RC response time of our solar cells. The $LADR$ results in Figure 6.5b show three important information. First, under dark condition the $PTB2:PCBM$ and $PTB4:PCBM$ solar cells exhibit a lager capacitance than the $P3HT:PCBM$ device. This implies that the $PTB2:PCBM$ and $PTB4:PCBM$ films have a higher dielectric constant relative to the $P3HT:PCBM$ film. This higher dielectric constant further indicates that the $PTB2:PCBM$ and $PTB4:PCBM$ bulk heterojunctions have stronger

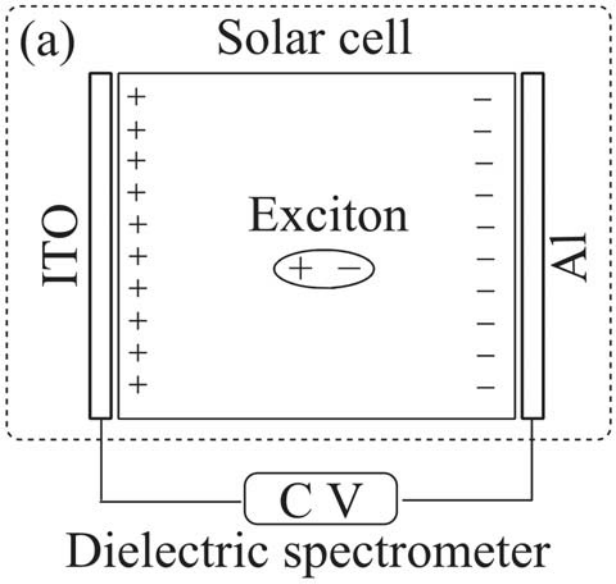

(a) Schematic diagram for LADR setup

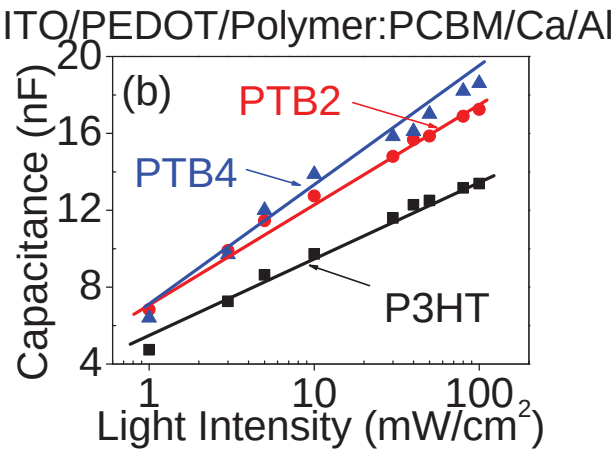

(b) LADR results

Figure 6.5: Light-assisted dielectric response (LADR) setup and results: (a): Schematic diagram for LADR setup. (b): LADR results for $P3HT : PCBM$, $PTB2 : PCBM$, and $PTB4 : PCBM$ solar cells.

local electrical fields from intra-molecular "Donor-Acceptor" interactions, which are accountable for the lower binding energies of CT complexes in the $PTB2$ and $PTB4$ based solar cells. Second, at a given photoexcitation intensity the $PTB2 : PCBM$ and $PTB4 : PCBM$ solar cells show higher capacitances as compared to the $P3HT : PCBM$ device. This result suggests that the photoexcitation leads to more charge collection at the respective electrodes in the $PTB2 : PCBM$ and $PTB4 : PCBM$ solar cells relative to the $P3HT : PCBM$ device. Third, the $PTB2 : PCBM$ and $PTB4 : PCBM$ solar cells have a larger increase-rate in the capacitance-photoexcitation characteristics than the $P3HT : PCBM$ device. This indicates that the $PTB2 : PCBM$ and $PTB4 : PCBM$ solar cells form more effective charge-transport channels to transport dissociated charge carriers to respective electrodes through the donor-acceptor interpenetrating networks. Especially, using stronger electron-withdrawing fluorine side-group can lead to a larger increase-rate in capacitance-photoexcitation characteristics in the $PTB4 : PCBM$ solar cell as compared to the $PTB2 : PCBM$ solar cell. This implies that stronger intra-molecular "Donor-Acceptor" interaction can enhance the charge transport and collection when the $PTB4$ is mixed with $PCBM$ to form bulk-heterojunction solar cell.

It can be seen in Figure 6.6 that the PTB derivatives-based solar cell shows larger photocurrents based on intra-molecular "Donor-Acceptor" interaction as compared to the $P3HT : PCBM$ device. Further increasing intra-molecular "Donor-Acceptor" interaction by using strong electron-withdrawing fluorine side-group can lead to a more efficient photovoltaic performance in the $PTB4 : PCBM$ solar cell. Therefore, we can confirm that intra-molecular "Donor-Acceptor" interaction can indeed enhance charge dissociation, transport, and collection towards the generation of photocurrent in the bulk-heterojunction solar cells.

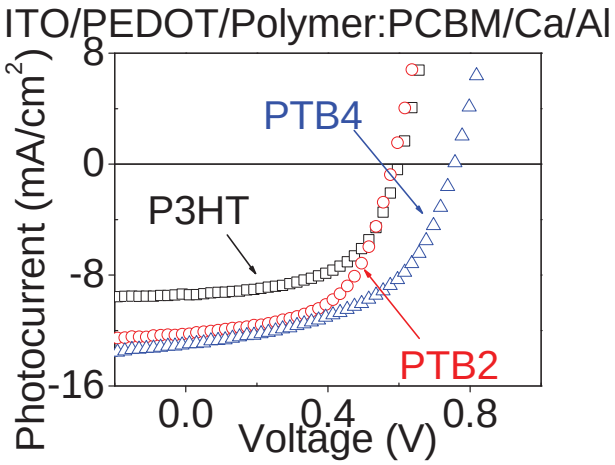

Figure 6.6: Photocurrent-voltage characteristics for $P3HT : PCBM$, $PTB2 : PCBM$ and $PTB4 : PCBM$ solar cells under the simulated sunlight illumination of 100 mW/cm^2.

6.4 Conclusion

In summary, the low-field MFE_{PC} reveals that the newly synthesized photovoltaic polymer $PTB2$ and $PTB4$ exhibit intra-molecular "Donor-Acceptor" interaction in their pristine forms. In particular, this intra-molecular "Donor-Acceptor" interaction in the pristine $PTB2$ and $PTB4$ is equivalent to the externally introduced donor-acceptor interaction in 5 wt% $PCBM$ doped $P3HT$ for charge dissociation. The high-field MFE_{PC} together with applied electric field indicates that the CT complexes in the PTB derivatives-based solar cells have much lower binding energies as compared to the $P3HT : PCBM$ device towards the generation of photocurrent. Furthermore, the light-assisted dielectric response: LADR indicates that when the $PTB2$ and $PTB4$ are mixed with the $PCBM$ to form bulk-heterojunctions, the charge transport and collection are more effective through donor and acceptor interpenetrating networks to generate photocurrent. Therefore, it can be suggested that the intra-molecular "Donor-Acceptor" interaction plays an important role to reduce the binding energies of CT complexes for charge dissociation and to enhance the charge transport and collection in bulk-heterojunction organic solar cells.

Chapter 7

CONCLUSIONS

The magnetic, optical and dielectric effect were studied toward the organic photovoltaics in this dissertation. The research includes the following three parts.

First, the origin of the open circuit voltage of bulk heterojunction solar cell was systematically studied, including the change of cathode, active layer thickness, donor material, and the modification the donor/acceptor weight ratio, etc. It was found that the open circuit voltage is mainly determined by the energy difference between HOMO of donor and LUMO of acceptor which is consistent with the published results by many groups. However, it was also found that the effective dielectric background of the heterojunction also can affect the open circuit voltage, which may not have been paid enough attention. Moreover, the photo-assisted impedance spectroscopy analysis was utilized to study the charge accumulation effect on the open circuit voltage in $P3HT : PCBM$ solar cells.

Second, the magnetic field effect on photocurrent change was studied in both pristine polymer, bulk heterojunction and double layer architecture based photovoltaic devices. It was found that in the heavily studied polymer material $P3HT$, the positive photocurrent change under external magnetic field is due to the change

of singlet/triplet polaron pair ratio through intersystem crossing together with the consideration of higher dissociation rate of singlet state due to its stronger ionic nature. The negative photocurrent change can be associated with the magnetic field depended triplet and charge reaction processes. For bulk heterojunction and double layer structure devices, it was found that the charge transfer complexes exist at the donor and accepter interfaces. The formation of the charge transfer complexes essentially form a loss channel towards the generation of free charge carriers. By combining the magnetic field effect on photocurrent change and the reversed bias electric field, the binding energy of charge transfer complex can be qualitatively studied between different systems or under different post treatment methods. Particularly, in double layer structure $P3HT/TiO_x$ photovoltaic device, the photocurrent change under magnetic field was studied under illumination with different wavelengths. It was found that the MFE_{PC} decreases with decreasing of excitation wavelength, and the results support the argument of the exist of hot exciton and also provide detailed information towards the internal photovoltaic processes of exciton dissociation and free charge generation.

Third, the "intra-molecular" interaction effect was found in the new low band gap polymers (PTBs). It was found that the push-pull group in the polymer chain can facilitate the exciton dissociation and free charge generation. The magnetic field effect study on photocurrent change in pristine polymers $PTB2$ and $PTB4$ and the system of 5% doping of $PCBM$ in $P3HT$ reveals that the polymers $PTB2$ and $PTB4$ in their pristine form is essentially equivalent to the condition of 5% doping of $PCBM$ in $P3HT$. Moreover, the study indicates that the intra-molecular "Donor-Acceptor" interaction plays an important role in reducing the binding energies of CT complexes for charge dissociation and then enhancing the charge transport and collection in organic bulk-heterojunction photovoltaics.

Bibliography

Bibliography

[1] A. E. Becquerel. Mémoire sur les effets électriques produits sous l'influence des rayons solaires. *Comptes Rendus des Séances Hebdomadaires*, 9:561–567, 1839. 1

[2] D. M. Chapin, C. S. Fuller, and G. L. Pearson. A new silicon p-n junction photocell for converting solar radiation into electrical power. *Journal of Applied Physics*, 25(5):676–677, 1954. 1

[3] M. A. Green, K. Emery, D. L. King, S. Igari, and W. Warta. Short communication: Solar cell efficiency tables (version 25). *Progress in Photovoltaics: Research and Applications*, 13(1):49–54, 2005. 1

[4] M. A. Green. *Solar cells: operating principles, technology, and system applications*. Prentice-Hall series in solid state physical electronics. Prentice-Hall, 1982. 1

[5] W Shockley and H. J. Queisser. Detailed balance limit of efficiency of p-n junction solar cells. *Journal of Applied Physics*, 32(3):510–519, 1961. 1

[6] *European Photovoltaic Industry Association (2012). "Market Report 2011"*. 2012. 2

[7] G. Li, V. Shrotriya, J. S. Huang, Y. Yao, T. Moriarty, K. Emery, and Y. Yang. High-efficiency solution processable polymer photovoltaic cells by

self-organization of polymer blends. *Nature Materials*, 4(11):864–868, 2005. 2, 43, 52, 65

[8] J. Zou, H. Wu, C. S. Lam, C. Wang, J. Zhu, C. Zhong, S. Hu, C. L. Ho, G. J. Zhou, H. Wu, W. C. H. Choy, J. Peng, Y. Cao, and W. Y. Wong. Simultaneous optimization of charge-carrier balance and luminous efficacy in highly efficient white polymer light-emitting devices. *Advanced Materials*, 23(26):2976–2980, 2011. 2, 87

[9] A. J. Heeger, S. Kivelson, J. R. Schrieffer, and W. P. Su. Solitons in conducting polymers. *Reviews of Modern Physics*, 60(3):781–850, 1988. 3

[10] A. J. Heeger. Semiconducting polymers: the third generation. *Chemical Society Reviews*, 39(7):2354–2371, 2010. 3

[11] A. Kohler and D. Beljonne. The singlet-triplet exchange energy in conjugated polymers. *Advanced Functional Materials*, 14(1):11–18, 2004. 11

[12] A. Köhler. The singlet-triplet energy gap in organic and pt-containing phenylene ethynylene polymers and monomers. *J. Chem. Phys.*, 116(21):9457, 2002. 11

[13] J. L. Brédas, J. Cornil, and A. J. Heeger. The exciton binding energy in luminescent conjugated polymers. *Advanced Materials*, 8(5):447–452, 1996. 11, 52, 72, 88

[14] V.M. Agranovich. *Excitations in Organic Solids*. International Series of Monographs on Physics. Oxford University Press, 2009. 12

[15] D.J. Griffiths. *Introduction to quantum mechanics*. Pearson Prentice Hall, 2005. 13, 14, 16

[16] M. Klessinger and J. Michl. *Excited states and photochemistry of organic molecules*. VCH, 1995. 14, 16

[17] D. R. Arnold. *Photochemistry: an introduction*. Academic Press rapid manuscript reproductions. Academic Press, 1974. 14, 16

[18] H. D. Burrows, J. Seixas de Melo, C. Serpa, L. G. Arnaut, M. da G. Miguel, A. P. Monkman, I. Hamblett, and S. Navaratnam. Triplet state dynamics on isolated conjugated polymer chains. *Chemical Physics*, 285(1):3–11, 2002. 15

[19] Igor V. Khudyakov, Yuri A. Serebrennikov, and Nicholas J. Turro. Spin-orbit coupling in free-radical reactions: on the way to heavy elements. *Chemical Reviews*, 93(1):537–570, 1993. 15

[20] V. Prigodin, J. Bergeson, D. Lincoln, and A. Epstein. Anomalous room temperature magnetoresistance in organic semiconductors. *Synthetic Metals*, 156(9-10):757–761, 2006. 15

[21] S. Difley, D. Beljonne, and T. Van Voorhis. On the singlet-triplet splitting of geminate electron-hole pairs in organic semiconductors. *Journal of the American Chemical Society*, 130(11):3420–3427, 2008. 17

[22] V. Dyakonov and E. Frankevich. On the role played by polaron pairs in photophysical processes in semiconducting polymers. *Chemical Physics*, 227(1-2):203–217, 1998. 18

[23] G. Yu, J. Gao, J. C. Hummelen, F. Wudl, and A. J. Heeger. Polymer photovoltaic cells - enhanced efficiencies via a network of internal donor-acceptor heterojunctions. *Science*, 270(5243):1789–1791, 1995. 18, 52, 72

[24] C. J. Brabec, A. Cravino, D. Meissner, N. S. Sariciftci, T. Fromherz, M. T. Rispens, L. Sanchez, and J. C. Hummelen. Origin of the open circuit voltage of plastic solar cells. *Advanced Functional Materials*, 11(5):374–380, 2001. 19

[25] C. M. Ramsdale, J. A. Barker, A. C. Arias, J. D. MacKenzie, R. H. Friend, and N. C. Greenham. The origin of the open-circuit voltage in polyfluorene-based photovoltaic devices. *Journal of Applied Physics*, 92(8):4266–4270, 2002. 19

[26] X. Deng, L. Zheng, C. Yang, Y. Li, G. Yu, and Y. Cao. Polymer photovoltaic devices fabricated with blend mehppv and organic small molecules. *The Journal of Physical Chemistry B*, 108(11):3451–3456, 2004. 19

[27] A. Gadisa, M. Svensson, M. R. Andersson, and O. Inganäs. Correlation between oxidation potential and open-circuit voltage of composite solar cells based on blends of polythiophenes/ fullerene derivative. *Applied Physics Letters*, 84(9):1609–1611, 2004. 19

[28] J. S. Kim, J. H. Park, J. H. Lee, J. Jo, D. Y. Kim, and K. Cho. Control of the electrode work function and active layer morphology via surface modification of indium tin oxide for high efficiency organic photovoltaics. *Applied Physics Letters*, 91(11):112111–3, 2007. 19

[29] H. L. Yip, S. K. Hau, N. S. Baek, H. Ma, and A. K. Y. Jen. Polymer solar cells that use self-assembled-monolayer-modified zno/metals as cathodes. *Advanced Materials*, 20(12):2376–2382, 2008. 19

[30] D. Veldman, S. C. J. Meskers, and R. A. J. Janssen. The energy of charge-transfer states in electron donor-acceptor blends: Insight into the energy losses in organic solar cells. *Advanced Functional Materials*, 19(12):1939–1948, 2009. 19, 45

[31] K. Vandewal, A. Gadisa, W. D. Oosterbaan, S. Bertho, F. Banishoeib, I. Van Severen, L. Lutsen, T. J. Cleij, D. Vanderzande, and J. V. Manca. The relation between open-circuit voltage and the onset of photocurrent generation by charge-transfer absorption in polymer: Fullerene bulk heterojunction solar cells. *Advanced Functional Materials*, 18(14):2064–2070, 2008. 19

[32] U. E. Steiner and T. Ulrich. Magnetic-field effects in chemical-kinetics and related phenomena. *Chemical Reviews*, 89(1):51–147, 1989. 19, 53, 54, 76, 91, 94

[33] E. L. Frankevich, A. A. Lymarev, I. Sokolik, F. E. Karasz, S. Blumstengel, R. H. Baughman, and H. H. Horhold. Polaron-pair generation in poly(phenylene vinylenes). *Physical Review B*, 46(15):9320–9324, 1992. 19, 52, 53, 54, 88, 91

[34] Zakhidov A. Yoshino K. Maruyama Y. Frankevich, E. and K. Yakushi. Photoconductivity of poly(2,5-diheptyloxy-p-phenylene vinylene) in the air atmosphere: Magnetic-field effect and mechanism of generation and recombination of charge carriers. *Phys Rev B Condens Matter*, 53(8):4498–4508, 1996. 19, 52, 53, 76, 91, 94

[35] J. Kalinowski, M. Cocchi, D. Virgili, P. Di Marco, and V. Fattori. Magnetic field effects on emission and current in alq3-based electroluminescent diodes. *Chemical Physics Letters*, 380(5-6):710–715, 2003. 20, 54, 74, 76, 89, 91

[36] I. V. Tolstov, A. V. Belov, M. G. Kaplunov, I. K. Yakuschenko, N. G. Spitsina, M. M. Triebel, and E. L. Frankevich. On the role of magnetic field spin effect in photoconductivity of composite films of meh-ppv and nanosized particles of pbs. *Journal of Luminescence*, 112(1-4):368–371, 2005. 20, 52, 53, 76, 89, 94

[37] Ikoma T. Akiyama K. Kobori Y. Ito, F. and S. Tero-Kubota. Long-range jump versus stepwise hops: magnetic field effects on the charge-transfer fluorescence from photoconductive polymer films. *Journal of the American Chemical Society*, 125(16):4722–3, 2003. 20, 52, 88

[38] Ikoma T. Akiyama K. Watanabe A. Ito, F. and S. Tero-Kubota. Carrier generation process on photoconductive polymer films as studied by magnetic field effects on the charge-transfer fluorescence and photocurrent. *Journal of Physical Chemistry B*, 109(18):8707–17, 2005. 20, 52, 74, 76, 91

[39] P. Desai, P. Shakya, T. Kreouzis, W. P. Gillin, N. A. Morley, and M. R. J. Gibbs. Magnetoresistance and efficiency measurements of al q3 -based oleds. *Physical Review B*, 75(9):094423, 2007. 20, 76

[40] P. Desai, P. Shakya, T. Kreouzis, and W. Gillin. Magnetoresistance in organic light-emitting diode structures under illumination. *Physical Review B*, 76(23):235202, 2007. 20, 94

[41] P. Shakya, P. Desai, T. Kreouzis, W. P. Gillin, S. M. Tuladhar, A. M. Ballantyne, and J. Nelson. The effect of applied magnetic field on photocurrent generation in poly-3-hexylthiophene:[6,6]-phenyl c61-butyric acid methyl ester photovoltaic devices. *Journal of Physics: Condensed Matter*, 20(45):452203, 2008. 20, 52, 66, 79, 89

[42] P. W. M. Blom, V. D. Mihailetchi, L. J. A. Koster, and D. E. Markov. Device physics of polymer : fullerene bulk heterojunction solar cells. *Advanced Materials*, 19(12):1551–1566, 2007. 22, 36, 48

[43] B. P. Rand, D. P. Burk, and S. R. Forrest. Offset energies at organic semiconductor heterojunctions and their influence on the open-circuit voltage of thin-film solar cells. *Physical Review B*, 75(11), 2007. 25, 52, 72

[44] H. Al-Dmour and D. M. Taylor. Revisiting the origin of open circuit voltage in nanocrystalline-tio[sub 2]/polymer heterojunction solar cells. *Applied Physics Letters*, 94(22):223309, 2009. 29

[45] Y. Y. Liang, S. Q. Xiao, D. Q. Feng, and L. P. Yu. Control in energy levels of conjugated polymers for photovoltaic application. *Journal of Physical Chemistry C*, 112(21):7866–7871, 2008. 29, 90

[46] M. Estrada, I. Mejia, A. Cerdeira, and B. Iñiguez. Polymeric tfts using pmma on p3ht layers. *Solid State ElectronSolid State Electron*, 52(2):53, 2008. 29

[47] V. D. Mihailetchi, J.K.J. van Duren, P.W.M. Blom, J.C. Hummelen, R.A.J. Janssen, J.M. Kroon, M.T. Rispens, W.J.H. Verhees, and M.M. Wienk. Electron transport in a methanofullerene. *Advanced Functional Materials*, 13(1):43–46, 2003. 29

[48] D. Veldman, O. Ipek, S.C.J. Meskers, J. Sweelssen, M.M. Koetse, S.C. Veenstra, J.M. Kroon, S.S. Bavel, J. Loos, and R.A.J. Janssen. Compositional and electric field dependence of the dissociation of charge transfer excitons in alternating polyfluorene copolymer/fullerene blends. *Journal of the American Chemical Society*, 130(24):7721–7735, 2008. 29

[49] Y. Kim, S. Cook, S. M. Tuladhar, S. A. Choulis, J. Nelson, J. R. Durrant, D. D. C. Bradley, M. Giles, I. McCulloch, C. S. Ha, and M. Ree. A strong regioregularity effect in self-organizing conjugated polymer films and high-efficiency polythiophene:fullerene solar cells. *Nature Materials*, 5(3):197–203, 2006. 31

[50] H. Hoppe and N. S. Sariciftci. Morphology of polymer/fullerene bulk heterojunction solar cells. *Journal of Materials Chemistry*, 16(1):45, 2006. 31, 32

[51] T. Erb, U. Zhokhavets, G. Gobsch, S. Raleva, B. Sthn, P. Schilinsky, C. Waldauf, and C. J. Brabec. Correlation between structural and optical properties of composite polymer/fullerene films for organic solar cells. *Advanced Functional Materials*, 15(7):1193–1196, 2005. 31, 32, 65

[52] X. N. Yang, J. Loos, S. C. Veenstra, W. J. H. Verhees, M. M. Wienk, J. M. Kroon, M. A. J. Michels, and R. A. J. Janssen. Nanoscale morphology of high-performance polymer solar cells. *Nano Letters*, 5(4):579–583, 2005. 32, 65, 88, 89

[53] S. L. M. van Mensfoort and R. Coehoorn. Determination of injection barriers in organic semiconductor devices from capacitance measurements. *Physical Review Letters*, 100(8):086802, 2008. 39

[54] T. F. Guo, T. C. Wen, G. L. Pakhomov, X. G. Chin, S. H. Liou, P. H. Yeh, and C. H. Yang. Effects of film treatment on the performance of poly(3-hexylthiophene)/soluble fullerene-based organic solar cells. *Thin Solid Films*, 516(10):3138–3142, 2008. 41

[55] J. Liu, Y. Shi, and Y. Yang. Solvation-induced morphology effects on the performance of polymer-based photovoltaic devices. *Advanced Functional Materials*, 11(6):420–424, 2001. 41

[56] P. Vanlaeke, A. Swinnen, I. Haeldermans, G. Vanhoyland, T. Aernouts, D. Cheyns, C. Deibel, J. Dhaen, P. Heremans, and J. Poortmans. P3ht/pcbm bulk heterojunction solar cells: Relation between morphology and electro-optical characteristics. *Solar Energy Materials and Solar Cells*, 90(14):2150–2158, 2006. 41

[57] McNeill C. R. Abrusci A. Marsh, R. A. A unified description of currentcvoltage characteristics in organic and hybrid photovoltaics under low light intensity. *Nano Letters*, 8(5):1393–1398, 2008. 43

[58] T. M. Clarke, A. M. Ballantyne, J. Nelson, D. D. C. Bradley, and J. R. Durrant. Free energy control of charge photogeneration in polythiophene/fullerene solar cells: The influence of thermal annealing on p3ht/pcbm blends. *Advanced Functional Materials*, 18(24):4029–4035, 2008. 44, 65, 82, 88

[59] M. Al-Ibrahim. Flexible large area polymer solar cells based on poly(3-hexylthiophene)/fullerene. *Solar Energy Materials and Solar Cells*, 85(1):13–20, 2004. 44

[60] S. Sensfuss, M. Al-Ibrahim, A. Konkin, G. Nazmutdinova, U. Zhokhavets, G. Gobsch, D. A. M. Egbe, E. Klemm, and H. K. Roth. Characterisation of potential donor acceptor pairs for polymer solar cells by esr, optical and

electrochemical investigations. *Proceedings of SPIE (San Diego, August 2003)*, 5215:129–140, 2003. 44

[61] V. D. Mihailetchi, H. X. Xie, B. de Boer, L. J. A. Koster, and P. W. M. Blom. Charge transport and photocurrent generation in poly (3-hexylthiophene): Methanofullerene bulk-heterojunction solar cells. *Advanced Functional Materials*, 16(5):699–708, 2006. 44, 45, 65, 67, 82

[62] P. C. Rusu, G. Giovannetti, C. Weijtens, R. Coehoorn, and G. Brocks. Work function pinning at metal-organic interfaces. *Journal of Physical Chemistry C*, 113(23):9974–9977, 2009. 48

[63] N. S. Sariciftci, L. Smilowitz, A. J. Heeger, and F. Wudl. Photoinduced electron-transfer from a conducting polymer to buckminsterfullerene. *Science*, 258(5087):1474–1476, 1992. 52, 72, 88

[64] M. Granstrom, K. Petritsch, A. C. Arias, A. Lux, M. R. Andersson, and R. H. Friend. Laminated fabrication of polymeric photovoltaic diodes. *Nature*, 395(6699):257–260, 1998. 52

[65] S. E. Shaheen, C. J. Brabec, N. S. Sariciftci, F. Padinger, T. Fromherz, and J. C. Hummelen. 2.5 *Applied Physics Letters*, 78(6):841–843, 2001. 52

[66] J. G. Xue, S. Uchida, B. P. Rand, and S. R. Forrest. 4.2resistances. *Applied Physics Letters*, 84(16):3013–3015, 2004. 52

[67] F. Zhang, W. Mammo, L. M. Andersson Andersson, S. M. R. Andersson Admassie, and Olle Inganäs. Low-bandgap alternating fluorene copolymer/methanofullerene heterojunctions in efficient near-infrared polymer solar cells. *Advanced Materials*, 18(16):2169–2173, 2006. 52

[68] J. Y. Kim, K. Lee, N. E. Coates, D. Moses, T. Q. Nguyen, M. Dante, and A. J. Heeger. Efficient tandem polymer solar cells fabricated by all-solution processing. *Science*, 317(5835):222–225, 2007. 52, 60

[69] F. Huang, K. S. Chen, H. L. Yip, S. K. Hau, O. Acton, Y. Zhang, J. Luo, and A. K. Y. Jen. Development of new conjugated polymers with donor pi bridge acceptor side chains for high performance solar cells. *Journal of the American Chemical Society*, 131(39):13886–13887, 2009. 52

[70] L. M. Blinov, S. P. Palto, G. Ruani, C. Taliani, A. A. Tevosov, S. G. Yudin, and R. Zamboni. Location of charge transfer states in [alpha]-sexithienyl determined by the electroabsorption technique. *Chemical Physics Letters*, 232(4):401–406, 1995. 52, 72, 88

[71] S. F. Alvarado, P. F. Seidler, D. G. Lidzey, and D. D. C. Bradley. Direct determination of the exciton binding energy of conjugated polymers using a scanning tunneling microscope. *Physical Review Letters*, 81(5):1082–1085, 1998. 52, 72

[72] R. Österbacka, M. Wohlgenannt, M. Shkunov, D. Chinn, and Z. V. Vardeny. Excitons, polarons, and laser action in poly(p-phenylene vinylene) films. *Journal of Chemical Physics*, 118(19):8905–8916, 2003. 52, 72

[73] H. Ohkita, S. Cook, Y. Astuti, W. Duffy, S. Tierney, W. Zhang, M. Heeney, I. McCulloch, J. Nelson, D. D. C. Bradley, and J. R. Durrant. Charge carrier formation in polythiophene/fullerene blend films studied by transient absorption spectroscopy. *Journal of the American Chemical Society*, 130(10):3030–3042, 2008. 52, 72, 88, 95

[74] L. J. A. Koster, V. D. Mihailetchi, and P. W. M. Blom. Bimolecular recombination in polymer/fullerene bulk heterojunction solar cells. *Applied Physics Letters*, 88(5):052104–3, 2006. 52

[75] J. M. Frost, F. Cheynis, S. M. Tuladhar, and J. Nelson. Influence of polymer-blend morphology on charge transport and photocurrent generation in donor-acceptor polymer blends. *Nano Letters*, 6(8):1674–1681, 2006. 52

[76] I. W. Hwang, C. Soci, D. Moses, Z. Zhu, D. Waller, R. Gaudiana, C. J. Brabec, and A. J. Heeger. Ultrafast electron transfer and decay dynamics in a small band gap bulk heterojunction material. *Advanced Materials*, 19(17):2307–2312, 2007. 52, 72, 88, 95

[77] S. De, T. Pascher, M. Maiti, K. G. Jespersen, T. Kesti, F. L. Zhang, O. Inganäs, A. Yartsev, and V. Sundstrom. Geminate charge recombination in alternating polyfluorene copolymer/fullerene blends. *Journal of the American Chemical Society*, 129(27):8466–8472, 2007. 52, 72, 88, 95

[78] S. Westenhoff, I. A. Howard, and R. H. Friend. Probing the morphology and energy landscape of blends of conjugated polymers with sub-10 nm resolution. *Physical Review Letters*, 101(Copyright (C) 2010 The American Physical Society):016102, 2008. 52, 62, 72

[79] K. Tvingstedt, K. Vandewal, A. Gadisa, F. L. Zhang, J. Manca, and O. Inganäs. Electroluminescence from charge transfer states in polymer solar cells. *Journal of the American Chemical Society*, 131(33):11819–11824, 2009. 52, 72

[80] Y. Zhou, K. Tvingstedt, F. Zhang, C. Du, W. X. Ni, M. R. Andersson, and O. Inganäs. Observation of a charge transfer state in low-bandgap polymer/fullerene blend systems by photoluminescence and electroluminescence studies. *Advanced Functional Materials*, 19(20):3293–3299, 2009. 52, 72

[81] D. L. Vangeneugden, D. J. M. Vanderzande, J. Salbeck, P. A. van Hal, R. A. J. Janssen, J. C. Hummelen, C. J. Brabec, S. E. Shaheen, and N. S. Sariciftci. Synthesis and characterization of a poly(1,3-dithienylisothianaphthene) derivative for bulk heterojunction photovoltaic cells. *The Journal of Physical Chemistry B*, 105(45):11106–11113, 2001. 52, 72

[82] M. Hallermann, S. Haneder, and E. Da Como. Charge-transfer states in conjugated polymer/fullerene blends: Below-gap weakly bound excitons for polymer photovoltaics. *Applied Physics Letters*, 93(5):053307–3, 2008. 52, 72

[83] Z. H. Xu, B. Hu, and J. Howe. Improvement of photovoltaic response based on enhancement of spinorbital coupling and triplet states in organic solar cells. *Journal of Applied Physics*, 103(4):043909, 2008. 52

[84] T. Ogiwara, T. Ikoma, K. Akiyama, and S. Tero-Kubota. Spin dynamics of carrier generation in a photoconductive c60-doped poly(n-vinylcarbazole) film. *Chemical Physics Letters*, 411(4-6):378–383, 2005. 52, 88

[85] Z. H. Xu and B. Hu. Photovoltaic processes of singlet states in organic solar cells. *Advanced Functional Materials*, 18(17):2611–2617, 2008. 52, 54, 74, 76, 77, 89, 91, 94, 95

[86] Z. H. Xu, H. D. Zang, and B. Hu. Solar energy-conversion processes in organic solar cells. *Jom*, 60(9):49–53, 2008. 52, 54, 77, 91, 95

[87] G. Veeraraghavan, T. D. Nguyen, Y. Sheng, O. Mermer, and M. Wohlgenannt. Magnetic field effects on current, electroluminescence and photocurrent in organic light-emitting diodes. *Journal of Physics: Condensed Matter*, 19(3):036209, 2007. 52

[88] B. Hu, L. A. Yan, and M. Shao. Magnetic-field effects in organic semiconducting materials and devices. *Advanced Materials*, 21(14-15):1500–1516, 2009. 53, 58, 89, 91, 96

[89] N. E. Geacintov, M. Pope, and S. Fox. Magnetic field effects on photo-enhanced currents in organic crystals. *Journal of Physics and Chemistry of Solids*, 31(6):1375–1379, 1970. 53, 94

[90] L. Onsager. Initial recombination of ions. *Physical Review*, 54(8):554–557, 1938. 53, 54, 74, 89, 91, 96

[91] M. Wohlgenannt and Z. V. Vardeny. Spin-dependent exciton formation rates in pi-conjugated materials. *Journal of Physics-Condensed Matter*, 15(3):R83–R107, 2003. 53, 54, 76, 89, 91, 96

[92] M. Schott and J. Berrehar. Detrapping of holes by singlet excitons or photons in crystalline anthracene. *Molecular Crystals and Liquid Crystals*, 20:13 – 25, 1973. 53

[93] M. Pope, J. Burgos, and N. Wotherspoon. Singlet exciton-trapped carrier interaction in anthracene. *Chemical Physics Letters*, 12(1):140–143, 1971. 53

[94] B. Hu and Y. Wu. Tuning magnetoresistance between positive and negative values in organic semiconductors. *Nature Materials*, 6(12):985–991, 2007. 53, 76, 94

[95] C. Doubleday, N. J. Turro, and J. F. Wang. Dynamics of flexible triplet biradicals. *Accounts of Chemical Research*, 22(6):199–205, 1989. 53

[96] Z. H. Xu, Y. Wu, and B. Hu. Dissociation processes of singlet and triplet excitons in organic photovoltaic cells. *Applied Physics Letters*, 89(13):131116, 2006. 53

[97] M. A. Baldo, C. Adachi, and S. R. Forrest. Transient analysis of organic electrophosphorescence. ii. transient analysis of triplet-triplet annihilation. *Physical Review B*, 62(16):10967–10977, 2000. 53

[98] A. H. Davis and K. Bussmann. Large magnetic field effects in organic light emitting diodes based on tris(8-hydroxyquinoline aluminum) (alq[sub 3])/n,n[sup]-di(naphthalen-1-yl)-n,n[sup]diphenyl-benzidine (npb) bilayers. *Journal of Vacuum Science & Technology A: Vacuum, Surfaces, and Films*, 22(4):1885, 2004. 53

[99] V. Ern and R. E. Merrifield. Magnetic field effect on triplet exciton quenching in organic crystals. *Physical Review Letters*, 21(9):609, 1968. 53, 94

[100] M Pope and CE Swenberg. *Electronic processes in organic crystals and polymers*. Oxford University Press, 1999. 54, 95

[101] J. Kalinowski and J. Godlewski. Magnetic-field effects on recombination radiation in tetracene crystal. *Chemical Physics Letters*, 36(3):345–348, 1975. 54, 95

[102] H. Tajima, M. Miyakawa, H. Isozaki, M. Yasui, N. Suzuki, and M. Matsuda. Magnetophotocurrent effect in organic photovoltaic cells at low temperatures. *Synthetic Metals*, 160(3-4):256–261, 2010. 54

[103] Wu, Naoki Kumagai, and Masahiro Yoshimura. Hydrothermal formation and growth of single and double layer batio3 and srtio3 films on the flexible polymer film substrates from sol gel amorphous titanium oxide films. *Chemistry of Materials*, 12(11):3356–3361, 2000. 55, 73

[104] S. Mandal, M. L. N. Goswami, K. Das, A. Dhar, and S. K. Ray. Temperature dependent photoluminescence characteristics of nanocrystalline zno films grown by sol-gel technique. *Thin Solid Films*, 516(23):8702–8706, 2008. 55

[105] D. R. Lide. Crc handbook of chemistry and physics, 89th edition. pages 12–52, 2008-2009. 60

[106] Z. H. Sun, C. X. Wang, J. X. Yang, B. Zhao, and J. R. Lombardi. Nanoparticle metal - semiconductor charge transfer in zno/patp/ag assemblies by surface-enhanced raman spectroscopy. *Journal of Physical Chemistry C*, 112(15):6093–6098, 2008. 60

[107] W. L. Ma, C. Y. Yang, X. Gong, K. Lee, and A. J. Heeger. Thermally stable, efficient polymer solar cells with nanoscale control of the interpenetrating network morphology. *Advanced Functional Materials*, 15(10):1617–1622, 2005. 65

[108] T. J. Savenije, J. E. Kroeze, X. N. Yang, and J. Loos. The effect of thermal treatment on the morphology and charge carrier dynamics in a polythiophene-fullerene bulk heterojunction. *Advanced Functional Materials*, 15(8):1260–1266, 2005. 65, 82

[109] Y. Kim, S. Choulis, J. Nelson, D. Bradley, S. Cook, and J. Durrant. Composition and annealing effects in polythiophene/fullerene solar cells. *Journal of Materials Science*, 40(6):1371–1376, 2005. 65

[110] G. Li, V. Shrotriya, Y. Yao, and Y. Yang. Investigation of annealing effects and film thickness dependence of polymer solar cells based on poly(3-hexylthiophene). *Journal of Applied Physics*, 98(4):043704, 2005. 65, 67, 82

[111] Y. Kim, S. A. Choulis, J. Nelson, D. D. C. Bradley, S. Cook, and J. R. Durrant. Device annealing effect in organic solar cells with blends of regioregular poly(3-hexylthiophene) and soluble fullerene. *Applied Physics Letters*, 86(6):063502, 2005. 65

[112] M. Reyes-Reyes, K. Kim, and D. L. Carroll. High-efficiency photovoltaic devices based on annealed poly(3-hexylthiophene) and 1-(3-methoxycarbonyl)-propyl-1-phenyl-(6,6)c-61 blends. *Applied Physics Letters*, 87(8):083506, 2005. 65

[113] L. H. Nguyen, H. Hoppe, T. Erb, S. Gunes, G. Gobsch, and N. S. Sariciftci. Effects of annealing on the nanomorphology and performance of poly(alkylthiophene): fullerene bulk-heterojunction solar cells. *Advanced Functional Materials*, 17(7):1071–1078, 2007. 65

[114] M. Dante, J. Peet, and T. Q. Nguyen. Nanoscale charge transport and internal structure of bulk heterojunction conjugated polymer/fullerene solar cells by scanning probe microscopy. *Journal of Physical Chemistry C*, 112(18):7241–7249, 2008. 65

[115] D. Chirvase, J. Parisi, J. C. Hummelen, and V. Dyakonov. Influence of nanomorphology on the photovoltaic action of polymerfullerene composites. *Nanotechnology*, 15(9):1317–1323, 2004. 65

[116] J. Jo, S. S. Kim, S. I. Na, B. K. Yu, and D. Y. Kim. Time-dependent morphology evolution by annealing processes on polymer:fullerene blend solar cells. *Advanced Functional Materials*, 19(6):866–874, 2009. 65

[117] P. Taneja, P. Ayyub, and R. Chandra. Size dependence of the optical spectrum in nanocrystalline silver. *Physical Review B*, 65(24):245412, 2002. 69

[118] Z. M. Ou, H. Yao, and K. Kimura. Organic nanoparticles of cyanine dye in aqueous solution. *Bulletin of the Chemical Society of Japan*, 80(2):295–302, 2007. 69

[119] K. Vandewal, K. Tvingstedt, A. Gadisa, O. Inganäs, and J. V. Manca. On the origin of the open-circuit voltage of polymer-fullerene solar cells. *Nature Materials*, 8(11):904–909, 2009. 69

[120] T. M. Clarke and J. R. Durrant. Charge photogeneration in organic solar cells. *Chemical Reviews*, 110(11):6736–6767, 2010. 72, 88, 95

[121] J. M. Frost, F. Cheynis, S. M. Tuladhar, and J. Nelson. Influence of polymer-blend morphology on charge transport and photocurrent generation in donoracceptor polymer blends. *Nano Letters*, 6(8):1674–1681, 2006. PMID: 16895355. 72

[122] L. J. A. Koster, V. D. Mihailetchi, and P. W. M. Blom. Ultimate efficiency of polymer/fullerene bulk heterojunction solar cells. *Applied Physics Letters*, 88(9):093511, 2006. 72

[123] M. Chandross, S. Mazumdar, S. Jeglinski, X. Wei, Z. V. Vardeny, E. W. Kwock, and T. M. Miller. Excitons in poly(para-phenylenevinylene). *Physical Review B*, 50(Copyright (C) 2010 The American Physical Society):14702, 1994. 72

[124] M. Knupfer. Exciton binding energies in organic semiconductors. *Applied Physics A: Materials Science & Processing*, 77(5):623–626, 2003. 72

[125] X. Y. Zhu, Q. Yang, and M. Muntwiler. Charge-transfer excitons at organic semiconductor surfaces and interfaces. *Accounts of Chemical Research*, 42(11):1779–1787, 2009. 72, 88

[126] B. Brocklehurst, R. S. Dixon, E. M. Gardy, V. J. Lopata, M. J. Quinn, A. Singh, and F. P. Sargent. The effect of a magnetic field on the singlet/triplet ratio in geminate ion recombination. *Chemical Physics Letters*, 28(3):361–363, 1974. 74, 76, 91

[127] V. M. Agranovich, D. M. Basko, K. Schmidt, G. C. LaRocca, F. Bassani, S. Forrest, K. Leo, and D. Lidzey. Charged frenkel excitons in organic crystals. *Chemical Physics*, 272(2-3):159–169, 2001. 76, 94

[128] M. Iltaf Khan, Guilermo C. Bazan, and Zoran D. Popovic. Evidence for electric field-assisted dissociation of the excited singlet state into charge carriers in meh-ppv. *Chemical Physics Letters*, 298(4-6):309–314, 1998. 77

[129] V. I. Arkhipov, E. V. Emelianova, and H. Bässler. Hot exciton dissociation in a conjugated polymer. *Physical Review Letters*, 82(Copyright (C) 2010 The American Physical Society):1321, 1999. 77

[130] V. I. Arkhipov, E. V. Emelianova, S. Barth, and H. Bässler. Ultrafast on-chain dissociation of hot excitons in conjugated polymers. *Phys. Rev. B*, 61:8207–8214, Mar 2000. 77

[131] V. Bessergenev. High-temperature anomalies of dielectric constant in tio2 thin films. *Materials Research Bulletin*, 44(8):1722–1728, 2009. 83

[132] G. Zhao, Y. He, and Y. Li. 6.5% efficiency of polymer solar cells based on poly(3-hexylthiophene) and indene-c60 bisadduct by device optimization. *Advanced Materials*, 22(39):4355–4358, 2010. 87

[133] Y. Y. Liang, Y. Wu, D. Q. Feng, S. T. Tsai, H. J. Son, G. Li, and L. P. Yu. Development of new semiconducting polymers for high performance solar cells. *Journal of the American Chemical Society*, 131(1):56–+, 2009. 87, 90

[134] R. Qin, W. Li, C. Li, C. Du, C. Veit, H. F. Schleiermacher, M. Andersson, Z. Bo, Z. Liu, O. Inganäs, U. Wuerfel, and F. Zhang. A planar copolymer for high efficiency polymer solar cells. *Journal of the American Chemical Society*, 131(41):14612–14613, 2009. 87

[135] S. H. Park, A. Roy, S. Beaupre, S. Cho, N. Coates, J. Moon, D. Moses, M. Leclerc, K. Lee, and A. J. Heeger. Bulk heterojunction solar cells with internal quantum efficiency approaching 100 *Nat Photon*, 3(5):297–302, 2009. 87

[136] R. H. Friend, D. D. C. Bradley, and P. D. Townsend. Photo-excitation in conjugated polymers. *Journal of Physics D: Applied Physics*, 20(11):1367–1384, 1987. 88

[137] A. C. Morteani, P. Sreearunothai, L. M. Herz, R. H. Friend, and C. Silva. Exciton regeneration at polymeric semiconductor heterojunctions. *Physical Review Letters*, 92(24):247402, 2004. 88

[138] M. G. Harrison, J. Grner, and G. C. W. Spencer. Analysis of the photocurrent action spectra of meh-ppv polymer photodiodes. *Physical Review B*, 55(12):7831, 1997. 88

[139] G. A. Chamberlain. Organic solar cells: A review. *Solar Cells*, 8(1):47–83, 1983. 88

[140] Y. Nishihara, E. Frankevich, A. Fujii, M. Ozaki, and K. Yoshino. Properties of polaron pairs in conjugated polymers studied by two-correlated-pulses technique. *Journal of the Physical Society of Japan*, 73(7):1888, 2004. 88

[141] Pedro Henrique de Oliveira Neto and Geraldo Magela e Silva. Photo-generation of polaron pairs in coupled chains of polyacetylene. *Journal of Molecular Structure: THEOCHEM*, 852(1-3):11–14, 2008. 88

[142] A. Ruseckas, M. Theander, M. R. Andersson, M. Svensson, M. Prato, O. Inganäs, and V. Sundström. Ultrafast photogeneration of inter-chain charge pairs in polythiophene films. *Chemical Physics Letters*, 322(1-2):136–142, 2000. 88

[143] H. Zang, Z. Xu, and B. Hu. Magneto-optical investigations on the formation and dissociation of intermolecular charge-transfer complexes at donor-acceptor interfaces in bulk-heterojunction organic solar cells. *The Journal of Physical Chemistry B*, 114(17):5704–5709, 2010. 88, 89

[144] E. L. Frankevich and E. I Balabanov. New effect of increasing photoconductivity of organic semiconductors in a weak magnetic field. *JETP letters*, 1:169, 1965. 88

[145] Geacinto.Ne, M. Pope, and S. Fox. Magnetic field effects on photo-enhanced currents in organic crystals. *Journal of Physics and Chemistry of Solids*, 31(6):1375–&, 1970. 88, 94

[146] H. Tajima, M. Miyakawa, M. Yasui, N. Suzuki, and M. Matsuda. Photovoltaic effect of organic devices at low temperature and under high magnetic field. *Thin Solid Films*, 518(2):781–785, 2009. 88

[147] T. Ikoma, F. Ito, T. Ogiwara, K. Akiyama, and S. Tero-Kubota. Evidence of photocarrier generation via the singlet and triplet states in a poly(n-vinylcarbazole) film. *Chemistry Letters*, 34(10):1424–1425, 2005. 88

[148] M. Reufer, M. J. Walter, P. G. Lagoudakis, A. B. Hummel, J. S. Kolb, H. G. Roskos, U. Scherf, and J. M. Lupton. Spin-conserving carrier recombination in conjugated polymers. *Nature Materials*, 4(4):340–346, 2005. 89, 91

[149] V. Dyakonov, ouml, G. sler, M. Schwoerer, and E. L. Frankevich. Evidence for triplet interchain polaron pairs and their transformations in polyphenylenevinylene. *Physical Review B*, 56(7):3852, 1997. 89, 91

[150] J. Szmytkowski, W. Stampor, J. Kalinowski, and Z. H. Kafafi. Electric field-assisted dissociation of singlet excitons in tris-(8-hydroxyquinolinato) aluminum (iii). *Applied Physics Letters*, 80(8):1465–1467, 2002. 89

[151] J. Peet, J. Y. Kim, N. E. Coates, W. L. Ma, D. Moses, A. J. Heeger, and G. C. Bazan. Efficiency enhancement in low-bandgap polymer solar cells by processing with alkane dithiols. *Nature Materials*, 6(7):497–500, 2007. 89, 95, 96

[152] H. Sakai, H. Murata, M. Murakami, K. Ohkubo, and S. Fukuzumi. Photoinduced change of dielectric permittivity in molecular doped polymer layer. *Applied Physics Letters*, 95(25):252901–3, 2009. 89

[153] Y. Y. Liang, D. Q. Feng, Y. Wu, S. T. Tsai, G. Li, C. Ray, and L. P. Yu. Highly efficient solar cell polymers developed via fine-tuning of structural and electronic properties. *Journal of the American Chemical Society*, 131(22):7792–7799, 2009. 89

[154] Y. Yao, Y. Liang, V. Shrotriya, S. Xiao, L. Yu, and Y. Yang. Plastic near-infrared photodetectors utilizing low band gap polymer. *Advanced Materials*, 19(22):3979–3983, 2007. 90

[155] Y. Liang, D. Feng, J. Guo, J. M. Szarko, C. Ray, L. X. Chen, and L. Yu. Regioregular oligomer and polymer containing thieno[3,4-b]thiophene moiety for efficient organic solar cells. *Macromolecules*, 42(4):1091–1098, 2009. 90

[156] J. Guo, H. Ohkita, H. Benten, and S. Ito. Charge generation and recombination dynamics in poly(3-hexylthiophene)/fullerene blend films with

different regioregularities and morphologies. *Journal of the American Chemical Society*, 132(17):6154–6164, 2010. 94

[157] D. J. D. Moet, M. Lenes, M. Morana, H. Azimi, C. J. Brabec, and P. W. M. Blom. Enhanced dissociation of charge-transfer states in narrow band gap polymer:fullerene solar cells processed with 1,8-octanedithiol. *Applied Physics Letters*, 96(21):213506–3, 2010. 95

[158] Z. Zhu, D. Waller, R. Gaudiana, M. Morana, D. Muhlbacher, M. Scharber, and C. Brabec. Panchromatic conjugated polymers containing alternating donor/acceptor units for photovoltaic applications. *Macromolecules*, 40(6):1981–1986, 2007. 95

[159] I. W. Hwang, S. Cho, J. Y. Kim, K. Lee, N. E. Coates, D. Moses, and A. J. Heeger. Carrier generation and transport in bulk heterojunction films processed with 1,8-octanedithiol as a processing additive. *Journal of Applied Physics*, 104(3):033706–9, 2008. 95

[160] T. Clarke, A. Ballantyne, F. Jamieson, C. Brabec, J. Nelson, and J. Durrant. Transient absorption spectroscopy of charge photogeneration yields and lifetimes in a low bandgap polymer/fullerene film. *Chemical Communications*, (1):89–91, 2009. 95

[161] M. Lenes, M. Morana, C. J. Brabec, and P. W. M. Blom. Recombination-limited photocurrents in low bandgap polymer/fullerene solar cells. *Advanced Functional Materials*, 19(7):1106–1111, 2009. 95

[162] P. J. Bounds, P. Petelenz, and W. Siebrand. Charge-transfer excitons in anthracene crystals. a theoretical investigation of their optical absorption and thermal dissociation. *Chemical Physics*, 63(3):303–320, 1981. 95

[163] C. L. Braun. Electric field assisted dissociation of charge transfer states as a mechanism of photocarrier production. *The Journal of Chemical Physics*, 80(9):4157–4161, 1984. 95

[164] D. Veldman, O. Ipek, S. C. J. Meskers, J. Sweelssen, M. M. Koetse, S. C. Veenstra, J. M. Kroon, S. S. van Bavel, J. Loos, and R. A. J. Janssen. Compositional and electric field dependence of the dissociation of charge transfer excitons in alternating polyfluorene copolymer/fullerene blends. *Journal of the American Chemical Society*, 130(24):7721–7735, 2008. 95

[165] T. Drori, J. Holt, and Z. V. Vardeny. Optical studies of the charge transfer complex in polythiophene/fullerene blends for organic photovoltaic applications. *Physical Review B*, 82(7):075207, 2010. 95

[166] C. Deibel, T. Strobel, and V. Dyakonov. Role of the charge transfer state in organic donoracceptor solar cells. *Advanced Materials*, 22(37):4097–4111, 2010. 95

[167] M. Cocchi, D. Virgili, C. Sabatini, and J. Kalinowski. Organic electroluminescence from singlet and triplet exciplexes: Exciplex electrophosphorescent diode. *Chemical Physics Letters*, 421(4-6):351–355, 2006. 95

[168] S. C. Price, A. C. Stuart, L. Yang, H. Zhou, and W. You. Fluorine substituted conjugated polymer of medium band gap yields 7 % efficiency in polymer-fullerene solar cells. *Journal of the American Chemical Society*, 133(12):4625–4631, 2011. 98

[169] H. Zhou, L. Yang, A. C. Stuart, S. C. Price, S. Liu, and W. You. Development of fluorinated benzothiadiazole as a structural unit for a polymer solar cell of 7 % efficiency. *Angewandte Chemie International Edition*, 50(13):2995–2998, 2011. 98

[170] K. Ohno and Y. Kawazoe. Abnormal intermolecular interaction between overlayer c60 molecules due to induced dipole moments in c60 thin films adsorbed on substrates. *Scripta Materialia*, 44(8-9):1579–1582, 2001. 98

[171] Z. Xu, L. Chen, G. Yang, C. Huang, J. Hou, Y. Wu, G. Li, C. Hsu, and Y. Yang. Vertical phase separation in poly(3-hexylthiophene): Fullerene derivative blends and its advantage for inverted structure solar cells. *Advanced Functional Materials*, 19(8):1227–1234, 2009. 98

Vita

Huidong Zang was born in Liaoyuan, Jilin, People's Republic of China, in January 1982. He went to Jilin University at 2000 to study in Electronic Science and Technology and obtained his Bachelors degree in July, 2004. He continued to study in Microelectronics and Solid State Electronics at Jilin University and obtained his Masters degree in July, 2007. Then he went to University of Tennessee-Knoxville to continue his study in Material Science and Engineering, pursuing his Ph.D. degree under the supervision of Prof. Bin Hu from August, 2007.

Index

π-bond, 3

π-electron, 3

σ-bond, 3

Bimolecular recombination, 7

binding energy, 83

capacitance-voltage analysis, 37

charge-transfer complex, 11

Coulomb attraction, 83

dielectric effect, 28

donor-acceptor interaction, 52

electrical polarizability, 69

electroluminescence, 58

electron hole pair, 11, 52

energy level pinning, 46

equivalent electric circuit, 8

exchange energy, 76

excited states, 10

exciton, 11

Exciton diffusion, 7

F8BT, 5

fill factor, 6

Frenkel exciton, 11

Geminated recombination, 7

Gibbs free energy, 29

HXS-1, 5

hydrogen bonding, 3

Hyperfine interaction, 16

intersystem crossing, 16, 74

Intra-molecular recombination, 7

kinetic energy, 63

LADR, 51

magnetic field effect, 17

MDMO-PPV, 5

MEH-PPV, 5

metal-semiconductor contact, 39

MIM model, 22

Onsager process, 53, 74

open circuit voltage, 6

P3HT, 5

parallel resistance, 8

PBnDT-DTBT, 5

PCBM, 5

photoinduced electron transfer, 6, 29

polaron pair, 11, 74

PTB1, 5

PTB2, 5

PTB4, 5

PTB7, 5

series resistance, 8

short circuit current, 6

singlet excited states, 10

spin conservation, 11

spin forbidden, 11

spin momentum conservation, 53

Spin-Orbit coupling, 14

spin-spin interaction, 11

surface charge density, 39

trion, 76

triplet charge reaction, 17

triplet excited states, 10

van der Waals force, 3

Wannier-Mott exciton, 12

Zeeman Effect, 13